ISSN 2413-9432

BIOMEDICAL PHOTONICS

Volume 15, # 2, 2026

In the issue:

BMP

Российская Фотодинамическая Ассоциация

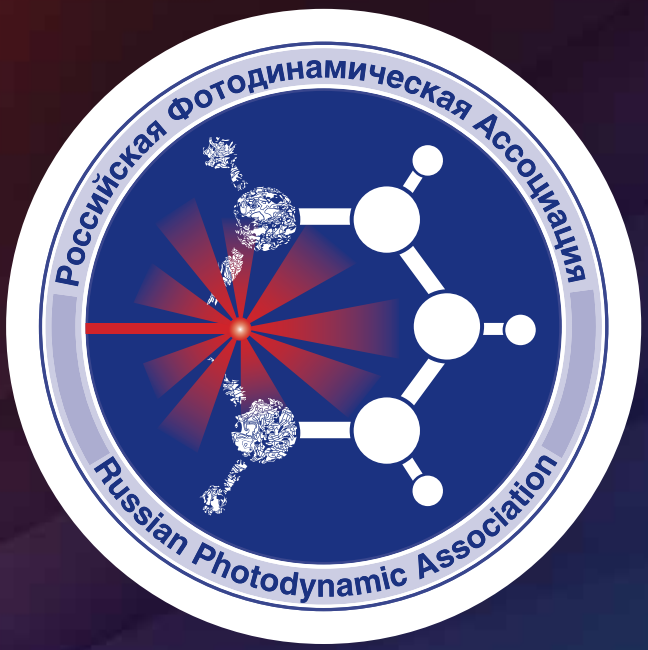

www.pdt-association.com

BIOMEDICAL PHOTONICS

FOUNDERS:
Russian Photodynamic Association
P.A. Herzen Moscow Cancer Research Institute

EDITOR-IN-CHIEF:
Filonenko E.V., Dr. Sci. (Med.), Professor, Head of the Centre of Laser and Photodynamic Diagnosis and Therapy of Tumors in P.A.Herzen Moscow Cancer Research Institute (Moscow, Russia)

DEPUTY CHIEF EDITOR:
Grin M.A., Dr. Sci. (Chem.), Professor, Chief of Department of Chemistry and Technology of Biological Active Substances named after Preobragenskiy N.A. in Moscow Technological University (Moscow, Russia)

Loschenov V.B., Dr. Sci. (Phys. and Math.), Professor, Chief of Laboratory of Laser biospectroscopy in the Natural Sciences Center of General Physics Institute of the Russian Academy of Sciences (Moscow, Russia)

EDITORIAL BOARD:

Kaprin A.D., Academician of the Russian Academy of Sciences, Dr. Sci. (Med.), Professor, General Director of National Medical Research Radiological Centre of the Ministry of Health of the Russian Federation (Moscow, Russia)

Romanko Yu.S., Dr. Sci. (Med.), Professor of the Department of Oncology, Radiotherapy and Plastic Surgery named after L.L. Lyovshina in I.M. Sechenov First Moscow State Medical University (Moscow, Russia)

Stranadko E.Ph., Dr. Sci. (Med.), Professor, Chief of department of Laser Oncology and Photodynamic Therapy of State Research and Clinical Center of Laser Medicine named by O.K.Skobelcin of FMBA of Russia (Moscow, Russia)

Blondel V., PhD, Professor at University of Lorraine, Joint-Head of the Health-Biology-Signal Department (SBS) (Nancy, France)

Bolotine L., PhD, Professor of Research Center for Automatic Control of Nancy (Nancy, France)

Douplik A., PhD, Professor in Ryerson University (Toronto, Canada)

Steiner R., PhD, Professor, the Honorary Director of Institute of Laser Technologies in Medicine and Metrology at Ulm University (Ulm, Germany)

BIOMEDICAL PHOTONICS –
research and practice, peer-reviewed, multidisciplinary journal.
The journal is issued 4 times per year.
The circulation – 1000 copies., on a quarterly basis.

The journal is included into the List of peer-reviewed science press of the State Commission for Academic Degrees and Titles of Russian Federation.
The journal is indexed in the international abstract and citation database – Scopus.

The publisher "Agentstvo MORE".
Moscow, Khokhlovskiy lane, 9

Editorial Staff:

Chief of the editorial Staff	Ivanova-Radkevich V.I.
Science Editor	Prof. Mamontov A.S.
Literary Editor	Moiseeva R.N.
Translators	Kalyagina N.A.
Computer Design	Kreneva E.I.
Desktop Publishing	Shalimova N.M.

The Address of Editorial Office:
Russia, Moscow, 2nd Botkinskiy Proezd, 3
Tel. 8 (495) 945–86–60
www: PDT-journal.com
E-mail: PDT-journal@mail.ru

Corresponding to:
125284, Moscow, p/o box 13

Registration certificate (PI), No. FS 77–51995, issued on 29.11.2012 by the Federal Service for Supervision of Communications, Information Technology, and Mass Media of Russia.

The subscription index of "Rospechat" agency – 70249

The editorial staff is not responsible for the content of promotional material. Articles represent the authors' point of view, which may be not consistent with view of the journal's editorial board. Editorial Board admits for publication only the articles prepared in strict accordance with guidelines for authors. Whole or partial presentation of the material published in the Journal is acceptable only with written permission of the Editorial board.

BIOMEDICAL PHOTONICS

BIOMEDICAL PHOTONICS –
научно-практический, рецензируемый,
мультидисциплинарный журнал.
Выходит 4 раза в год.
Тираж – 1000 экз., ежеквартально.

Входит в Перечень ведущих рецензируемых научных журналов ВАК РФ.
Индексируется в международной реферативной базе данных Scopus.

Издательство «Агентство МОРЕ».
Москва, Хохловский пер., д. 9

Редакция:

Зав. редакцией	Иванова-Радкевич В.И.
Научный редактор	проф. Мамонтов А.С.
Литературный редактор	Моисеева Р.Н.
Переводчик	Калягина Н.А.
Компьютерный дизайн	Кренева Е.И.
Компьютерная верстка	Шалимова Н.М.

Адрес редакции:
Россия, Москва, 2-й Боткинский пр., д. 3
Тел. 8 (495) 945–86–60
www: PDT-journal.com
E-mail: PDT-journal@mail.ru

Адрес для корреспонденции:
125284, Москва, а/я 13

Свидетельство о регистрации ПИ
№ ФС 77–51995, выдано 29.11.2012 г.
Федеральной службой по надзору в сфере связи, информационных технологий и массовых коммуникаций (Роскомнадзор).

Индекс по каталогу агентства «Роспечать» – 70249

Редакция не несет ответственности за содержание рекламных материалов.

В статьях представлена точка зрения авторов, которая может не совпадать с мнением редакции журнала.

К публикации принимаются только статьи, подготовленные в соответствии с правилами для авторов, размещенными на сайте журнала.

Полное или частичное воспроизведение материалов, опубликованных в журнале, допускается только с письменного разрешения редакции.

УЧРЕДИТЕЛИ:
Российская Фотодинамическая Ассоциация,
Московский научно-исследовательский онкологический институт им. П.А. Герцена

ГЛАВНЫЙ РЕДАКТОР:
Филоненко Е.В., доктор медицинских наук, профессор, руководитель Центра лазерной и фотодинамической диагностики и терапии опухолей Московского научно-исследовательского онкологического института им. П.А. Герцена (Москва, Россия)

ЗАМ. ГЛАВНОГО РЕДАКТОРА:
Грин М.А., доктор химических наук, профессор, заведующий кафедрой химии и технологии биологически активных соединений им. Н.А. Преображенского Московского технологического университета (Москва, Россия)

Лощенов В.Б., доктор физико-математических наук, профессор, заведующий лабораторией лазерной биоспектроскопии в Центре естественно-научных исследований Института общей физики им. А.М. Прохорова РАН (Москва, Россия)

РЕДАКЦИОННАЯ КОЛЛЕГИЯ:

Каприн А.Д., академик РАН, доктор медицинских наук, профессор, генеральный директор Национального медицинского исследовательского центра радиологии Минздрава России (Москва, Россия)

Романко Ю.С., доктор медицинских наук, профессор кафедры онкологии, радиотерапии и пластической хирургии им. Л.Л. Лёвшина Первого Московского государственного медицинского университета им. И.М. Сеченова (Москва, Россия)

Странадко Е.Ф., доктор медицинских наук, профессор, руководитель отделения лазерной онкологии и фотодинамической терапии ФГБУ «Государственный научный центр лазерной медицины им. О.К.Скобелкина ФМБА России»

Blondel V., профессор Университета Лотарингии, руководитель отделения Здравоохранение-Биология-Сигналы (SBS) (Нанси, Франция)

Bolotine L., профессор научно-исследовательского центра автоматики и управления Нанси (Нанси, Франция)

Douplik A., профессор Университета Райерсона (Торонто, Канада)

Steiner R., профессор, почетный директор Института лазерных технологий в медицине и измерительной технике Университета Ульма (Ульм, Германия)

ORIGINAL ARTICLES

ОРИГИНАЛЬНЫЕ СТАТЬИ

REVIEWS OF LITERATURE

ОБЗОРЫ ЛИТЕРАТУРЫ

FLUORESCENCE-GUIDED LYMPHATIC MAPPING IN PATIENTS WITH DIFFERENTIATED THYROID CANCER

Vetshev F.P., Popov K.K., Vetshev S.P., Ippolotov L.I., Gabaidze D.I., Kharnas S.S., Saliba M.B., Tugusheva V.S.
Sechenov University, Moscow, Russia

Abstract

The role of prophylactic central neck dissection in patients with differentiated thyroid cancer without clinically evident lymph node involvement remains controversial despite its importance for staging and risk stratification. In this context, intraoperative lymphatic mapping may provide an opportunity to reduce the extent of surgical intervention.

The study included 125 patients with cN0 differentiated thyroid cancer who underwent thyroidectomy or hemityroidectomy. Central neck dissection was performed in 98 patients, while 27 patients underwent fluorescence-guided lymphatic mapping using indocyanine green with selective lymph node removal. The mean number of removed lymph nodes was significantly lower in the ICG group (3.67 vs 10.3; $p < 0.001$), while the rate of metastatic node detection did not differ between groups (33.3% vs 34.7%; $p = 0.62$). The incidence of transient hypoparathyroidism was comparable (14.8% vs 13.3%; $p = 0.74$), whereas permanent hypoparathyroidism was observed only in the central neck dissection group (17.3% vs 0%; $p = 0.02$). However, in the subgroup of patients undergoing thyroidectomy, no difference in transient hypoparathyroidism was found (15.5% vs 15.4%; $p = 1.00$). Permanent recurrent laryngeal nerve palsy occurred in 4.1% of patients in the control group and was not observed in the ICG group.

These findings suggest that fluorescence-guided lymphatic mapping allows selective lymph node removal with a reduced extent of dissection while maintaining a comparable rate of metastatic detection. The differences in postoperative complications appear to be primarily related to the extent of surgery. Further studies are required to evaluate the diagnostic accuracy and long-term outcomes of this approach.

Key words: indocyanine green, fluorescence imaging, lymphatic mapping, differentiated thyroid cancer, lymph node dissection, thyroidectomy

Contacts: Popov K.K., e-mail: popov_k_k_1@staff.sechenov.ru

For citations: Vetshev F.P., Popov K.K., Vetshev S.P., Ippolotov L.I., Gabaidze D.I., Kharnas S.S., Saliba M.B., Tugusheva V.S. Fluorescence-guided lymphatic mapping in patients with differentiated thyroid cancer, *Biomedical Photonics*, 2026, vol. 15, no. 2, pp. 4–8. doi: 10.24931/2413–9432–2026–15-2-4-8

ПРИМЕНЕНИЕ ФЛУОРЕСЦЕНТНОГО КАРТИРОВАНИЯ ЛИМФООТТОКА У ПАЦИЕНТОВ С ДИФФЕРЕНЦИРОВАННЫМ РАКОМ ЩИТОВИДНОЙ ЖЕЛЕЗЫ

Ф.П. Ветшев, К.К. Попов, С.П. Ветшев, Л.И. Ипполитов, Д.И. Габаидзе, С.С. Харнас, М.Б. Салиба, В.С. Тугушева
ФГАОУ ВО «Первый Московский государственный медицинский университет имени И.М. Сеченова» Министерства здравоохранения Российской Федерации (Сеченовский университет), Москва, Россия

Резюме

Целесообразность профилактической центральной лимфаденэктомии у пациентов с дифференцированным раком щитовидной железы (ЩЖ) без клинических признаков поражения лимфатических узлов остаётся предметом дискуссии, несмотря на её значение для уточнения стадии заболевания и стратификации риска рецидива. В связи с этим представляют интерес методы интраоперационного картирования лимфатического оттока, позволяющие ограничить объём хирургического вмешательства.

В исследование включено 125 пациентов с cN0 дифференцированным раком ЩЖ, которым была проведена тиреоидэктомия либо гемитиреоидэктомия. У 98 пациентов выполнена центральная лимфаденэктомия, у 27 – флуоресцентное картирование лимфатического оттока с использованием индоцианина зелёного (ИЦЗ) с последующим селективным удалением лимфатических узлов. Среднее

число удалённых лимфатических узлов было ниже в группе ИЦ3 (3,67 против 10,3; $p < 0,001$), при этом частота выявления метастатического поражения статистически не различалась (33,3% и 34,7%; $p = 0,62$). Частота транзиторного гипопаратиреоза была сопоставимой между группами (14,8% и 13,3%; $p = 0,74$), тогда как постоянный гипопаратиреоз отмечен только в группе центральной лимфаденэктомии (17,3% против 0%; $p = 0,02$). При анализе пациентов, перенесших тиреоидэктомию, различия в частоте транзиторного гипопаратиреоза отсутствовали (15,5% и 15,4%; $p = 1,00$). Постоянный парез возвратного гортанного нерва отмечен у 4,1% пациентов в группе ЦЛД и не наблюдался в группе ИЦ3.
Полученные данные свидетельствуют о возможности выполнения селективного удаления лимфатических узлов на основании результатов флуоресцентного картирования для стадирования заболевания и определения послеоперационного лечения больных. Различия в частоте осложнений, вероятно, связаны с объёмом хирургического вмешательства. Для оценки диагностической точности метода и его влияния на отдалённые результаты необходимы дальнейшие исследования.

Ключевые слова: дифференцированный рак щитовидной железы, индоцианин зелёный, флуоресцентная визуализация, лимфатическое картирование, лимфодиссекция, тиреоидэктомия.

Контакты: Попов К.К., e-mail: popov_k_k_1@staff.sechenov.ru

Для цитирования: Ветшев Ф.П., Попов К.К., Ветшев С.П., Ипполитов Л.И., Габаидзе Д.И., Харнас С.С., Салиба М.Б., Тугушев В.С. Применение флуоресцентного картирования лимфооттока у пациентов с дифференцированным раком щитовидной железы // Biomedical Photonics. – 2026. – Т. 15, № 2. – С. 4–8. doi: 10.24931/2413–9432–2026–15-2-4-8

Introduction

Differentiated thyroid cancer (DTC), which includes papillary thyroid carcinoma (PTC), follicular carcinoma, and oncocytic carcinoma, accounts for more than 90% of all malignant neoplasms of the thyroid gland (TG) and represents the most common form of endocrine cancer [1]. In recent decades, a steady increase in the incidence of DTC has been observed in many countries worldwide [2,3]. According to GLOBOCAN 2020, more than 580,000 new cases of thyroid cancer are registered annually worldwide [2]. In the Russian Federation, approximately 12,000 new patients are registered annually [4]. Despite a high 10-year survival rate exceeding 90%, disease recurrence can be detected in a significant proportion of patients and is generally dependent on the number of affected lymph nodes in the central compartment [3,5]. According to surgical and pathomorphological studies, involvement of regional lymph nodes is detected in 30–80% of patients with DTC in the absence of clinical signs of their involvement, with the frequency substantially depending on the extent of lymph node dissection and the thoroughness of morphological analysis [6,7]. The central compartment (paratracheal lymph nodes or level VI) is the most common site of primary metastasis [6].

Given the high frequency of lymphogenous metastasis, the need for prophylactic central lymph node dissection in the absence of clinical signs of regional lymph node involvement (cN0) has been widely discussed in recent years. On the one hand, prophylactic central lymphadenectomy allows for accurate disease staging. At the same time, a number of studies have shown that performing prophylactic central lymph node dissection does not lead to a significant improvement in long-term treatment outcomes [8]. Prophylactic central lymph node dissection is falling out of routine practice, as its performance may be accompanied by an increased risk of postoperative complications, primarily hypoparathyroidism and recurrent laryngeal nerve (RLN) injury [9].

In current guidelines for the management of patients with DTC, a key role is given to stratifying the risk of disease recurrence. According to the American Thyroid Association (ATA, 2025) guidelines, the assessment of local recurrence risk is based on a combination of clinical and morphological factors, including the size and location of the primary tumor, the presence of extrathyroidal extension, histological features of the tumor, and the status of regional lymph nodes [1]. Based on these data, patients are stratified into low-risk, low-intermediate risk, intermediate-high risk, and high-risk of recurrence groups, thereby determining postoperative treatment or observation strategies. One of the main criteria for risk stratification is histologically confirmed lymph node involvement.

Routine abandonment of central lymphadenectomy may lead to underestimation of regional metastasis status and incorrect choice of postoperative management strategy. In turn, this may lead to an increased rate of recurrence or disease progression. Of particular interest is the use of lymphatic drainage mapping techniques. Identifying lymph nodes involved in the lymphatic drainage from the tumor could potentially contribute to a more accurate assessment of the regional extent of the tumor process without increasing the rate of postoperative complications.

One of the current directions in the development of intraoperative navigation is the use of fluorescence diagnostics with indocyanine green (ICG). After injection of the dye into the thyroid tissue, it binds to proteins in the interstitial fluid and plasma and spreads through the lymphatic vessels, allowing visualization of lymphatic drainage using a near-infrared fluorescence imaging system.

Aim of the study is to develop and investigate the necessity of a method for intraoperative fluorescence mapping of lymphatic drainage in differentiated thyroid cancer.

Materials and Methods

An open prospective study with a retrospective control group was conducted at the N.N. Burdenko Clinic of Faculty Surgery.

For intraoperative mapping of lymphatic pathways, 0.1 ml of ICG (0.5 mg/ml; Fig. 1) was injected into the thyroid tumor under ultrasound guidance 15 minutes before the skin incision. After completion of the main stage of the operation – thyroidectomy or hemithyroidectomy – the regional drainage zones were identified using a Stryker SPY-PHI near-infrared fluorescence imaging system (Fig. 2). The intraoperative photograph shows fluorescence of lymphatic vessels and regional lymph nodes (marked with a square) in the near-infrared range. The collector or tissue containing lymph nodes draining the injection zone was identified. The identified area of tissue with lymph nodes was excised. The removed thyroid gland or thyroid lobe with the selectively excised tissue was sent for routine histological examination. Based on the results of the routine histological examination, the postoperative clinical diagnosis was formulated, the disease stage was determined, the further treatment plan was established, and the follow-up program was defined.

Inclusion criteria for patients in the study:

1. Newly diagnosed DTC: category VI or V according to the results of a cytological examination of the punctate nodule according to the Bethesda System with a normal level of calcitonin in the blood.
2. Stages T1-T3 according to the TNM classification 9th edition.
3. Absence of clinical signs of metastasis – cN0, cM0.
4. Planned surgical treatment – thyroidectomy or hemithyroidectomy.

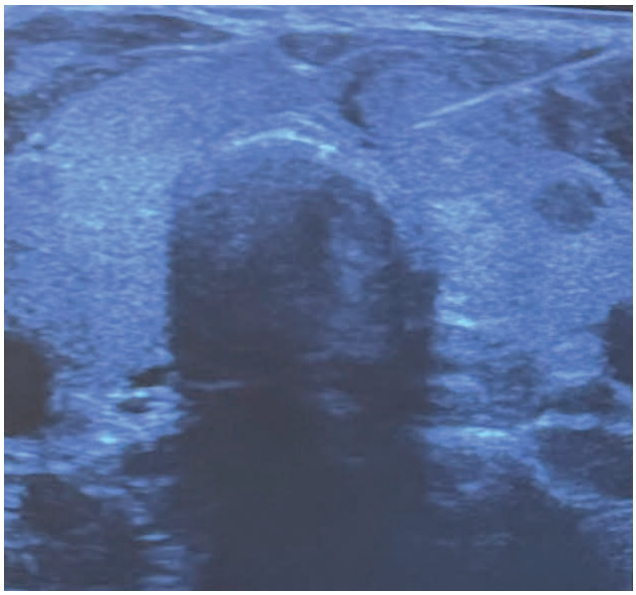

Рис. 1. Ультразвуковая сканограмма. Введение ИЦЗ в опухоль ЩЖ под контролем УЗИ.
Fig. 1. Ultrasound scan. Intratumoral ultrasound-guided injection of ICG.

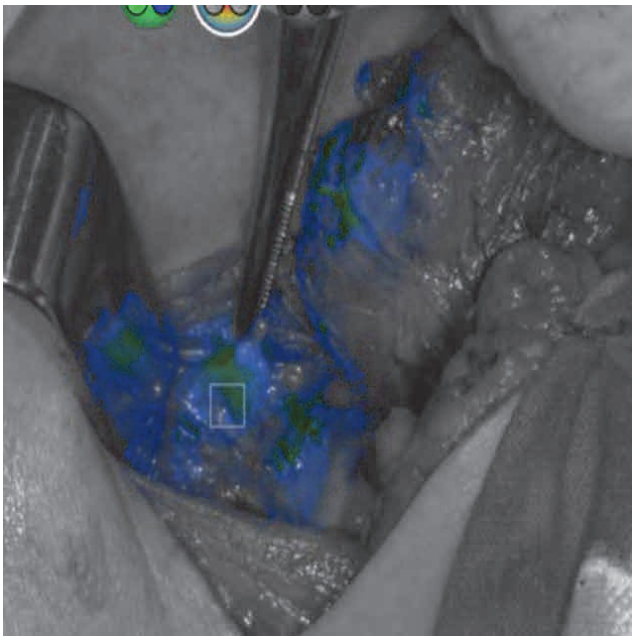

Рис. 2. Пути лимфатического оттока после введения ИЦЗ.
Fig. 2. The pathways of lymphatic outflow after the introduction of ICG.

5. Patient age from 18 to 75 years.
6. Signed informed consent to participate in the study.

Non-inclusion criteria:

1. Recurrent forms of thyroid cancer.
2. Presence of regional and distant metastases – N+ and/or M+.
3. Allergic reactions to ICG in history.
4. Pregnancy and lactation period.
5. Severe concomitant diseases: chronic heart failure class III-IV, renal failure.

Exclusion criteria:

1. Absence of signs of a malignant process according to the results of postoperative histological examination.
2. Cancer type confirmed by postoperative histological examination that is not DTC.
3. Patient's refusal to continue participation in the study.

Results

The study included 125 patients operated on at the Clinic of Faculty Surgery from 2023 to 2025. In 98 cases, thyroidectomy or hemithyroidectomy was performed with central lymph node dissection (CLND), and in 27 cases, thyroidectomy or hemithyroidectomy was supplemented with intraoperative lymphatic drainage mapping using ICG followed by selective excision of lymph nodes (Table 1). The mean age of patients in the CLND group was 47 (39-59) years, and in the ICG group – 43 (33-45) years ($p = 0.12$). In the CLND group, the proportion of men was 17.3%, in the ICG group – 33.3%, no statistically significant differences in sex were found between the groups ($p = 0.29$).

Thyroidectomy was performed in 71 (72.4%) patients in the CLND group and in 13 (48.1%) patients in the ICG group (p = 0.08). The mean number of removed lymph nodes in the control group was 10.3 per patient, whereas in the ICG group it was 3.67 (Mann-Whitney U test, ***p <0.001). Metastatic lymph node involvement according to histological examination was detected in 34 (34.7%) patients in the CLND group and in 9 (33.3%) patients in the ICG group (p = 0.62).

Transient hypoparathyroidism was registered in 13 (13.3%) patients in the control group and in 4 (14.8%) patients in the ICG group; the differences did not reach statistical significance (p = 0.74). Permanent hypoparathyroidism developed in 17 (17.3%) patients in the control group and was not registered in the ICG group (p = 0.02). Transient recurrent laryngeal nerve palsy was detected in 16 (16.3%) patients in the control group and in 2 (7.4%) patients in the ICG group (p = 0.32). Permanent recurrent laryngeal nerve palsy was not registered in the ICG group.

When analyzing the subgroup of patients who underwent thyroidectomy, transient hypoparathyroidism was registered in 11 (15.5%) out of 71 patients in the CLND group and in 2 (15.4%) out of 13 patients in the ICG group; no statistically significant differences were found between the groups (p = 1.00). Permanent hypoparathyroidism developed in 17 (23.9%) out of 71 patients in the control group, whereas no such complication occurred in the ICG group; the differences did not reach statistical significance (p = 0.061; Table 2). Permanent RLN palsy developed in 4 (4.1%) patients in the control group and was not registered in the ICG group (p = 0.57).

Discussion

Intraoperative fluorescence mapping of lymphatic drainage may potentially be used for disease staging in settings where prophylactic lymphadenectomy is not indicated. At the same time, the rate of detecting metastatic lymph node involvement did not differ statistically between the groups. The comparable rate of metastasis detection with a significant reduction in the number of removed lymph nodes may indicate the possibility of targeted removal of nodes specifically involved in lymphatic drainage from the tumor. A similar principle underlies sentinel lymph node biopsy. The possibility of its application in PTC has been discussed previously, including studies on the use of ICG for intraoperative lymphatic mapping [9,10].

Although performing central lymph node dissection increases the accuracy of staging and is used for recurrence risk stratification [1], meta-analysis data do not confirm its impact on long-term oncological outcomes. At the same time, an increased rate of postoperative complications has been noted [8,11], particularly hypoparathyroidism and RLN palsy. With a comparable rate of postoperative

Таблица 1
Характеристика пациентов
Table 1
Baseline characteristics

Показатель Variable	Число наблюдений, абс. (%) Number of observations, abs. (%)		p-value
	ЦЛД CLND	ИЦЗ ICG	
Всего In total	98	27	-
Мужчин Men	17 (17,3)	9 (33,3)	0,29
Перенесших тиреоидэктомию Thyroidectomy	71 (72,4)	13 (48,1)	0,08
С опухолью T1 T1 tumor	67 (68,4)	21 (77,8)	0,29
С опухолью T2 T2 tumor	12 (12,2)	4 (14,8)	
С опухолью T3 T3 tumor	19 (19,4)	2 (7,4)	

Таблица 2
Хирургические результаты и послеоперационные осложнения
Table 2
Surgical outcomes and postoperative complications

Показатель Variable	Число наблюдений, абс. (%) Number of observations, abs. (%)		p-value
	ЦЛД CLND	ИЦЗ ICG	
Всего In total	98	27	-
Метастазы в лимфоузлах Lymph node metastases	34 (34,7)	9 (33,3)	0,62
Транзиторный гипопаратиреоз Transient hypoparathyroidism	13 (13,3)	4 (14,8)	0,74
Пациентов с постоянным гипопаратиреозом Persistent hypoparathyroidism	17 (17,3)	-	0,02*
Транзиторный парез ВГН Transient paresis RLN	16 (16,3)	2 (7,4)	0,32
Постоянный парез ВГН Persistent RLN paresis	4 (4,1)	-	0,57

*результат статистически значим / the result is statistically significant

transient hypoparathyroidism, the rate of permanent hypoparathyroidism and the rate of postoperative RLN palsy were significantly lower in patients who underwent selective lymphadenectomy.

The use of ICG for intraoperative diagnostics is based on detecting a signal in the near-infrared range, which allows assessment of lymphatic drainage in real time. The method does not require ionizing radiation and can be integrated into the standard surgical protocol. At the same time, its application is limited by the depth of signal penetration and depends on the injection technique and visualization conditions [12,13]. A significant technical limitation of the method is the anatomically close location of the injection site to the potential area of sentinel lymph nodes. If the drug is injected incorrectly or if the thyroid tissue is inadvertently damaged during surgery, the drug may spread throughout the surgical field, making further lymphatic system mapping impossible.

The obtained data allow considering fluorescence mapping of lymphatic drainage using ICG as a potential and accessible tool for disease staging in patients with DTC without significantly increasing the extent of surgical intervention.

Conclusion

Intraoperative fluorescence mapping of lymphatic drainage using ICG represents a reproducible and technologically accessible method that expands the possibilities of intraoperative navigation in differentiated thyroid cancer. The use of this method allows surgeons to rely on individual lymphatic drainage characteristics and perform selective removal of lymph nodes involved in drainage from the tumor.

Thus, more accurate determination of the disease stage is quite feasible using modern fluorescence mapping methods without increasing the complication rate. The identified differences in complication rates are likely primarily related to the extent of surgical intervention. Further studies are required for the final assessment of the clinical significance of the method.

REFERENCES

1. Ringel M.D., Sosa J.A., Baloch Z. et al. 2025 American Thyroid Association Management Guidelines for Adult Patients with Differentiated Thyroid Cancer. *Thyroid*, 2025, vol. 35(8), pp. 841-985. doi:10.1177/10507256251363120
2. Sung H., Ferlay J., Siegel R.L. et al. Global Cancer Statistics 2020: *CA Cancer J Clin*, 2021, vol. 71(3), pp. 209–249. doi:10.3322/caac.21660
3. Pizzato M. et al. The epidemiological landscape of thyroid cancer worldwide. *Lancet Diabetes Endocrinol*, 2022, vol. 10(4), pp. 264–272. doi:10.1016/S2213-8587(22)00035-3
4. Kaprin A.D., Starinsky V.V., Shakhzadova A.O. The state of oncological care for the Russian population in 2023. Moscow: P.A. Herzen Moscow Institute of Medical Sciences – branch of the Federal State Budgetary Institution "NMITS of Radiology" of the Ministry of Health of the Russian Federation, 2024, pp. 248.
5. Lee J., Song Y., Soh E.Y. Prognostic Significance of the Number of Metastatic Lymph Nodes to Stratify the Risk of Recurrence. *World J Surg*, 2014, vol. 38(4), pp. 858–62. doi:10.1007/s00268-013-2345-6
6. Randolph G.W. et al. The prognostic significance of nodal metastases. *Thyroid*, 2012, vol. 22(11), pp. 1144–1152. doi:10.1089/thy.2012.0043
7. Miličić B. et al. Skip metastases in papillary thyroid carcinoma – prevalence, predictive and clinicopathological factors. *Acta Clin Croat*, 2020, vol. 59(1), pp. 123–131. doi:10.20471/acc.2020.59.s1.16.
8. Chen L., Wu Y.H., Lee C.H., Chen H.A., Loh E.W., Tam K.W. Prophylactic central neck dissection for papillary thyroid carcinoma with clinically uninvolved central neck lymph nodes: a systematic review and meta-analysis. *World J Surg*, 2018, vol. 42(9), pp. 2846–2857. doi:10.1007/s00268-018-4547-4.
9. Garau L.M., Rubello D., Ferretti A. et al. Sentinel lymph node biopsy in small papillary thyroid cancer. *Endocrine*, 2018, vol. 62(2), pp. 340–350. doi:10.1007/s12020-018-1658-5
10. Zhang X., Ning L., Liu D. et al. Clinical feasibility of imaging with indocyanine green combined with methylene blue for sentinel lymph node identification in papillary thyroid microcarcinoma. *Medicine (Baltimore)*, 2019, vol. 98(36), pp. e16935. doi:10.1097/MD.0000000000016935
11. Sitges-Serra A., Ruiz S., Girvent M. et al. Outcome of protracted hypoparathyroidism after total thyroidectomy. *Br J Surg*, 2010, vol. 97(11), pp. 1687–1695. doi:10.1002/bjs.7219
12. Fanaropoulou N.M., Chorti A., Markakis M., Papaioannou M., Michalopoulos A., Papavramidis T. The use of Indocyanine green in endocrine surgery of the neck: A systematic review. *Medicine*, 2019, vol. 98(10), pp. e14765. doi:10.1097/MD.0000000000014765
13. Di Marco A.N., Palazzo F.F. Near-infrared autofluorescence in thyroid and parathyroid surgery. *Gland Surg*, 2020, vol. 9(2), pp. 136–46. doi:10.21037/gs.2020.01.04

ЛИТЕРАТУРА

1. Ringel M.D., Sosa J.A., Baloch Z. et al. 2025 American Thyroid Association Management Guidelines for Adult Patients with Differentiated Thyroid Cancer. Thyroid. – 2025. – Vol. 35(8). – P. 841-985. doi:10.1177/10507256251363120
2. Sung H., Ferlay J., Siegel R.L. et al. Global Cancer Statistics 2020: CA Cancer J Clin. – 2021. – Vol. 71(3). – P. 209–249. doi:10.3322/caac.21660
3. Pizzato M. et al. The epidemiological landscape of thyroid cancer worldwide. Lancet Diabetes Endocrinol. – 2022. – Vol. 10(4). – P. 264–272. doi:10.1016/S2213-8587(22)00035-3
4. Каприн А.Д., Старинский В.В., Шахзадова А.О. Состояние онкологической помощи населению России в 2023 году. – М.: МНИОИ им. П.А. Герцена – филиал ФГБУ «НМИЦ радиологии» Минздрава России, 2024. – 248 с.
5. Lee J., Song Y., Soh E.Y. Prognostic Significance of the Number of Metastatic Lymph Nodes to Stratify the Risk of Recurrence. World j surg. – 2014. – Vol. 38(4). – P. 858–62. doi:10.1007/s00268-013-2345-6
6. Randolph G.W. et al. The prognostic significance of nodal metastases. Thyroid. – 2012. – Vol. 22(11). – P. 1144-1152. doi:10.1089/thy.2012.0043
7. Miličić B. et al. Skip metastases in papillary thyroid carcinoma – prevalence, predictive and clinicopathological factors. Acta Clin Croat. – 2020. – Vol. 59(1). – P. 123–131. doi:10.20471/acc.2020.59.s1.16.
8. Chen L, Wu YH, Lee CH, Chen HA, Loh EW, Tam KW. Prophylactic central neck dissection for papillary thyroid carcinoma with clinically uninvolved central neck lymph nodes: a systematic review and meta-analysis. World J Surg. – 2018. – Vol. 42(9). - P. 2846–2857. doi:10.1007/s00268-018-4547-4.
9. Garau L.M., Rubello D., Ferretti A. et al. Sentinel lymph node biopsy in small papillary thyroid cancer. Endocrine. – 2018. – Vol. 62(2). – P. 340–350. doi:10.1007/s12020-018-1658-5
10. Zhang X., Ning L., Liu D. et al. Clinical feasibility of imaging with indocyanine green combined with methylene blue for sentinel lymph node identification in papillary thyroid microcarcinoma. Medicine (Baltimore). – 2019. – Vol. 98(36). – P. e16935. doi:10.1097/MD.0000000000016935
11. Sitges-Serra A., Ruiz S., Girvent M. et al. Outcome of protracted hypoparathyroidism after total thyroidectomy. Br J Surg. – 2010. – Vol. 97(11). – P. 1687–1695. doi:10.1002/bjs.7219
12. Fanaropoulou N.M., Chorti A., Markakis M., Papaioannou M., Michalopoulos A., Papavramidis T. The use of Indocyanine green in endocrine surgery of the neck: A systematic review. Medicine. – 2019. – Vol. 98(10). – P. e14765. doi:10.1097/MD.0000000000014765
13. Di Marco A.N., Palazzo F.F. Near-infrared autofluorescence in thyroid and parathyroid surgery. Gland Surg. – 2020. – Vol. 9(2). – P. 136–46. doi:10.21037/gs.2020.01.04

IMPACT OF SYSTEMIC PHOTODYNAMIC THERAPY ON QUALITY OF LIFE IN PATIENTS WITH METASTATIC PROSTATE CANCER

Kazbekov K.T.[1], Shanazarov N.A.[1], Zinchenko S.V.[2], Kazbekova A.T.[3], Benberin V.V.[1]
[1]Medical Center Hospital of the President's affairs Administration of the Republic of Kazakhstan, Astana, Republic of Kazakhstan
[2]Kazan Federal University, Kazan, Russia
[3]Astana Medical University, Astana, Republic of Kazakhstan

Abstract

Quality of life is an important integrative indicator of treatment effectiveness in oncology and reflects patients' subjective physical, psychological, and social well-being. Data regarding the impact of systemic photodynamic therapy on quality of life in patients with metastatic prostate cancer remains limited. The aim of this study was to evaluate the effect of systemic photodynamic therapy on quality-of-life outcomes in patients with metastatic prostate cancer. A prospective longitudinal study was conducted involving 14 patients with a mean age of 69 years. Quality of life was assessed before and after treatment using the Quality of Life-Cancer Survivor (QOL-CS) questionnaire. Internal consistency of the scales was evaluated using Cronbach's alpha. Changes in quality-of-life scores were analyzed using the paired Student's t-test, and effect sizes were calculated using Cohen's d. The QOL-CS questionnaire demonstrated high reliability ($\alpha = 0.91$). After treatment, statistically significant improvements were observed in the physical, psychological, and social domains, as well as in the overall quality-of-life score ($p < 0.001$), with large effect sizes (Cohen's $d > 1.8$). Changes in spiritual well-being did not reach statistical significance ($p = 0.134$). Systemic photodynamic therapy is associated with clinically meaningful improvements in quality of life among patients with metastatic prostate cancer.

Keywords: systemic photodynamic therapy, quality of life, prostate cancer, QOL-CS.

Contacts: Kazbekov K.T., e-mail: kazbekovkt@gmail.com

For citations: Kazbekov K.T., Shanazarov N.A., Zinchenko S.V., Kazbekova A.T., Benberin V.V. Impact of systemic photodynamic therapy on quality of life in patients with metastatic prostate cancer, *Biomedical Photonics*, 2026, vol. 15, no. 2, pp. 9–17. doi: 10.24931/2413–9432–2026–15-2-9-17

ВЛИЯНИЕ СИСТЕМНОЙ ФОТОДИНАМИЧЕСКОЙ ТЕРАПИИ НА КАЧЕСТВО ЖИЗНИ ПАЦИЕНТОВ С МЕТАСТАТИЧЕСКИМ РАКОМ ПРЕДСТАТЕЛЬНОЙ ЖЕЛЕЗЫ

К.Т. Казбеков[1], Н.А. Шаназаров[1], С.В. Зинченко[2], А.Т. Казбекова[3], В.В. Бенберин[1]
[1]Больница Медицинского центра Управления делами Президента Республики Казахстан, Астана, Республика Казахстан
[2]Казанский (Приволжский) федеральный университет, Казань, Россия
[3]Медицинский Университет Астана, Астана, Республика Казахстан

Резюме

Качество жизни является важным интегральным показателем эффективности лечения онкологических пациентов и отражает субъективное физическое, психологическое и социальное благополучие. Данные о влиянии системной фотодинамической терапии на качество жизни пациентов с метастатическим раком предстательной железы ограничены. Целью исследования являлось изучение влияния системной фотодинамической терапии на показатели качества жизни у пациентов с метастатическим раком предстательной железы. Проведено проспективное продольное исследование с участием 14 пациентов, со средним возрастом 69 лет. Качество жизни оценивали до и после лечения с использованием опросника QOL-CS. Надёжность шкал определяли с помощью коэффициента α Кронбаха. Для сравнения показателей до и после лечения использовали парный t-критерий Стьюдента с расчётом размера эффекта (Cohen's d). Опросник QOL-CS продемонстрировал высокую надёжность ($\alpha = 0,91$). После лечения выявлено статистически значимое улучшение по физическому, психологическому и социальному доменам, а также по интегральному показателю качества жизни ($p < 0,001$), при больших величинах эффекта (Cohen's $d > 1,8$). Изменения показателей духовного благополучия не достигли статистической

значимости (p = 0,134). Системная фотодинамическая терапия ассоциируется с клинически значимым улучшением качества жизни пациентов с метастатическим раком предстательной железы.

Ключевые слова: системная фотодинамическая терапия, качество жизни, рак предстательной железы, QOL-CS.

Контакты: Казбеков К.Т., e-mail: kazbekovkt@gmail.com

Для цитирования: Казбеков К.Т., Шаназаров Н.А., Зинченко С.В., Казбекова А.Т., Бенберин В.В. Влияние системной фотодинамической терапии на качество жизни пациентов с метастатическим раком предстательной железы // Biomedical Photonics. – 2026. –Т. 15, № 2. – С. 9–17. doi: 10.24931/2413–9432–2026–15-2-9-17

Introduction

Quality of life (QOL) is a multidisciplinary health-related concept that has been used in medicine for more than four decades. It has become an integral component of modern clinical practice and is widely regarded as an individual's subjective assessment of overall well-being [1]. The term "quality of life" in relation to patients first appeared in Index Medicus in 1977 [2]. In 1982, R.M. Kaplan and J.W. Bush introduced the concept of "health-related quality of life" (HRQOL), referring specifically to quality of life as it relates to health status [3, 4].

According to the World Health Organization (WHO), health is defined as a state of complete physical, social, and psychological well-being rather than merely the absence of disease. In this framework, the WHO defines QOL as an individual's subjective perception of their position in life, in relation to their culture, value systems, and relationships with the surrounding environment. The WHOQOL instruments (WHOQOL-100 and WHOQOL-BREF) enable standardized assessment of physical, psychological, social, and environmental well-being, providing a valid and reliable approach to measuring QOL in both clinical and population-based studies [5].

In 1990, at a joint conference of the U.S. National Cancer Institute (NCI) and the American Society of Clinical Oncology (ASCO), QOL was recognized as the second most important endpoint after overall survival and was considered more informative than objective tumor response in assessing treatment outcomes [6].

In modern medicine, improving patients' QOL has become a primary goal of medical care and one of the key criteria for treatment evaluation, thereby driving the development of new diagnostic and therapeutic approaches for malignant neoplasms, including prostate cancer [4].

These developments have necessitated the establishment of a unified methodological framework for QOL assessment. Despite ongoing discussions regarding the diversity of available measurement instruments, a key methodological requirement is the appropriate selection of instruments capable of objectively capturing an individual's physical, spiritual, psychological, and social well-being. Standardized questionnaires represent the primary instruments for this purpose. These instruments must meet strict psychometric standards, and only when such criteria are satisfied can the resulting data be considered reliable and meaningful. A questionnaire may be defined as a structured method of data collection in social research that involves obtaining written responses from a defined population through questions relevant to the research problem [7].

Currently, more than 400 QOL questionnaires have been developed worldwide. In oncology practice, several cancer-specific instruments are most commonly used, including the American Functional Assessment of Cancer Therapy-General (FACT-G), the European Organisation for Research and Treatment of Cancer Quality of Life Questionnaire-Core 30 (EORTC QLQ-C30), and the Quality of Life-Cancer Survivor (QOL-CS). In addition, other instruments are occasionally employed, such as the Rotterdam Symptom Checklist (RSC), the Functional Living Index-Cancer (FLIC), the Cancer Inventory of Problem Situations (CIPS), and the Cancer Rehabilitation Evaluation System (CARES). Measures assessing physical functioning, symptom burden, and pain are also commonly used, including the Karnofsky Performance Index (KPI), the McGill Pain Questionnaire (MPQ), the Symptom Distress Scale (SDS), visual analogue scales such as the Spitzer Quality of Life Index (SQLI), the Linear Analogue Self-Assessment Scale (LASA), the Quality of Life Tool (QOLT), and the BREAST-Q [4, 8, 9].

S.A. Muslov et al. (2022) conducted a QOL assessment among 100 patients with prostate cancer at baseline using the EORTC QLQ-PR25 module, applying both classical test theory and modern Rasch model-based approaches. Both methods demonstrated high internal consistency (Cronbach's α = 0.81) and strong correlations between the two approaches (r = 0.93-0.97). The overall QOL score ranged from 76% to 79%, supporting the validity and comparability of these measurement methods in patients with prostate cancer [10].

A.A. Zhuravlev et al. (2025) adapted the Functional Assessment of Cancer Therapy-Prostate (FACT-P) questionnaire for Russian-speaking patients with prostate cancer, confirming high reliability (α = 0,78-0,89) and validity. The

Russian-language version showed good clinical utility for QOL assessment in both clinical practice and oncourological research [9].

The validation of the "Universal QOL Questionnaire for Patients with Prostate Cancer" demonstrated its high reliability and validity. The instrument enables the assessment of urinary, bowel, sexual, and hormonal functions, as well as patients' social and emotional well-being before and after treatment, making it a valuable tool for guiding therapeutic decisions and for clinical research [11].

Specific QOL assessment instruments complement traditional indicators of morbidity and mortality, providing researchers and clinicians with valuable means of evaluating the impact of cancer and its treatment. However, their psychometric refinement and cross-cultural adaptation remain subjects of ongoing development [12].

A comprehensive analysis of methodological approaches to measuring QOL in medicine, drawing on both classical test theory and modern latent variable models, as well as reviews of historical perspectives, psychometric properties of questionnaires, and applications of traditional and novel assessment methods across various clinical settings, underscores the importance of accurate QOL measurement in clinical research and healthcare practice [13].

Drawing on international experience in QOL assessment, researchers at the City of Hope National Medical Center (California, USA) developed the QOL-CS questionnaire to measure QOL in patients with different types of cancer. The instrument comprises 41 items grouped into four domains: physical, social, psychological, and spiritual well-being. It is regarded as one of the most comprehensive instruments for evaluating changes across multiple dimensions of QOL in patients with cancer and has been validated in several countries [14, 15, 16].

Quality of life assessment in prostate cancer

Individual QOL assessment is conducted across all stages of medical care and has important prognostic value, facilitating prediction of disease course and outcomes while supporting informed treatment decision-making. Longitudinal evaluation enables monitoring of therapeutic effectiveness, comparison of different treatment modalities and pharmacological interventions, and broad application in the development of prognostic, rehabilitation, and palliative care programs, as well as in treatment standardization and pharmacoeconomic research [2, 17].

The development of new approaches to QOL assessment in patients with urological malignancies plays a key role in both clinical research and routine practice. An analysis of 17 original studies employing instruments such as EPIC-26/CP, EORTC QLQ-C30/PR25, FACT-P, PROMIS, and FoP-Q-SF demonstrated that QOL in patients with prostate cancer is influenced by a complex interplay of clinical, anatomical, and psychosocial factors [10, 18, 19].

The primary goal of prostate cancer treatment is not only to maximize survival but also to maintain a high QOL. Prostate cancer is frequently detected at an early stage and often presents as a low-risk disease. An increasing number of patients opt for active surveillance, which reduces treatment-related morbidity and helps preserve QOL [11, 20].

A favorable prognosis in prostate cancer has been associated with greater patient engagement in daily life and active participation in social activities, better disease awareness, partial independence from others, minimal emotional limitations in role functioning, and overall better social functioning, as well as positive worldviews and a perceived sense of control over life circumstances [21].

Treatment strategies for prostate cancer are heterogeneous and often aggressive. Advanced prostate cancer has a significant impact on patients' QOL. In routine clinical practice, impairments such as reduced physical functioning, generalized weakness, bone pain due to metastatic involvement, and urinary dysfunction are frequently underestimated. In the absence of overt clinical symptoms, the disease often presents predominantly with psychological distress, particularly depression and anxiety [1, 22].

QOL in patients with prostate cancer is strongly associated with disease stage, treatment modalities, and overall disease severity, highlighting the clinical importance of comprehensive patient assessment when selecting optimal treatment strategies [23].

The management of prostate cancer in elderly patients is closely linked to disease duration and QOL considerations, necessitating comprehensive geriatric assessment to individualize treatment strategies. Patients with prostate cancer, particularly those over 80 years of age, require multidisciplinary management involving not only oncologists but also clinical psychologists, geriatric specialists, and, when necessary, social services. QOL in older patients declines with advancing disease stage, while urinary dysfunction becomes more pronounced. The greatest improvement in urinary symptoms has been observed following palliative transurethral resection of the prostate, whereas the highest QOL scores are reported after radical prostatectomy. Assessment of both QOL and urinary function may serve as prognostic markers in prostate cancer staging [24, 25].

In recent years, accumulating evidence suggests a close association between prostate cancer and cardiovascular disease, with psychological disorders and QOL emerging as important prognostic factors. Patients with newly diagnosed prostate cancer and concomitant ischemic heart disease exhibit higher levels of depression, greater anxiety, and poorer QOL scores on general health perception and mental health subscales compared with those without ischemic heart disease [26].

QOL in patients with prostate cancer is substantially affected by sexual dysfunction, emotional disturbances,

and pain, particularly at advanced stages of the disease. Studies evaluating QOL following radical treatment have shown that a considerable proportion of patients experience functional impairments and a decline in overall well-being. Only approximately 17% of patients reported high QOL scores, underscoring the significant impact of both the disease and its treatment on daily functioning and psychological well-being. Preservation of the neurovascular bundles during radical prostatectomy has been associated with improved sexual function outcomes, while comprehensive QOL assessment facilitates treatment optimization by balancing survival benefits against treatment-related adverse effects [27, 28].

In the context of ongoing healthcare digitalization, emerging approaches to QOL assessment in prostate cancer enable optimization of treatment and rehabilitation strategies, facilitate longitudinal monitoring of patients' clinical status, and promote individualized therapy. Digital solutions and personalized assessment tools further enhance tracking of treatment-related adverse effects, thereby improving the overall effectiveness of patient care [29].

Photodynamic therapy in prostate cancer and its impact on quality of life

International clinical experience with photodynamic therapy (PDT) has demonstrated considerable efficacy for both radical and palliative management of malignancies across various anatomical sites. PDT may be used either as a standalone modality or in combination with surgery and radiotherapy. In certain clinical situations, including patient refusal of surgery or contraindications to surgical intervention, it may represent the only feasible antitumor treatment option [4].

PDT is a modern therapeutic modality based on the interaction of three key components: a photosensitizer, light of a specific wavelength, and molecular oxygen. This approach enables selective destruction of tumor cells while simultaneously stimulating immune responses. As a minimally invasive, tissue-preserving technique, PDT has been increasingly adopted in recent years in oncology.

PDT consists of two main stages and involves administration of a photosensitizer followed by localized irradiation of the target area. Its mechanism of action is based on selective accumulation of the photosensitizer in tumor cells and its activation by light of a specific wavelength, resulting in the generation of reactive oxygen species and tumor cell destruction. The efficacy and safety of PDT are ensured by precise selection of both the light source and the photosensitizer, allowing selective targeting of pathological tissues while minimizing damage to surrounding healthy cells.

Upon light activation of the photosensitizer, reactive oxygen species and free radicals are generated, resulting in oxidative damage to tumor cells, disruption of cellular membranes and intracellular structures, and ultimately cell death. Concurrently, PDT activates antitumor immune responses by stimulating phagocytosis and cell-mediated immunity, thereby facilitating the elimination of residual malignant cells and reducing the risk of disease recurrence.

Systemic photodynamic intravenous laser blood irradiation enhances therapeutic effectiveness by improving the rheological and functional properties of blood, activating both cellular and humoral immunity, and increasing oxygen transport capacity together with antioxidant and bactericidal activity. Collectively, these effects promote a systemic immune response [30, 31].

In prostate cancer, QOL assessment plays a key role in selecting optimal treatment strategies that balance therapeutic efficacy with minimal adverse effects. Studies indicate that combined treatment approaches provide better pain control and improved emotional well-being. Longitudinal QOL evaluation before and after treatment enables therapy to be tailored according to urinary, sexual, hormonal, and psychological functioning [32].

Following vascular-targeted photodynamic therapy, most patients with low-risk localized prostate cancer reported no decision regret, with only 9.7% reporting significant regret due to local recurrence or tumor progression. Overall QOL remained stable, indicating good tolerability and minimal invasiveness of the procedure [33].

O.E. Popovkina et al. (2022) report on the development of photodynamic diagnostic and therapeutic approaches at the A. Tsyb Medical Radiological Research Cente, highlighting advances in photosensitizer application, optimization of treatment parameters, and the implementation of focal, interstitial, and systemic photodynamic therapy in clinical oncology practice. These findings highlight the potential of PDT as both a diagnostic and therapeutic modality in contemporary oncology [34].

Systemic photodynamic therapy (SPDT) for localized low-risk prostate cancer has demonstrated a high rate of negative biopsy results at 6 months, good tolerability, and preservation of QOL, with only moderate effects on erectile and urinary function. In a European prospective study, SPDT reduced disease progression and prolonged time to progression compared with active surveillance. Adverse events were predominantly mild to moderate and transient, indicating good tolerability and supporting the potential of this approach as a promising focal therapy option [35].

QOL analysis using the QOL-CS questionnaire in patients with advanced cancer demonstrated that SPDT improves patient outcomes. QOL assessment serves as an important prognostic indicator and aids in individualizing treatment by guiding the selection of optimal therapeutic strategies [36].

The importance of QOL assessment as a sensitive endpoint in the management of metastatic prostate cancer highlights its value in detecting changes in functional and

emotional well-being during therapy and in informing optimal treatment strategies [37].

The aim of the study was to evaluate the effect of systemic photodynamic therapy on QOL outcomes in patients with metastatic prostate cancer.

Materials and methods

The study was conducted at the Center for Photodynamic Therapy of the Medical Center Hospital of the President's affairs Administration of the Republic of Kazakhstan from 2024 to 2025. Patients with metastatic prostate cancer were enrolled. The mean age of the participants was 69 years. None of the participants had cognitive impairment, which ensured their ability to independently complete the questionnaires. Written informed consent was obtained from all patients prior to study initiation and treatment.

This prospective longitudinal study assessed QOL indicators at baseline (before treatment initiation) and after completion of systemic photodynamic therapy.

Changes in QOL parameters were evaluated over time relative to baseline values. This design enabled objective evaluation of the treatment effect on patients' subjective well-being. The study design is illustrated in Fig. 1.

Subjective evaluation of overall health and psychological well-being was performed in patients with metastatic prostate cancer before initiation of systemic photodynamic therapy and after treatment completion to assess QOL related outcomes.

QOL assessment and analysis were performed using the Quality of Life/Cancer Survivor (QOL-CS) questionnaire, which comprises 41 items and has been adapted and validated for use in clinical research. The instrument enables comprehensive evaluation of patients' physical, psychological, social, and functional well-being.

Scores were calculated on a 0-10 scale, where 0 indicated the worst outcome and 10 the best. Items 1-7, 9, 16-27, 29-34, and 38 were reverse-scored.

Internal consistency of the QOL-CS questionnaire scales was assessed using Cronbach's alpha. Values of $\alpha > 0.70$ were considered indicative of acceptable reliability of the instrument.

Statistical analysis was performed using parametric methods. Normality of QOL score distribution variables was assessed using the Shapiro-Wilk test. Differences in QOL scores before and after treatment were evaluated using the paired Student's t-test. Results are presented as mean ± standard deviation (M ± SD). To assess the clinical significance of the observed changes, effect size was additionally calculated using Cohen's d.

A p-value < 0.05 was considered statistically significant.

Results

Based on a processed data, internal consistency of the QOL-CS questionnaire domains was assessed using Cronbach's alpha after reverse scoring of relevant items and calculation of domain scores. The obtained coefficients were comparable to those reported in the original validation study by B.R. Ferrell et al. (2003) in a cohort of cancer survivors [15, 16].

In the original study, the authors reported high internal consistency for the overall QOL score ($\alpha = 0.93$), as well as high Cronbach's alpha values for the individual domains: physical ($\alpha = 0.77$), psychological ($\alpha = 0.89$), social ($\alpha = 0.81$) and spiritual well-being ($\alpha = 0.71$).

In the present study, the overall QOL-CS score demonstrated high reliability ($\alpha = 0.91$), consistent with the original validation findings and confirming the robustness of the instrument.

Internal consistency indices for the physical ($\alpha = 0.88$) and psychological well-being ($\alpha = 0.91$) domains indicated high reliability and were comparable to those reported in the original validation study. In contrast, Cronbach's alpha values for the social ($\alpha = 0.49$) and spiritual ($\alpha = 0.29$) domains were lower. Similar reductions in internal consis-

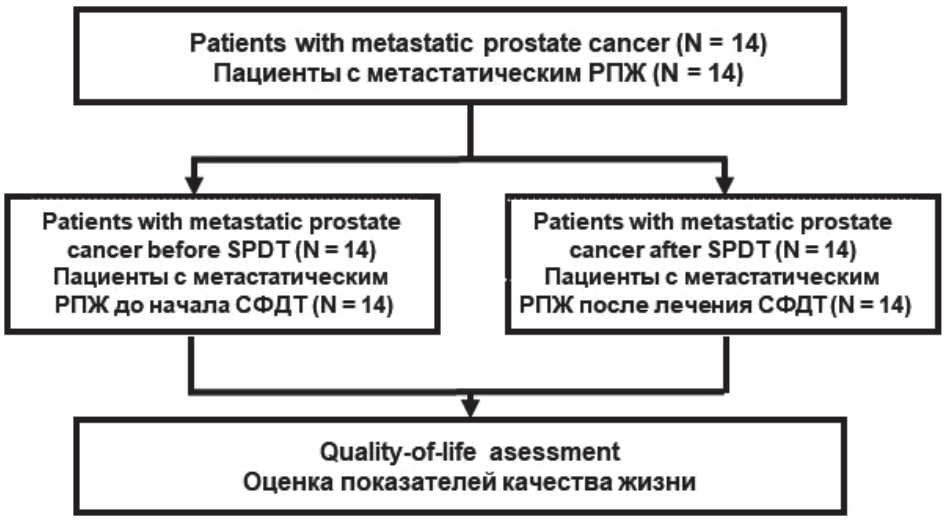

Рис. 1. Дизайн исследования.
Fig. 1. Study design.

tency have been reported in subsequent studies and are commonly attributed to the conceptual heterogeneity of these scales, which encompass diverse aspects of social adaptation and spiritual experience.

Overall, the findings confirm the psychometric reliability of the QOL-CS questionnaire and are consistent with those of the original validation study.

Normality of quantitative variables distribution was assessed using the Shapiro-Wilk test separately for each QOL domain and the overall score before and after treatment. According to analysis, no statistically significant deviations from normality were observed for any QOL domain (physical, psychological, social, and spiritual) or for the total QOL-CS score ($p > 0.05$) These findings indicate no evidence to reject the assumption of normal distribution of the data (Table 1).

Таблица 1
Проверка гипотезы о нормальности распределения показателей качества жизни (QOL-CS) до и после лечения (критерий Шапиро-Уилка)

Table 1
Shapiro-Wilk test for normality of quality-of-life (QOL-CS) scores before and after treatment

Домен QOL-CS QOL-CS Domain	W, до лечения W, before treatment (n = 14)	p	W, после лечения W, after treatment (n = 14)	p
Физическое благополучие Physical well-being	0.955	0.647	0.960	0.727
Психологическое благополучие Psychological well-being	0.939	0.404	0.943	0.452
Социальное благополучие Social well-being	0.890	0.080	0.930	0.308
Духовное благополучие Spiritual well-being	0.962	0.753	0.950	0.552
Общий показатель Overall score	0.957	0.677	0.904	0.128

Accordingly, parametric statistical methods were applied for subsequent analysis of differences in QOL scores before and after treatment.

Differences in quality-of-life scores before and after treatment were analyzed using the paired Student's t-test.

Statistically significant improvements were observed in the physical, psychological, and social domains, as well as in the overall QOL-CS score ($p < 0.001$). These differences remained significant after adjustment for multiple comparisons. Large effect sizes were observed across these domains (Cohen's $d > 1.8$), indicating substantial clinical significance.

Changes in spiritual well-being did not reach statistical significance ($p = 0.134$), with a small-to-moderate effect size (Cohen's $d = 0.43$) (Table 2).

Thus, treatment was associated with statistically significant improvements in physical, psychological, social, and overall QOL scores, indicating the clinical relevance of these changes. No statistically significant changes were observed in spiritual well-being. Overall, these findings support the effectiveness of treatment in improving key aspects of patients' quality of life.

Discussion

In the present study, QOL in patients with metastatic prostate cancer was comprehensively assessed before and after SPDT using the QOL-CS questionnaire. The findings confirm the instrument's psychometric reliability and sensitivity to clinically meaningful treatment-related changes,

Таблица 2
Сравнение показателей качества жизни (QOL-CS) до и после лечения (парный t-критерий Стьюдента, с коррекцией Бонферрони)

Table 2
Comparison of QOL-CS scores before and after treatment using paired Student's t-tests with Bonferroni correction

Домен QOL-CS QOL-CS Domain	n	M, до лечения M, before treatment	M, после лечения M, after treatment	t-критерий Стьюдента Student's t-test	p	d Коэна Cohen's d
Физическое благополучие Physical well-being	14	2.79	3.48	8.322	<0.001	2.224
Психологическое благополучие Psychological well-being	14	1.69	2.37	8.677	<0.001	2.319
Социальное благополучие Social well-being	14	2.88	3.37	6.790	<0.001	1.815
Духовное благополучие Spiritual well-being	14	5.03	5.22	1.598	0.134	0.427
Общий показатель Overall score	**14**	**3.10**	**3.61**	**8.228**	**<0.001**	**2.199**

supporting its use for longitudinal QOL assessment in this patient population.

Analysis of internal consistency demonstrated high Cronbach's alpha values for the overall QOL-CS score and for the physical and psychological well-being domains, consistent with the original validation findings and indicating item homogeneity. Lower alpha values for the social and spiritual domains are in line with previous reports and likely reflect the conceptual heterogeneity of these scales, which encompass diverse aspects of social adaptation and existential experience, as well as the limited sample size.

Assessment of normality revealed no statistically significant deviations from normal distribution for any domain or for the overall QOL score, either before or after treatment, supporting the use of parametric statistical methods. Application of the paired Student's t-test demonstrated significant improvements in the physical, psychological, social domains, and overall QOL-CS score. These changes were accompanied by large effect sizes, indicating their clinical relevance.

In contrast to the aforementioned domains, changes in spiritual well-being did not reach statistical significance, which may reflect the relative stability of spiritual and existential aspects of quality of life and their lower sensitivity to short-term clinical interventions. Overall, the findings support the effectiveness of the treatment in improving the main dimensions of patients' quality of life and underscore the importance of incorporating QOL assessment into the comprehensive evaluation of treatment outcomes.

Conclusion

The study demonstrated that SPDT in patients with metastatic prostate cancer was associated with statistically and clinically significant improvements in QOL scores, particularly in the physical, psychological, social, and overall QOL-CS domains. The magnitude of these effects supports their clinical relevance.

The QOL-CS questionnaire demonstrated high psychometric reliability and sensitivity to clinically meaningful changes, supporting its use for assessing QOL dynamics during treatment. The absence of statistically significant changes in spiritual well-being highlights the relative stability of this domain and underscores the need for further investigation using additional or alternative instruments.

These findings underscore the importance of incorporating QOL assessment into the overall evaluation of treatment outcomes in patients with advanced prostate cancer and may help optimize therapeutic and supportive interventions aimed at improving QOL in this population.

REFERENCES

1. Petrov S.B., Rakul S.A. Prostate cancer and quality of life. *Onkourologiya*, 2006, Vol. 4, pp. 9-14. doi: 10.17650/1726-9776-2006-2-4-9-14
2. Ionova T.I., Novik A.A., Sukhonos Yu.A. The concept of quality of life in oncology patients. *Onkologiya*, 2000, Vol. 2 (1-2), pp. 25-28.
3. Kaplan R.M., Bush J.W. Health-related quality of life measurement for evaluation research and policy analysis. *Health Psychology*, 1982, Vol. 1, pp. 61-80. doi: 10.1037/0278-6133.1.1.61.
4. Benberin V.V., Shanazarov N.A., Rakhimzhanova R.I. et al. Assessment of quality of life in patients with cutaneous breast cancer metastases. *Methodological guidelines*, 2021. ISBN 978-601-305-439-1.
5. World Health Organization. WHOQOL: Measuring quality of life. (WHO/HIS/HSI Rev.2012.03), 2012. – Geneva.
6. American Society of Clinical Oncology. Outcomes of cancer treatment for technology assessment and cancer treatment guidelines. *Journal of Clinical Oncology*, 1996, Vol. 14(3), pp. 671-679.
7. Novik A.A., Ionova T.I. Guide to quality-of-life research in medicine. *Sankt-Peterburg. Neva*, OLMA-PRESS, 2002, pp. 321.
8. Escobar A., Trujillo-Martin M., Rueda A. et al. Cross-cultural adaptation, reliability and validity of the Spanish version of the Quality of Life in Adult Cancer Survivors (QLACS) questionnaire: application in a sample of short-term survivors. *Health Quality Life Outcomes*, 2015, Vol. 13, pp. 182. doi: 10.1186/s12955-015-0378-2.
9. Zhuravlev A.A., Shkolnik M.I., Bogomolov O.A. et al. Quality-of-life assessment in prostate cancer patients using the FACT-P questionnaire: Linguistic and cultural adaptation of the Russian version. *Science and Innovations in Medicine*, 2025, Vol. 10(4), pp. 315-320. doi: 10.35693/2500-1388-2025-10-4-315-320
10. Muslov S.A., Lapshikhina E.A., Maslak A.A. et al. Quality-of-life assessment in prostate cancer patients using the EORTC QLQ-PR25 questionnaire based on classical and modern test theories. *Effective Pharmacotherapy*, 2022, Vol. 18(27), pp. 6-24. doi: 10.33978/2307-3586-2022-18-27-6-24

ЛИТЕРАТУРА

1. Петров С.Б., Ракул С.А. Рак предстательной железы и качество жизни // Онкоурология. – 2006. – № 4. – С. 9-14. doi.org/10.17650/1726-9776-2006-2-4-9-14.
2. Ионова Т.И., Новик А.А., Сухонос Ю.А. Понятие качества жизни больных онкологического профиля // Онкология. – 2000. – Т. 2, № 1-2. – С. 25-28.
3. Kaplan R.M., Bush J.W. Health-related quality of life measurement for evaluation research and policy analysis // Health. Psychol. – 1982. – Vol. 1. – P. 61-80. doi: 10.1037/0278-6133.1.1.61.
4. Бенберин В.В., Шаназаров Н.А., Рахимжанова Р.И. и др. Оценка качества жизни пациентов с кожными метастазами рака молочной железы (методические рекомендации) // 2021. – ISBN 978-601-305-439-1.
5. World Health Organization. WHOQOL: Measuring quality of life (WHO/HIS/HSI Rev.2012.03) // 2012. – Geneva.
6. American Society of Clinical Oncology. Outcomes of cancer treatment for technology assessment and cancer treatment guidelines // Journal of Clinical Oncology. – 1996. – Vol. 14(3). – P. 671-679.
7. Новик А.А., Ионова Т.И. Руководство по исследованию качества жизни в медицине // СПб.: Нева. – ОЛМА-ПРЕСС. – 2002. – С. 321.
8. Escobar A., Trujillo-Martin M., Rueda A. et al. Cross-cultural adaptation, reliability and validity of the Spanish version of the Quality of Life in Adult Cancer Survivors (QLACS) questionnaire: application in a sample of short-term survivors. // Health Qual Life Outcomes. 2015. – Vol. 13. – P. 182. doi: 10.1186/s12955-015-0378-2.
9. Журавлев А.А., Школьник М.И., Богомолов О.А. и др. Оценка качества жизни больных раком предстательной железы с помощью опросника FACT-P: языковая и культурная адаптация русскоязычной версии // Наука и инновации в медицине. – 2025. – Т. 10, № 4. – С. 315-320. doi: 10.35693/2500-1388-2025-10-4-315-320.
10. Муслов С.А., Лапшихина Е.А., Маслак А.А. и др. Исследование качества жизни больных раком предстательной железы с помощью опросника EORTC QLQ-PR25 на основе классической и современной теорий тестирования // Эффективная фармакотерапия. – 2022. – Т. 18, № 27. – С. 6-24. doi: 10.33978/2307-3586-2022-18-27-6-24.

11. Rakul S.A., Petrov S.B., Ivanova M.D. et al. Validation of the universal quality-of-life questionnaire for patients with prostate cancer. *Onkourologiya*, 2009, Vol. 5(2), pp. 64-74. doi: 10.17650/1726-9776-2009-5-2-64-74.
12. Grant M., Padilla G.V., Ferrell B.R. et al. Assessment of quality of life with a single instrument. *Seminars in Oncology Nursing*, 1990, Vol. 6(4), pp. 260-270. doi: 10.1016/0749-2081(90)90028-4.
13. Muslov S.A., Maev I.V., Arutyunov S.D. et al. Measurement of quality-of-life indicators in medicine based on classical and modern theory. *Practical Medicine*, 2023, pp. 216. ISBN 978-5-98811-756-8.
14. Van Dis F.W., Mols F., Vingerhoets A.J. et al. A validation study of the Dutch version of the Quality of Life-Cancer Survivor (QOL-CS) questionnaire in a group of prostate cancer survivors. *Qual Life Res*, 2006, Vol. 15(10), pp. 1607-1612. doi: 10.1007/s11136-006-0015-y.
15. Ferrell B.R, Virani R., Smith S. et al. The Role of Oncology Nursing to Ensure Quality Care for Cancer Survivors: A Report Commissioned by the National Cancer Policy Board and Institute of Medicine. *Oncology Nursing Forum*, 2003, Vol. 30(1), pp. E1-11 doi: 10.1188/03.ONF.E1-E11.
16. Ferrell B.R., Dow K.H., Grant M. Measurement of the quality of life in cancer survivors. *Qual Life Res*, 1995, Vol. 4(6), pp. 523-531. doi: 10.1007/BF00634747.
17. Hann D.M., Jacobsen P.B., Azzarello L.M. et al. Measurement of fatigue in cancer patients: development and validation of the Fatigue Symptom Inventory. *Qual Life Res*, 1998, Vol. 7(4), pp. 301-310. doi: 10.1023/a:1026475015471.
18. Maksimova M.I., Vasiliev A.O., Govorov A.V. et al. Quality of life and its predictors in prostate cancer patients. *Health of the Megalopolis*, 2025, Vol. 6(3), pp. 109-118. doi: 10.47619/2713-2617.zm.2025.v.6i3p2;109-118.
19. Maksimova M.I., Vasiliev A.O., Govorov A.V. New vectors in quality-of-life assessment in prostate cancer patients. *Voprosy onkologii*, 2025, Vol. 71(S3), pp. 656-657.
20. Zhuravlev A.A., Sukhanova T.V., Kneev A.Yu. Quality-of-life assessment in prostate cancer patients under active surveillance. *St. Petersburg Scientific Readings - 2024: Proceedings of the X International Youth Medical Congress. Saint Petersburg: Pavlov University,* 2024, pp. 162-163.
21. Ponomareva I.V., Kuznetsova A.I., Vazhenin A.V. et al. Rehabilitation potential in prostate cancer patients: psychological aspects. *Permskiy meditsinskiy zhurnal*, 2024, Vol. 41(2), pp. 19-32. doi: 10.17816/pmj41219-32.
22. Bessmertnykh D.V., Pavlova T.V. Quality of life in prostate cancer patients. *Nauchnye vedomosti Belgorodskogo gosudarstvennogo universiteta. Seriya: Meditsina. Farmatsiya*, 2009, Vol. 12(67), pp. 68-70.
23. Pavlova T.V., Bessmertnykh D.V., Pavlov I.A. Prostate cancer: treatment methods and quality of life. *Vrach*, 2014, Vol. 7, pp. 55-56.
24. Suchalkin E.B., Pavlova T.V. Analysis of quality of life in men with prostate pathology in the geriatric continuum. *Sovremennye problemy zdravookhraneniya i meditsinskoy statistiki*, 2024, Vol. 2, pp. 520-530.
25. Pavlova T.V., Bessmertnykh D.V., Pavlov I.A. Modern aspects of treatment and quality of life in elderly prostate cancer patients. *Nauchnye vedomosti Belgorodskogo gosudarstvennogo universiteta. Seriya: Meditsina. Farmatsiya*, 2010, Vol. 22-1(93), pp. 67-70.
26. Pomeshkin V.E., Shamin M.V., Pomeshkin E.V. Quality of life and psychoemotional status in comorbid patients with newly diagnosed prostate cancer. *Proceedings of the 8th Scientific and Practical Conference of Urologists of the Northwestern Federal District. – St. Petersburg: Eco-Vector*, 2025, pp. 57.
27. Golovachev S.V., Makimbetov E.K. Quality of life in prostate cancer patients. *Vestnik Tambovskogo universiteta. Seriya: Estestvennye i tekhnicheskie nauki*, 2017, Vol. 22(2), pp. 257-260.

11. Ракул С.А., Петров С.Б., Иванова М.Д. и др. Апробация «Универсального опросника качества жизни больных раком предстательной железы» // Онкоурология. – 2009. – Т. 5, № 2. – С. 64-74. doi: 10.17650/1726-9776-2009-5-2-64-74.
12. Grant M., Padilla G.V., Ferrell B.R. et al. Assessment of quality of life with a single instrument // Seminars in Oncology Nursing – 1990. – Vol. 6(4). – P. 260-270. doi: 10.1016/0749-2081(90)90028-4.
13. Муслов С.А., Маев И.В., Арутюнов С.Д. и др. Измерение показателей качества жизни в медицине на основе классической и современной теории // Москва: Общество с ограниченной ответственностью «ПРАКТИЧЕСКАЯ МЕДИЦИНА» – 2023. – 216 с. – ISBN 978-5-98811-756-8.
14. van Dis F.W., Mols F., Vingerhoets A.J. et al. A validation study of the Dutch version of the Quality of Life-Cancer Survivor (QOL-CS) questionnaire in a group of prostate cancer survivors // QualLifeRes. – 2006. – Vol. 15(10). – P. 1607-1612. doi: 10.1007/s11136-006-0015-y.
15. Ferrell B.R, Virani R., Smith S. et al. The Role of Oncology Nursing to Ensure Quality Care for Cancer Survivors: A Report Commissioned by the National Cancer Policy Board and Institute of Medicine // Oncology Nursing Forum. – 2003. – Vol. 30(1). – P. E1-11. doi: 10.1188/03.ONF.E1-E11.
16. Ferrell B.R., Dow K.H., Grant M. Measurement of the quality of life in cancer survivors // Qual Life Res. – 1995. – Vol. 4(6). – P. 523-31. doi: 10.1007/BF00634747.
17. Hann D.M., Jacobsen P.B., Azzarello L.M. et al. Measurement of fatigue in cancer patients: development and validation of the Fatigue Symptom Inventory // Qual Life Res. – 1998. – Vol. 7(4). – P. 301-310. doi: 10.1023/a:1026475015471.
18. Максимова М.И., Васильев А.О., Говоров А.В. и др. Оценка качества жизни и его предикторы у больных раком предстательной железы // Здоровье мегаполиса. – 2025. – Т. 6, № 3. – С. 109-118. doi: 10.47619/2713-2617.zm.2025.v.6i3p2;109-118.
19. Максимова М.И., Васильев А.О., Говоров А.В. Новые векторы оценки качества жизни больных раком предстательной железы // Вопросы онкологии. – 2025. – Т. 71(S3). – С. 656-657.
20. Журавлев А.А., Суханова Т.В., Кнеев А.Ю. Оценка качества жизни больных раком предстательной железы, находящихся на активном наблюдении // Санкт-Петербургские научные чтения – 2024: сборник тезисов X международного молодежного медицинского конгресса, Санкт-Петербург, 04–06 декабря 2024 года. – Санкт-Петербург: Первый Санкт-Петербургский государственный медицинский университет им. академика И.П. Павлова. – 2024. – С. 162-163.
21. Пономарева И.В., Кузнецова А.И., Важенин А.В. и др. Реабилитационный потенциал у больных раком предстательной железы: психологический аспект // Пермский медицинский журнал. – 2024. – Т. 41, № 2. – С. 19-32. doi: 10.17816/pmj41219-32.
22. Бессмертных Д.В., Павлова Т.В. Оценка качества жизни больных раком предстательной железы // Научные ведомости Белгородского государственного университета. Серия: Медицина. Фармация. – 2009. – № 12(67). – С. 68-70.
23. Павлова Т.В., Бессмертных Д.В., Павлов И.А. Рак предстательной железы: методы лечения и качество жизни // Врач. – 2014. – № 7. – С. 55-56.
24. Сучалкин Е.Б., Павлова Т.В. Анализ качества жизни мужчин с патологией предстательной железы в гериатрическом континууме // Современные проблемы здравоохранения и медицинской статистики. – 2024. – № 2. – С. 520-530.
25. Павлова Т.В., Бессмертный Д.В., Павлов И.А. Современные аспекты лечения и оценка качества жизни пожилых больных раком предстательной железы // Научные ведомости Белгородского государственного университета. Серия: Медицина. Фармация. – 2010. – № 22-1(93). – С. 67-70.
26. Помешкин В.Е., Шамин М.В., Помешкин Е.В. Качество жизни и психоэмоциональный статус у коморбидного пациента с впервые выявленным раком предстательной железы // Материалы 8-й Научно-практической конференции урологов Северо-Западного федерального округа: Материалы конференции, Санкт-Петербург, 10–11 апреля 2025 года. – Санкт-Петербург: ООО "Эко-Вектор", 2025. – С. 57.
27. Головачев С.В., Макимбетов Э.К. Качество жизни пациентов с раком предстательной железы // Вестник Тамбовского университета. Серия: Естественные и технические науки. – 2017. – Т. 22, № 2. – С. 257-260.

28. Sosnovsky I.B. Prostate cancer and quality of life. *Obshchestvennoe zdorovye i zdravookhranenie*, 2009, Vol. 1(21), pp. 109-111.
29. Maksimova M.I., Vasiliev A.O., Govorov A.V. et al. New directions in quality-of-life assessment in prostate cancer patients. *Proceedings of the Research Institute for Healthcare Organization and Medical Management. Moscow: Research Institute for Healthcare Organization and Medical Management*, 2025, pp. 87-96.
30. Nam M., Seo S.S., Jung S. et al. Comparable plasma lipid changes in patients with cervical neoplasia. *J Proteome Res*, 2021, Vol. 20(1), pp. 740-750. doi: 10.1021/acs.jproteome.0c00640
31. Pak R., Sadykova T., Kaidarova D. et al. The Life Quality and Sexual Function of Women Underwent Radical Hysterectomy. *Asian Pac J Cancer Prev*, 2021, Vol. 22(2), pp.581-589. doi: 10.31557/APJCP.2021.22.2.581.
32. Isaeva N.K. Quality-of-life assessment in prostate cancer patients. *Izvestiya VUZov (Kyrgyzstan)*, 2010, Vol. 1, pp. 62-65.
33. Flegar L., Baunacke M., Buerk B.T. et al. Decision Regret and Quality of Life after Focal Therapy with Vascular-Targeted Photodynamic Therapy (TOOKAD®) for Localized Prostate Cancer. *Urol Int*, 2021, Vol. 105(6), pp. 464-471. doi: 10.1159/000517157.
34. Popovkina O.E., Kapinus V.N., Yaroslavtseva-Isaeva E.V. et al. Development of photodynamic diagnostic and therapy methods at the A.F. Tsyb Medical Radiological Research Centre. *Radiation and Risk (Bulletin of the National Radiation and Epidemiological Registry)*, 2022, Vol. 31(2), pp. 139-150. doi: 10.21870/0131-3878-2022-31-2-139-150.
35. Kleinclauss F., Frontczak A., Balssa L. et al. Vascular targeted photodynamic therapy in low-risk prostate cancer. A literature review. *Prog Urol*, 2019, Vol. 29(8-9), pp. 393-401. doi: 10.1016/j.purol.2019.05.003.
36. Shanazarov N.A., Usenbay M.U., Zinchenko S.V. The impact of systemic photodynamic therapy on quality of life in advanced cancer patients. *High Technologies in Modern Surgery: Proceedings of the III International Scientific and Practical Forum. Kazan: Praktika*, 2025, pp. 26.
37. Chernyshev I.V., Samsonov Yu.V., Zhernov A.A. et al. Quality-of-life assessment in advanced prostate cancer treatment. *Nauchno-meditsinskiy vestnik Tsentralnogo Chernozemya*, 2008, Vol. 34, pp. 62-63.

28. Сосновский И.Б. Рак предстательной железы и качество жизни // Общественное здоровье и здравоохранение. – 2009. – № 1(21). – С. 109-111.
29. Максимова М.И., Васильев А.О., Говоров А.В. и др. Новые векторы оценки качества жизни больных раком предстательной железы // Труды Научно-исследовательского института организации здравоохранения и медицинского менеджмента: Сборник научных трудов. – Москва: Научно-исследовательский институт организации здравоохранения и медицинского менеджмента. – 2025. – С. 87-96.
30. Nam M., Seo S.S., Jung S. et al. Comparable plasma lipid changes in patients with high-grade cervical intraepithelial neoplasia and patients with cervical cancer // J Proteome Res. – 2021. – Vol. 20(1). – P. 740–750. doi: 10.1021/acs.jproteome.0c00640
31. Pak R., Sadykova T., Kaidarova D. et al. The Life Quality and Sexual Function of Women Underwent Radical Hysterectomy // Asian Pac J Cancer Prev. – 2021. – Vol. 22(2). – P. 581-589. doi: 10.31557/APJCP.2021.22.2.581.
32. Исаева Н.К. Оценка качества жизни у больных раком предстательной железы // Известия ВУЗов (Кыргызстан). – 2010. – № 1. – С. 62-65.
33. Flegar L., Baunacke M., Buerk B.T. et al. Decision Regret and Quality of Life after Focal Therapy with Vascular-Targeted Photodynamic Therapy (TOOKAD®) for Localized Prostate Cancer // Urol Int. – 2021. – Vol. 105(6). – P. 464-471. doi: 10.1159/000517157.
34. Поповкина О.Е., Капинус В.Н., Ярославцева-Исаева Е.В. и др. Развитие методов фотодинамической диагностики и терапии в МРНЦ им. А.Ф. Цыба // Радиация и риск (Бюллетень Национального радиационно-эпидемиологического регистра). – 2022. – Т. 31, № 2. – С. 139-150. doi: 10.21870/0131-3878-2022-31-2-139-150.
35. Kleinclauss F., Frontczak A., Balssa L. et al. Vascular targeted photodynamic therapy in low-risk prostate cancer. A literature review // Prog Urol. – 2019. – Vol. 29(8-9). – P. 393-401. doi: 10.1016/j.purol.2019.05.003.
36. Шаназаров Н.А., Усенбай М.У., Зинченко С.В. Влияние системной фотодинамической терапии на улучшение качества жизни пациентов с поздними стадиями рака // Высокие технологии в современной хирургии : сборник материалов III Международного научно-практического форума, Казань, 16–17 мая 2025 года. – Казань: ООО Практика. – 2025. – С. 26.
37. Чернышев И.В., Самсонов Ю.В., Жернов А.А. и др. Оценка качества жизни пациентов при лечении распространенных форм рака предстательной железы // Научно-медицинский вестник Центрального Черноземья. – 2008. – № 34. – С. 62-63.

INVESTIGATION OF LIPOFUSCIN PHOTOOXIDATION EXTENT USING VISIBLE SPECTROSCOPY AND FLUORESCENCE LIFETIME IMAGING MICROSCOPY

Morozov P.V.[1,2], **Andreev V.S.**[1,2,3], **Tokarev M.A.**[1], **Yakovleva M.A.**[4,5], **Kostyukov A.A.**[4,5], **Feldman T.B.**[4,5], **Kuzmin V.A.**[4], **Ostrovsky M.A.**[4,5], **Goltsman G.N.**[1,3]
[1]Moscow Pedagogical State University, Moscow, Russia
[2]LLC "Supconductor Nanotehnology", Moscow, Russia
[3]National Research University Higher School of Economics, Moscow, Russia
[4]N.M. Emanuel Institute of Biochemical Physics RAS, Moscow, Russia
[5]M.V. Lomonosov Moscow State University, Moscow, Russia

Abstract

The study is devoted to the development of an early preclinical method for the diagnosis of age-related macular degeneration using time-correlated fluorescence microscopy and visible spectroscopy data for the analysis of fluorescence lifetimes and spectra for lipofuscin granules. Lipofuscin granules were obtained from cells of the retinal pigment epithelium of human cadaveric eyes without signs of pathology. To research the fluorescence lifetimes of lipofuscin granules we used the fluorescence excitation method with time-correlated single photon counting technique and the fluorescence lifetimes imaging microscopy (FLIM) method in combination with a superconducting single-photon detector. Photo-oxidized granules were used as a model of age-related macular degeneration. A comparative analysis of the fluorescence lifetimes and spectra before and after photooxidation of lipofuscin granules showed significant differences in the characteristic lifetimes, as well as a shift of the maximum of the fluorescence spectrum to the short-wavelength region. Analysis of the obtained data confirms the possibility of developing a comprehensive method for the spectral and lifetime characterization of fundus autofluorescence. It is necessary to take into account the changes in the contribution of the τ_2 and τ_3 components of the decomposition of the lifetimes curve of fluorescence decay with the longest characteristic lifetime and the shift in the peak of the fluorescence spectrum. This approach will make it possible to determine diagnostic criteria for norm and pathology in the diagnosis of degenerative diseases of the retina and retinal pigment epithelium. Analysis of the data obtained showed that the FLIM method might become promising for the development of an early preclinical method for the diagnosis of age-related macular degeneration of the retina.

Keywords: lipofuscin granule FLIM, fundus autofluorescence (FAF), bisretinoid, fluorescence lifetime, SSPD.

Contacts: Morozov P.V., e-mail: 1pavelmorozov@mail.ru

For citations: Morozov P.V., Andreev V.S., Tokarev M.A., Yakovleva M.A., Kostyukov A.A., Feldman T.B., Kuzmin V.A., Ostrovsky M.A., Goltsman G.N. Investigation of lipofuscin photooxidation extent using visible spectroscopy and fluorescence lifetime imaging microscopy, *Biomedical Photonics*, 2026, vol. 15, no. 2, pp. 18–26. doi: 10.24931/2413–9432–2026–15-2-18-26

ИССЛЕДОВАНИЕ СТЕПЕНИ ФОТООКИСЛЕНИЯ ЛИПОФУСЦИНА МЕТОДАМИ ВИДИМОЙ СПЕКТРОСКОПИИ И ВРЕМЯ-КОРРЕЛИРОВАННОЙ ФЛУОРЕСЦЕНТНОЙ МИКРОСКОПИИ

П.В. Морозов[1,2], **В.С. Андреев**[1,2,3], **М.А. Токарев**[1], **М.А. Яковлева**[4,5], **А.А. Костюков**[4,5], **Т.Б. Фельдман**[4,5], **В.А. Кузьмин**[4], **М.А. Островский**[4,5], **Г.Н. Гольцман**[1,3]
[1]Московский Педагогический Государственный Университет, Москва, Россия
[2]ООО «Сверхпроводниковые нанотехнологии», Москва, Россия
[3]Национальный Университет Высшая Школа Экономики, Москва, Россия
[4]Институт биохимической физики имени Н.М. Эмануэля РАН, Москва, Россия
[5]Московский государственный университет имени М.В. Ломоносова, Москва, Россия

Резюме

Исследование посвящено разработке раннего доклинического метода диагностики возрастной макулярной дегенерации с использованием данных время-коррелированной флуоресцентной микроскопии и видимой спектроскопии при анализе кинетик затухания и спектров флуоресценции для липофусциновых гранул. Липофусциновые гранулы были получены из клеток ретинального пигментного эпителия кадаверных глаз человека без признаков патологии. Для изучения кинетики затухания флуоресценции липофусциновых гранул использовали метод возбуждения флуоресценции с усредненной по образцу корреляцией по времени и метод время-разрешенной флуоресцентной визуализированной микроскопии (FLIM) в сочетании со сверхпроводниковым однофотонным детектором. В качестве модели возрастной макулярной дегенерации использовали фотоокисленные гранулы. Сравнительный анализ кинетик затухания и спектров флуоресценции до и после фотоокисления липофусциновых гранул показал достоверные различия характерных времен жизни, а также смещение максимума спектра флуоресценции в коротковолновую область по мере окисления образцов. Полученные данные позволяют сделать вывод о том, что для разработки метода спектрально-кинетического анализа аутофлуоресценции глазного дна необходимо учитывать изменение вклада τ_2 и τ_3 компонент разложения кинетической кривой затухания флуоресценции τ_m с наибольшим характерным временем жизни и смещение пика спектра флуоресценции. Такой подход позволит определить диагностические критерии для нормы и патологии при диагностике дегенеративных заболеваний сетчатки и ретинального пигментного эпителия. Анализ полученных данных показал, что метод FLIM, может стать перспективным для разработки раннего доклинического метода диагностики возрастной макулярной дегенерации сетчатки.

Ключевые слова: липофусциновая гранула, FLIM, аутофлуоресценция глазного дна (FAF), бисретиноид, кинетика затухания флуоресценции, SSPD.

Контакты: Морозов П.В., e-mail: 1pavelmorozov@mail.ru

Для цитирования: Морозов П.В., Андреев В.С., Токарев М.А., Яковлева М.А., Костюков А.А., Фельдман Т.Б., Кузьмин В.А., Островский М.А., Гольцман Г.Н. Исследование степени фотоокисления липофусцина методами видимой спектроскопии и время-коррелированной флуоресцентной микроскопии // Biomedical Photonics. – 2026. –Т. 15, № 2. – С. 18–26. doi: 10.24931/2413–9432–2026–15-2-18-26

Introduction

One of the most common causes of vision loss in the elderly is age-related macular degeneration (AMD) [1]. The development of AMD is accompanied by pathological changes in the retinal pigment epithelium (RPE) and, ultimately, by the death of retinal photoreceptor cells [1, 2]. Currently, the disease is considered practically incurable; therefore, an important task is the earliest possible detection of AMD with the aim of taking timely protective and preventive measures that can slow the progression of this severe ocular pathology and preserve vision and a good quality of life for the patient for many years. In this regard, particular attention is paid to the development of methods for early, preclinical diagnosis of degenerative diseases of the retina and RPE, in particular, the improvement and expansion of the diagnostic capabilities of the existing modern non-invasive diagnostic method – fundus autofluorescence [3, 4]. This method makes it possible to study pathological areas of the fundus in considerable detail when investigating, for example, early manifestations of AMD and its progression. The method of recording fundus autofluorescence allows one to assess the state of RPE cells in patients with AMD, choose a treatment strategy, and make a prognosis regarding the development of the disease. It is one of the most sensitive modern methods for studying early changes in the retina/RPE complex [5], which provides an opportunity for the prevention of early stages of the disease, as well as for qualitative objective assessment of treatment effectiveness.

The autofluorescence method is based on obtaining an image created mainly by the intrinsic fluorescence of the so-called "age pigment" – lipofuscin granules (LG), which are formed and accumulate in RPE cells as a result of incomplete lysosomal degradation of phagocytosed photoreceptor cell debris during aging and especially intensely during the development of degenerative diseases of the retina and RPE [6]. The fluorescent properties of LG are mainly determined by the presence in them of conjugates of all-trans retinal, the so-called bisretinoids – bis-retinylidene-ethanolamine (A2E) [7] and other compounds, as well as products of their photooxidation and photodegradation (oxidized bisretinoids) [8].

LG are photosensitive and, upon absorption of light in the visible spectral region, contribute to the formation of reactive oxygen species (ROS) [9]. The source of ROS in LG are bisretinoids. In this case, the bisretinoids themselves are readily oxidized upon interaction with ROS to form oxidized bisretinoids. The fluorescence spectrum of these products shifts to the short-wavelength region [10]. Oxidized bisretinoids are extremely toxic; accumulating in RPE cells, they are capable of damaging vital cellular structures even in the absence of light [11].

It was previously shown that in AMD, an increased content of oxidized bisretinoids is observed compared to the norm [12]. Therefore, the change in fluorescence spectra caused by an increase in the content of oxidized bisretinoids can be considered a diagnostic sign of the early preclinical stage of the disease [13]. Intensive attempts are currently being made to improve the non-invasive diagnostic method of fundus autofluorescence [14]. It is quite obvious that the qualitative and quantitative recording of LG fluorescent characteristics (fluorescence spectra,

fluorescence decay kinetics) can serve as an important prognostic criterion for the development of degenerative diseases of the retina. Experiments on studying the fluorescence decay kinetics of LG using time-correlated single-photon counting have been conducted [12, 15]. The research results showed that oxidized bisretinoids have the longest characteristic fluorescence lifetimes compared to non-oxidized bisretinoids. This result allowed explaining the phenomenon of increased mean fluorescence lifetime in AMD [16, 17]. In other words, an increased content of oxidized bisretinoids in LG of RPE cells leads to an increase in the mean fluorescence lifetime in pathology [13]. However, it should be noted that in the works of Feldman T.B. *et al.* [12] and Yakovleva M.A. *et al.* [15], averaged data of characteristic lifetimes were obtained when studying samples of RPE cell suspension or chloroform extract of LG.

A limitation of the classical method is that it is one-dimensional and does not transmit an image directly, nor can it be used in combination with fast scanning used in modern laser scanning microscopes [18]. To confirm these conclusions, experiments using fluorescence lifetime imaging microscopy (FLIM) are necessary. This method allows obtaining higher accuracy of lifetime or photon registration efficiency at a given number of photons detected from the sample [19], and the result of lifetime measurement does not depend on the concentration of fluorophores and variations in absorption in the studied sample [20]. Using the FLIM method, it is possible to analyze the spatial distribution of characteristic lifetimes in a LG sample before and after their photooxidation.

Simultaneous measurement of decay kinetics and fluorescence spectra of LG provides more data for analysis and, consequently, for improving the method of early diagnosis of eye diseases.

Thus, the aim of this work was a comparative analysis of the fluorescence decay kinetics of individual LGs obtained from RPE of human cadaveric eyes before and after photooxidation, using the FLIM method based on a laser galvanometer scanner and a superconducting single-photon detector (SSPD/SNSPD), with simultaneous measurement of LG fluorescence spectra. In addition, the aim of the research was to visualize the spatial distribution of LG fluorescence lifetimes by the FLIM method to determine the contributions of bisretinoids and oxidized bisretinoids to the overall fluorescence kinetics.

Materials and Methods

Object - Lipofuscin Granules

Human cadaveric eyes were obtained from the Federal State Autonomous Institution "National Medical Research Center "Microsurgery of the Eye" named after Academician S.N. Fedorov" from more than 100 donors in the age group 50-75 years without signs of pathology, from the thanatology departments of the Moscow Bureau of Forensic Medical Examination [10], according to the method described in the work of Boulton M. *et al.* [9]. Human cadaveric eyes were obtained within 10 hours after donor death after removal of the cornea for transplantation. Each cadaveric eye was carefully examined by an ophthalmologist. Analysis and screening selection of donor material were carried out according to clinical signs. The study of samples was carried out under subdued lighting.

Setup for Simultaneous Measurement of Fluorescence Spectra and Fluorescence Lifetimes

To simultaneously measure fluorescence spectra and fluorescence decay kinetics, a radiation collection scheme from a quartz cuvette placed in a holder was used: optical fibers for radiation collection were installed on two sides of the cuvette, one connected to the SSPD, the signal from which, together with the laser synchronization signal, was connected to a Time Tagger Ultra device for time-correlated counting and measurement of decay kinetics (Swabian, Germany), the second fiber was connected to an ATP5020P spectrometer (OptoSky, China). 500 LP filters (Chroma, USA) were installed in front of the optical fibers to cut off the possibility of laser excitation radiation entering. The sample was irradiated with a laser from the third side – perpendicular to the edges of the cuvette, from which the useful signal was collected. To excite fluorescence, a BDL-472-SMC laser with a wavelength of 473 nm and a picosecond pulse repetition rate of 50 MHz was used; the average laser power did not exceed 57 μW/s. The experimental setup is shown in Fig. 1.

Superconducting Single-Photon Detector

The manufacturing method of the SSPD is described in the article by Smirnov K. *et al.* [21]. The active area of the detector was 15×15 μm^2, and the detector was combined with a single-mode fiber SMF-28e (Corning, USA). The dependence of dark counts and detection system efficiency was measured using an SC-PRO 7 supercontinuum laser [YSL Photonics, China]. The method for measuring the efficiency of the optical system consists of measuring the number of detector counts compared to the incident radiation power on the detector [22]. The measured detection efficiency of the system was more than 60% in a wide wavelength range of 500-950 nm. The main advantages of the SSPD are low dark count rate (up to 0.1 counts/s) [23], low jitter [22], and high quantum efficiency [21].

Visualization of the Spatial Distribution of Fluorescence Lifetimes

During measurements by the FLIM method, a scanning system based on a DCS-120 confocal galvanometer scanner (Becker & Hickl, Germany) with a Zeiss AXIO Observer A1 microscope (Zeiss, Germany), with objectives (x20, x40, x60), and a picosecond diode laser BDL-472-SMC were used; time-correlated counting was performed using an SPC-150NX board. The optical system of the laser confocal galvanometer scanner was modified to interface with the

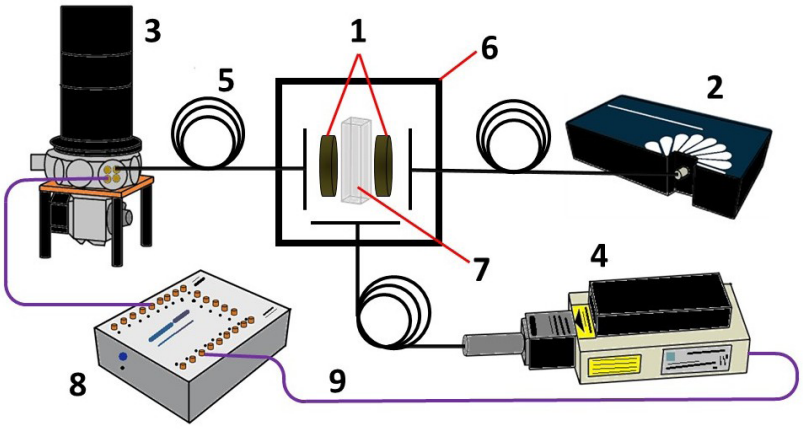

Рис. 1. Схема одновременного измерения спектров флуоресценции и времен жизни флуоресценции: 1 – фильтры (500 LP); 2 – спектрометр, 3 – SSPD криостат; 4 – лазер 473 нм; 5 – оптическое волокно; 6 – черный ящик; 7 – кварцевая кювета с суспензией ЛГ; 8 – время-разрешающая электроника Swabian; 9 – коаксиальный кабель.
Fig. 1. Scheme for simultaneous measurements of fluorescence spectra and lifetimes: 1 – filters (500 LP); 2 – spectrometer; 3 – cryostat with SSPD; 4 – laser 473 nm; 5 – optical fiber; 6 – black Box; 7 – quartz cuvette with suspension of lipofuscin granules; 8 – time tagger Swabian; 9 – coaxial cable.

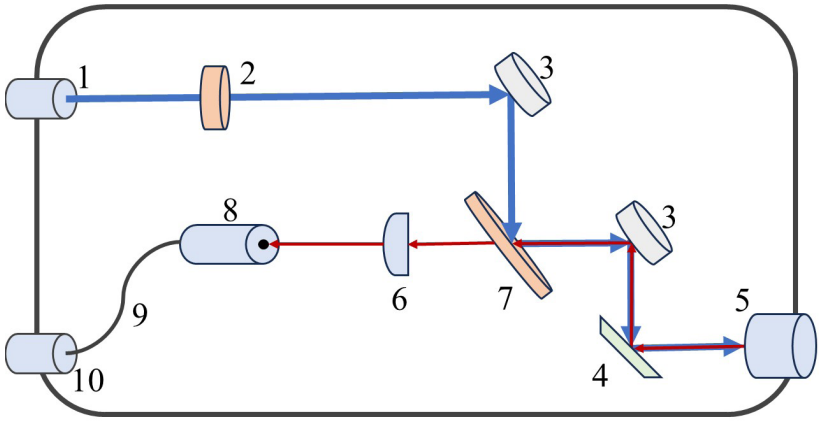

Рис. 2. Оптическая схема установки: 1 – вход лазера; лазерное излучение (синие стрелки); 2 – полосовой фильтр 473+-20 нм; 3 – зеркала; 4 – гальвано-зеркала; 5 – выход на микроскоп, сигнал люминесценции (красные стрелки); 6 – фокусирующая линза; 7 – дихроическое зеркало (500 LP); 8 – коллиматор одномодового оптического волокна; 9 – одномодовое оптическое волокно; 10 – вход на SSPD.
Fig. 2. Optical scanning scheme: 1 – laser In, laser signal (blue arrows); – band pass filter 473+-20 nm; 3 – mirrors; 4 – galvano-mirrors; 5 – to microscope, luminescence signal (red arrows); 6 – focusing lens; 7 – dichroic mirror (500 LP); 8 – SM-fiber coupler; 9 – SM-fiber; 10 – to SSPD.

optical fiber input of a single-photon superconducting detector (Fig. 2) located in an OPRS-SW-70-WB-SMF closed-cycle machine (Scontel, Russia). For FLIM analysis, the LG suspension was applied with a pipette onto the glass of a special bottom Petri dish (Fluorodish, USA) and then placed under the microscope objective, selecting a position with an accumulation of granules in the objective focus.

When measuring the temporal resolution of the entire system, a silver mirror was placed on the objective in the microscope focus. The measurement technique is described in the work of Shcheslavskiy V. *et al*. [22]. The measured temporal resolution (jitter) of the entire system at a wavelength of 473 nm was 76 ps: including the picosecond 473 nm laser (51 ps), the SSPD-based detection system (48 ps), consisting of the detector and electronics, and the SPC-150NX correlation measurement board (2.7 ps).

The laser excitation radiation was directed via the optical scheme to two galvanometer mirrors, which, in turn, performed pixel-by-pixel scanning of the sample in the working plane of the microscope. The fluorescence signal from the LG sample then hit the same mirror system and was redirected via a dichroic mirror to a lens, which focused the signal onto a coupler coupled to the optical fiber input of the detector. A 500 LP long-pass filter (Chroma, USA) was used to register fluorescence in the required range. Using the signal correlation program with pixel scanning, data on the distribution of intensities and fluorescence lifetime components at each point were constructed. The obtained data were processed using the SPCImage program (B&H, Germany).

Photooxidation of Lipofuscin Granules

The LG suspension was placed in a quartz cuvette or in a Petri dish (Fluorodish). LG samples were exposed to a 473 nm laser in CW mode with an average power of 1.5 mW for 1, 3, and 5 minutes. Laser irradiation caused the photooxidation process of LG.

Results

Fluorescent Properties of Lipofuscin Granules Before and After Their Photooxidation

The optical properties of the suspension of native and photooxidized LGs were studied using a setup for simultaneous registration of fluorescence spectra and fluorescence decay kinetics. Fig. 3 presents the fluorescence spectra of LGs; measurements were carried out on an ATP5020P spectrometer (Optosky, China) in the wavelength range of 500-800 nm.

The data in Fig. 3, it follows that upon gradual irradiation with a 473 nm CW laser with an average power of 1.5 mW, the fluorescence spectrum maximum shifts to the short-wavelength region. From the obtained data for photooxidized samples, a redistribution of spectrum intensities in the short-wavelength region of 500-550 nm and in the long-wavelength region of 650-800 nm can be observed. This is due to the oxidation process of LG and the formation of oxidized bis-retinoids, which have a shorter wavelength spectrum compared to the initial sample. It can be seen that in photooxidized LGs, the fluorescence intensity increases in the short-wavelength part of the spectrum and decreases in the long-wavelength part. Spectrum 4 in Fig. 3 reflects the extreme degree of LG photooxidation, after which the spectral shift is no longer observed and does not depend on either irradiation time or laser power – this may indicate that all LGs have transitioned to an oxidized state.

In this work, a detailed, step-by-step study of the dependence of the fluorescence maximum on the LG irradiation time was carried out; Fig. 4 shows a linear dependence of the shift of the fluorescence maximum on the duration of laser irradiation. However, at irradiation times of LG with the laser exceeding 160-170 min, the graph reaches a plateau (Fig. 4), leading to the conclusion of complete photooxidation of the sample.

The spectroscopy data are in good agreement with the results of high-performance liquid chromatography of previous studies [24]; thus, in photooxidized LG samples, there are more oxidized bisretinoids compared to non-oxidized ones. It is the increased content of oxidized bisretinoids in photooxidized LGs that leads to a shift of the fluorescence maximum to the short-wavelength region of the spectrum [9, 11].

Registrarion of Fluorescence Decay Kinetics of Lipofuscin Granules

Measurement of fluorescence lifetimes for the LG suspension was carried out using the time-correlated single-photon counting (TCSPC) method. During the experiment,

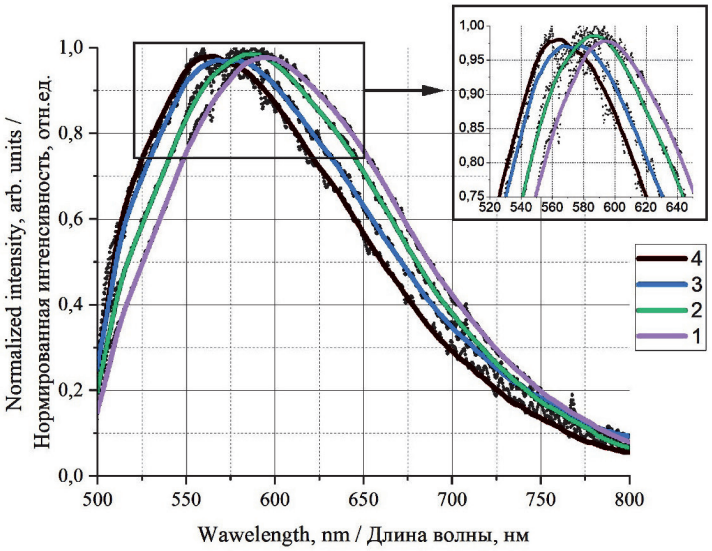

Рис. 3. Нормированные спектры флуоресценции ЛГ в исходном (спектр 1) и фотоокисленном состояниях (спектр 2, 3, 4). Вставка: Увеличенное изображение спектра флуоресценции в области максимума.
Fig. 3. Normalized fluorescence spectra of lipofuscin granules: native (curve 1) and photooxidized (curves 2, 3, 4).
Insert: enlarged image of the fluorescence spectra in the maximum region.

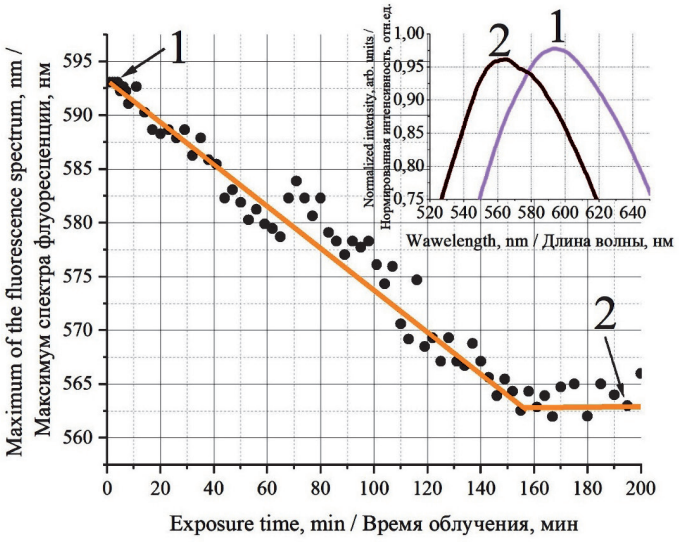

Рис. 4. Смещение максимума в спектрах флуоресценции для суспензии ЛГ от времени облучения CW-лазером (λ_{exc} = 473 нм): кривая 1 – до фотоокисления, кривая 2 – после фотоокисления.
Вставка: Крайние положения максимумов спектра флуоресценци ЛГ: 1 – до облучения, 2 – после облучения и выхода на плато.
Fig. 4. Fluorescence spectra maximum shift of lipofuscin granules in dependence of CW-laser exposition time, (λ_{exc} = 473 nm): curve 1 – native, curve 2 – photooxidized.
Insert: Extreme positions of the fluorescence spectrum maxima of lipofuscin granules: 1 – before irradiation, 2 – after irradiation and reaching a plateau.

the stepwise change in the mean lifetime τ_1 before and after the photooxidation process of LG was recorded. The obtained data are shown in Fig. 5. Signal accumulation using the TCSPC method was carried out for 2 minutes. The excitation laser wavelength was λ_{exc} = 473 nm, with a pulse repetition rate of 50 MHz; fluorescence lifetimes were recorded at wavelengths λ_{reg} >500 nm.

The mean fluorescence lifetime τm was calculated using the formula, within the framework of a three-exponential model [25]:

$$\boldsymbol{\tau}_m = (A_1 \times \tau_1 + A_2 \times \tau_2 + A_3 \times \tau_3)/(A_1 + A_2 + A_3).$$

From Fig. 5, it can be seen that with increasing laser irradiation time, the lifetime for the first component τ1 increases from 226 to 552 ps, which indicates an increase in the content of oxidized bisretinoids in the LG composition, which have a larger proportion of long-lived components $\boldsymbol{\tau}_2$ and $\boldsymbol{\tau}_3$ compared to the non-oxidized sample. Table 1 presents the individual components $\boldsymbol{\tau}_j$ of the fluorescence lifetime decay and the amplitudes ($\mathbf{A}_j$) of each component.

From Table 1, it follows that in photooxidized LGs, the contribution ($\mathbf{A}_3$) of the long-lived component ($\boldsymbol{\tau}_3$) increases, while the contribution of the first component ($\mathbf{A}_1$) with the shortest characteristic time ($\boldsymbol{\tau}_1$) decreases. It is also seen here that the mean fluorescence lifetime ($\boldsymbol{\tau}_m$) increases, which is consistent with literature data [26, 27].

Spatial Distribution of Fluorescence Lifetimes

Using a laser confocal scanner with the FLIM method combined with SSPD, data on the spatial distribution of characteristic fluorescence lifetimes depending on spatial coordinates in samples of native and photooxidized LGs were obtained (Fig. 6).

In contrast to the averaged data obtained from the analysis of fluorescent characteristics for the LG suspension (Fig. 4, Fig. 5), this section presents the results of detailed FLIM imaging of the spatial distribution of characteristic fluorescence lifetimes ($\boldsymbol{\tau}_j$) in LG samples placed on the bottom of a Petri dish (Fluorodish). Such analysis allows for a more detailed study of the lifetime distribution across the LG sample and the creation of a surface lifetime map, and also provides the opportunity to examine individual components of the fluorescence decay kinetic curves in more detail and track changes in the temporal characteristics of LG fluorescence decay during their stepwise photooxidation.

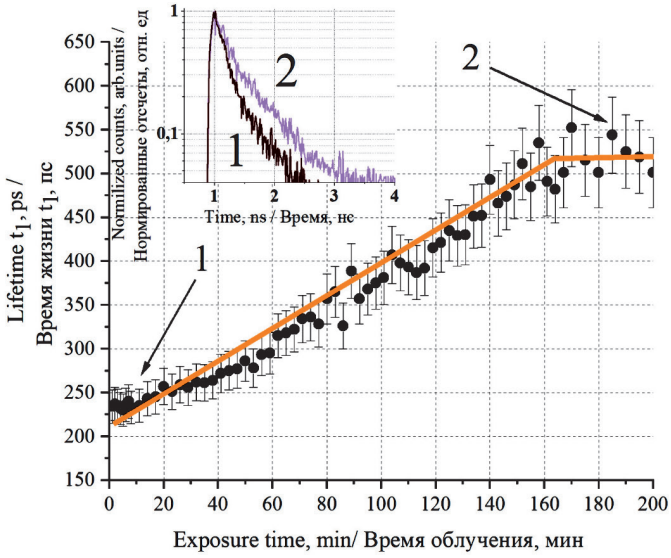

Рис. 5. Зависимость времени жизни первой компоненты флуоресценции τ_1 от времени облучения суспензии ЛГ лазером 473 нм в CW режиме.
Вставка: кинетики затухания флуоресценции для суспензии ЛГ до (кривая затухания 1) и после полного фотоокисления (кривая затухания 2), выхода графика на плато.
Fig. 5. The dependence of the first lifetime τ_1 component of fluorescence on the irradiation time of the suspension of lipofuscin granules with a 473 nm laser in CW mode.
Insert: kinetics of fluorescence lifetimes for a suspension of lipofuscin granules before (curve 1) and after (curve 2) complete photooxidation, the graph reaches a plateau.

Таблица 1
Компоненты разложения τ_j времен жизни флуоресценции для суспензии ЛГ до и после их фотоокисления (λ_{exc} = 473 нм, λ_{reg} > 500 нм), полученные методом TCSPC (из данных рис. 5)

Table 1
Components of the decomposition τ_j of the fluorescence lifetimes for a suspension of lipofuscin granules before and after photooxidation (λ_{exc} = 473 nm, λ_{reg} > 500 nm), obtained by the TCSPC method (from the data of Fig. 5).

Образец Sample	τ_1, пс τ_1, ps	A_1% A_1%	τ_2, пс τ_2, ps	A_2% A_2%	τ_3, пс τ_3, ps	A_3% A_3%	τ_m, пс τ_m, ps	A_2+A_3/A_1 A_2+A_3/A_1
Нативные ЛГ Native LG	226	66	649	27	2012	7	583	0.51
Фотоокисленные ЛГ Photooxidized LG	552	55	1594	31	4106	14	1671	0.82

ЛГ – липофусциновые гранулы, А – амплитуда в % для j-компоненты разложения времени жизни флуоресценции, τ – время жизни флуоресценции для j-компоненты.
LG – lipofuscin granules, A – is the amplitude in % of the j-component of the fluorescence lifetime decomposition, τ – is the fluorescence lifetime for the j-component.

Discussion of Results

Within the framework of the three-exponential model [25], characteristic fluorescence lifetimes were calculated for both experiments based on averaged data obtained by the TCSPC method for the LG suspension (Fig. 5 and Table 1) and the results of FLIM imaging of the spatial distribution of fluorescence lifetimes (Fig. 6, Table 2).

From Table 2, it can be seen that in photooxidized LGs, the contribution of the long-lived component (τ_3) increases, while the contribution of the component (τ_1) with the shortest characteristic time decreases. At the same time, the mean fluorescence lifetime (τ_m) increases, which correlates well with previous studies [15, 26, 27].

Thus, the analysis of fluorescence decay curves of the suspension of native and photooxidized LGs showed that the kinetics of changes in characteristic fluorescence lifetimes obtained on both setups have the same trend: there is an increase in the value of τm, which is the characteristic average lifetime for the fluorescence of oxidized bisretinoids [15, 24], and an increase in the contribution of long-lived (A_2, A_3) components to the fluorescence decay kinetic curve (Tables 1 and 2). Previous studies [15, 24, 26] have shown that it is oxidized bisretinoids that have the longest characteristic fluorescence lifetimes compared to non-oxidized bisretinoids.

A detailed analysis of fluorescence lifetimes for native LGs and photooxidized ones shows that for searching numerical criteria of normal and pathological conditions in diagnostics using the FLIM method, using only averaged values of characteristic fluorescence lifetimes and their contribution to the overall kinetics can lead to incorrect conclusions, since it is known that LG contain more than 20 types of fluorophores [28, 29, 30] and the distribution of τ_1, τ_2, and τ_3 across the LG sample in the Petri dish can vary within a certain range of decay times; if only the mean lifetime τm is taken into account, this valuable diagnostic information is lost.

Since the FLIM method is considered a promising approach for expanding the capabilities of the fundus autofluorescence method [31], it is necessary to define clear criteria for normal and pathological conditions. This concerns not only the fluorescent properties of the object under study itself, but also the methods of recording and determining numerical criteria. Analyzing the obtained data, it can be concluded that determining the exact values of characteristic fluorescence lifetimes for normal and pathological conditions, and especially their averaged values, can cause certain difficulties. Perhaps this is why the FLIM method has not yet been widely introduced into clinical practice.

Conclusion

In this work, a comparative analysis of the fluorescence decay kinetics of native and photooxidized LGs was carried out using two time-resolved fluorescence microscopy methods: the classical (sample-averaged) time-correlated single-photon counting (TCSPC) method and the fluorescence lifetime imaging (FLIM) method using a

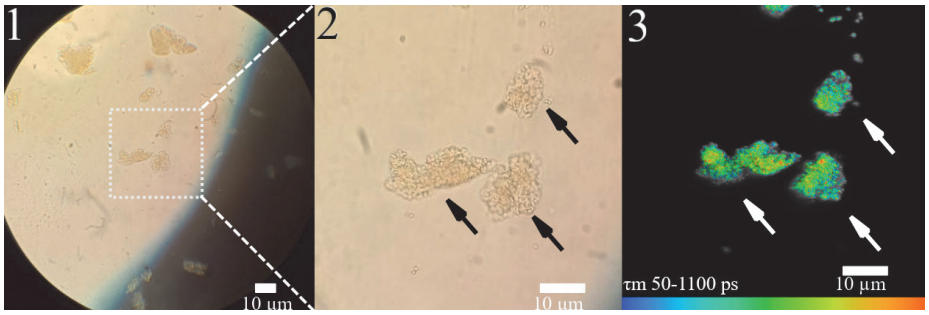

Рис. 6. Изображение ЛГ (1), полученное на микроскопе (объектив 40x, NA 0.8), область сканирования (2) и программно-увеличенное изображение FLIM (3). Разрешение FLIM 512x512 пикс 1024 каналов на пикс.
Fig. 6. Image of lipofuscin granules (1) obtained on a microscope (40x objective NA 0.8), scanning area (2) and programmatically enlarged FLIM image (3). FLIM resolution is 512x512 pixels, 1024 bins per pixel.

Таблица 2
Отдельные компоненты разложения τ_i времен жизни флуоресценции ЛГ до и после их фотоокисления (λ_{exc} = 473 нм, λ_{reg} > 500 нм), полученные методом FLIM (из данных рис. 6 (3))

Table 2
Individual components of decomposition τ_i of the fluorescence lifetimes of lipofuscin granules before and after photooxidation (λ_{exc} = 473 nm, λ_{reg} > 500 nm), obtained by the FLIM method (from the data of Fig. 6(3))

Образец Sample	τ_1, пс τ_1, ps	A_1% A_1%	τ_2, пс τ_2, ps	A_2% A_2%	τ_3, пс τ_3, ps	A_3% A_3%	τ_m, пс τ_m, ps	A_2+A_3/A_1 A_2+A_3/A_1
Нативные ЛГ Native LG	214	68	670	24	2104	8	502	0.47
Фотоокисленные ЛГ Photooxidized LG	567	52	1650	35	4030	13	1412	0.92

ЛГ – липофусциновые гранулы, A – амплитуда в % для j-компоненты разложения времени жизни флуоресценции, τ – время жизни флуоресценции для j-компоненты.
LG – lipofuscin granules, A – is the amplitude in % of the j-component of the fluorescence lifetime decomposition, τ – is the fluorescence lifetime for the j-component.

laser galvanometer scanner for direct measurement of fluorescence with picosecond temporal resolution combined with a superconducting single-photon detector.

Fluorescence analysis and high-performance liquid chromatography [24] showed that irradiation of LG leads to their photooxidation. Photooxidized samples were used as a model of AMD.

The study of fluorescence decay kinetics by two methods on different experimental setups showed good correlation both with each other and with literature data. It was established that during LG photooxidation, there is a change in the contribution of characteristic lifetimes to the overall fluorescence decay kinetics. The contribution with the shortest characteristic time decreases, while the contributions of the intermediate and longest lifetimes increase. This change in parameters occurs due to an increase in the content of oxidized bisretinoids in photooxidized LGs, which, in turn, leads to an increase in the value of the mean fluorescence decay time.

Currently, one of the approaches in the development of spectral methods for analyzing autofluorescence is the measurement of the mean fluorescence decay time using the TCSPC method. It is now beyond doubt that in some visual pathologies, particularly AMD, there is an increase in the mean fluorescence decay time, which allows considering this parameter as a potential criterion for degenerative processes in the retina and RPE during early diagnosis. It should be noted, however, that a universal diagnostic criterion value for normal and pathological conditions has not yet been determined.

FLIM imaging of the spatial distribution of characteristic LG fluorescence lifetimes made it possible to analyze the kinetics of changes in characteristic lifetimes during LG photooxidation across the entire sample surface, in the center and at the periphery (Fig. 6). Considering the fact that the degree of retinoid oxidation in LG can vary, it can be concluded that the FLIM distribution pattern of fluorescence lifetimes will also change. It follows that determining a diagnostic criterion for degenerative processes in the retina and RPE based solely on measuring the mean LG fluorescence decay time τm cannot provide an objective assessment of the degree of pathology progression; changes in fluorescence spectra must be taken into account, as well as the contribution of individual decay components τ_j of fluorescence lifetimes, as was demonstrated in the present study.

This work was supported by grant No. 23-65-10005 from the Russian Science Foundation.

This work was supported by the Ministry of Science and Higher Education of the Russian Federation (project No. 122041400102-9) and as part of a state assignment to Lomonosov Moscow State University.

REFERENCES

1. Rózanowska M.B. Lipofuscin, its origin, properties, and contribution to retinal fluorescence as a potential biomarker of oxidative damage to the retina. *Antioxidants*, 2023, vol. 12, pp. 2111. doi: 10.3390/antiox12122111.
2. Dorey K.C., Wu G., Ebensrein D., Garsd A. Cell loss in the aging retina: relationship to lipofuscin accumulation and macular degeneration. *Invest. Ophthalmol. Vis. Sci*., 1989, vol. 30, pp. 1691–1699. doi: 10.1016/S0161-8105(89)31221-5.
3. Schmitz Valckenberg S., Holz F.G., Fitzke F.W. Perspectives in imaging technologies. In: Holz F.G., Schmitz Valckenberg S., Spaide R.F., Bird A.C. (eds). *Atlas of fundus autofluorescence imaging.* Berlin: Springer, 2007, pp. 331–338. doi: 10.1007/978-3-540-71994-6_19.
4. Sharifzadeh M., Gellermann W. Systems and methods for optical detection of lipofuscin concentration in a subject's eye. *US Patent*, 2011, no. 7,914,147 B2.
5. Holz F.G., Schmitz Valckenberg S., Spaide R.F., Bird A.C. *Autofluorescence imaging.* Berlin, Heidelberg: Springer Verlag, 2007, pp. 342. doi: 10.1007/978-3-540-71994-6.
6. Holz F.G., Schutt F., Kopotz J. Inhibition of lysosomal degradative functions in RPE cells by a retinoid component of lipofuscin. *Invest. Ophthalmol. Vis. Sci*., 1999, vol. 40, pp. 737. PMID: 10067978.
7. Eldred G.E., Lasky M.R. Retinal age pigments generated by self-assembling lysosomotropic detergents. *Nature,* 1993, vol. 361, pp. 724. doi: 10.1038/361724a0.
8. Von Ruckmann A., Fitzke F.W., Bird A.C. In vivo fundus autofluorescence in macular dystrophies. *Arch. Ophthalmol*., 1997, vol. 115, pp. 609–615. doi: 10.1001/archopht.1997.01100150611006.
9. Boulton M., Dontsov A., Jarvis Evans J., Ostrovsky M., Svistunenko D. Lipofuscin is a photoinducible free radical generator. *J. Photochem. Photobiol. B: Biol*., 1993, vol. 19, pp. 201–204. doi: 10.1016/1011-1344(93)07173-3.
10. Yakovleva M.A., Feldman T.B., Krupennikova A.S., Borzenok S.A., Ostrovsky M.A. Fluorofory lipofuscinovych granul, otvetstvennie za autofluorescenciyu glaznogo dna cheloveka. *Izvestiya Akademii Nauk. Seriya Khimicheskaya*, 2010, no. 12, pp. 2252–2260.
11. Sparrow J.R., Vollmer Snarr H.R., Zhou J. et al. A2E epoxides damage DNA in retinal pigment epithelial cells. Vitamin E and other antioxidants inhibit A2E epoxide formation. *J. Biol. Chem*., 2003, vol. 278, no. 20, pp. 18207–18213. doi: 10.1074/jbc.M300155200.

ЛИТЕРАТУРА

1. Rózanowska M.B. Lipofuscin, its origin, properties, and contribution to retinal fluorescence as a potential biomarker of oxidative damage to the retina // Antioxidants. – 2023. – Vol. 12. – P. 2111. doi: 10.3390/antiox12122111.
2. Dorey K.C., Wu G., Ebensrein D., Garsd A. Cell loss in the aging retina: relationship to lipofuscin accumulation and macular degeneration // Invest. Ophthalmol. Vis. Sci. – 1989. – Vol. 30. – P. 1691–1699. doi: 10.1016/S0161-8105(89)31221-5.
3. Schmitz-Valckenberg S., Holz F.G., Fitzke F.W. Perspectives in imaging technologies // In: Holz F.G., Schmitz-Valckenberg S., Spaide R.F., Bird A.C. (Eds). Atlas of fundus autofluorescence imaging. – Berlin: Springer, 2007. – P. 331–338. doi: 10.1007/978-3-540-71994-6_19.
4. Sharifzadeh M., Gellermann W. Systems and methods for optical detection of lipofuscin concentration in a subject's eye // US Patent. – 2011. – No. 7,914,147 B2.
5. Holz F.G., Schmitz-Valckenberg S., Spaide R.F., Bird A.C. Autofluorescence imaging. – Berlin, Heidelberg: Springer-Verlag, 2007. – P. 342. doi: 10.1007/978-3-540-71994-6.
6. Holz F.G., Schutt F., Kopotz J. Inhibition of lysosomal degradative functions in RPE cells by a retinoid component of lipofuscin // Invest. Ophthalmol. Vis. Sci. – 1999. – Vol. 40. – P. 737. PMID: 10067978.
7. Eldred G.E., Lasky M.R. Retinal age pigments generated by self-assembling lysosomotropic detergents // Nature. – 1993. – Vol. 361. – P. 724. doi: 10.1038/361724a0.
8. Von Ruckmann A., Fitzke F.W., Bird A.C. In vivo fundus autofluorescence in macular dystrophies // Arch. Ophthalmol. – 1997. – Vol. 115. – P. 609–615. doi: 10.1001/archopht.1997.01100150611006.
9. Boulton M., Dontsov A., Jarvis-Evans J., Ostrovsky M., Svistunenko D. Lipofuscin is a photoinducible free radical generator // J. Photochem. Photobiol. B: Biol. – 1993. – Vol. 19. – P. 201–204. doi: 10.1016/1011-1344(93)07173-3.
10. Yakovleva M.A., Feldman T.B., Krupennikova A.S., Borzenok S.A., Ostrovsky M.A. Fluorofory lipofuscinovych granul, otvetstvennie za autofluorescenciyu glaznogo dna cheloveka // Izvestiya Akademii Nauk. Seriya Khimicheskaya. – 2010. – No. 12. – P. 2252–2260.
11. Sparrow J.R., Vollmer-Snarr H.R., Zhou J. et al. A2E-epoxides damage DNA in retinal pigment epithelial cells. Vitamin E and other antioxidants inhibit A2E-epoxide formation // J. Biol. Chem. – 2003. – Vol. 278, No. 20. – P. 18207–18213. doi: 10.1074/jbc.M300155200.

12. Feldman T.B., Yakovleva M.A., Arbukhanova P.M., Borzenok S.A., Kononikhin A.S., Popov I.A. et al. Changes in spectral properties and composition of lipofuscin fluorophores from human retinal pigment epithelium with age and pathology. *Anal. Bioanal. Chem*., 2015, vol. 407, pp. 1075–1088. doi: 10.1007/s00216-014-8366-9.
13. Feldman T.B., Yakovleva M.A., Larichev A.V., Arbukhanova P.M., Radchenko A.Sh., Borzenok S.A., Kuzmin V.A., Ostrovsky M.A. Spectral analysis of fundus autofluorescence pattern as a tool to detect early stages of degeneration in the retina and retinal pigment epithelium. *Eye*, 2018, vol. 32, no. 9, pp. 1440–1448. doi: 10.1038/s41433-018-0090-7.
14. Bourauel L., Vaisband M., von der Emde L. et al. Spectral analysis of human retinal pigment epithelium cells in healthy and AMD eyes. *Invest. Ophthalmol. Vis. Sci*., 2024, vol. 65, pp. 10. doi: 10.1167/iovs.65.1.10.
15. Yakovleva M.A., Radchenko A.Sh., Feldman T.B., Kostyukov A.A., Arbukhanova P.M., Borzenok S.A., Kuzmin V.A., Ostrovsky M.A. Fluorescence characteristics of lipofuscin fluorophores from human retinal pigment epithelium. *Photochem. Photobiol. Sci*., 2020, vol. 19, no. 7, pp. 920–930. doi: 10.1039/C9PP00406H.
16. Schweitzer D., Quick S., Schenke S. et al. Comparison of parameters of time resolved autofluorescence between healthy subjects and patients suffering from early AMD. *Ophthalmologe*, 2009, vol. 106, pp. 714–722. doi: 10.1007/s00347-009-1975-4.
17. Sauer L., Gensure R.H., Andersen K.M., Kreilkamp K.M., Hageman G.S., Hammer M., Bernstein P.S. Patterns of fundus autofluorescence lifetimes in eyes of individuals with non-exudative age-related macular degeneration. *Invest. Ophthalmol. Vis. Sci*., 2018, vol. 59, pp. AMD65. doi: 10.1167/iovs.17-23764.
18. Pawley J. (ed.). Handbook of biological confocal microscopy. *3rd ed. Springer*, 2006. doi: 10.1007/978-0-387-45524-2.
19. Philip J.P., Carlsson K. Theoretical investigation of the signal-to-noise ratio in fluorescence lifetime imaging. *J. Opt. Soc. Am. A*, 2003, vol. 20, pp. 368–379. doi: 10.1364/JOSAA.20.000368.
20. Becker W. Fluorescence lifetime imaging — techniques and applications. *J. Microsc*., 2012, vol. 247, iss. 2, pp. 119–136. doi: 10.1111/j.1365-2818.2012.03618.x.
21. Smirnov K., Divochiy A., Vakhtomin Y., Morozov P., Zolotov P., Antipov A., Seleznev V. NbN single photon detectors with saturated dependence of quantum efficiency. *Superconductor Scienceand Technology*, 2018, vol. 31, no. 3, pp. 035011. doi: 10.1088/1361-6668/aaa56a.
22. Shcheslavskiy V., Morozov P., Divochiy A., Vakhtomin Yu., Smirnov K., Becker W. Ultrafast time measurements by time-correlated single photon counting coupled with superconducting single photon detector. *Rev. Sci. Instrum*., 2016, vol. 87, pp. 053117. doi: 10.1063/1.4952963.
23. Wang S., Yin Z.-Q., He D.-Y., Chen W., Wang R.-Q., Ye P., Zhou Y., Fan-Yuan G.-J., Wang F.-X., Zhu Y.-G., Morozov P.V., Divochiy A.V., Zhou Z., Guo G.-C., Han Z.-F. Twin field quantum key distribution over 830 km fibre. *Nature Photonics*, 2022, vol. 16, pp. 154–161. doi: 10.1038/s41566-021-00928-2.
24. Dontsov A., Yakovleva M., Trofimova N., Sakina N., Gulin A., Aybush A., Gostev F., Vasin A., Feldman T., Ostrovsky M. Water-soluble products of photooxidative destruction of the bisretinoid A2E cause proteins modification in the dark. *Int. J. Mol. Sci*., 2022, vol. 23, no. 3, pp. 1534. doi: 10.3390/ijms23031534.
25. Docchio F., Boulton M., Cubeddu R., Ramponi R., Dayhaw-Barker P. Age-related changes in the fluorescence of melanin and lipofuscin granules of the retinal pigment epithelium: a time-resolved fluorescence spectroscopy study. *Photochemistry and Photobiology*, 1991, vol. 54, pp. 247–253. doi: 10.1111/j.1751-1097.1991.tb02013.x.
26. Semenov A.N., Maksimov E.G., Moysenovich A.M., Yakovleva M.A., Tsoraev G.V., Ramonova A.A., Shirshin E.A., Sluchanko N.N., Feldman T.B., Rubin A.B., Kirpichnikov M.P., Ostrovsky M.A. Protein-mediated carotenoid delivery suppresses the photoinducible oxidation of lipofuscin in retinal pigment epithelial cells. *Antioxidants*, 2023, vol. 12, no. 2, pp. 413. doi: 10.3390/antiox12020413.
27. Dysli C., Wolf S., Berezin M.Y., Sauer L., Hammer M., Zinkernagel M.S. Fluorescence lifetime imaging ophthalmoscopy. *Prog. Retin. Eye Res*., 2017, vol. 60, pp. 120–143. doi: 10.1016/j.preteyeres.2017.06.005.
28. Eldred G.E., Katz M.L. Fluorophores of the human retinal pigment epithelium: separation and spectral characterization. *Exp. Eye Res*., 1988, vol. 47, pp. 71–86. doi: 10.1016/0014-4835(88)90055-2.
29. Sparrow J.R., Wu Y., Kim C.Y., Zhou J. Phospholipid meets all-trans retinal: the making of RPE bisretinoids. *J. Lipid Res*., 2009, vol. 51, pp. 247–261. doi: 10.1194/jlr.R000687.
30. Miura Y., Bernstein P., Dysli C., Sauer L., Zinkernagel M. Fluorophores in the eye. In: Zinkernagel M., Dysli C. (eds). Fluorescence Lifetime Imaging Ophthalmoscopy. *Cham: Springer International Publishing*, 2019, pp. 35–48. doi: 10.1007/978-3-030-22878-1_7.
31. Sonntag S., Klein B., Brinkmann R., Grisanti S., Miura Y. Fluorescence lifetime imaging ophthalmoscopy of mouse models of age-related macular degeneration. *Transl. Vis. Sci. Technol*., 2024, vol. 13, pp. 24. doi: 10.1167/tvst.13.1.24.

12. Feldman T.B., Yakovleva M.A., Arbukhanova P.M., Borzenok S.A., Kononikhin A.S., Popov I.A. et al. Changes in spectral properties and composition of lipofuscin fluorophores from human retinal pigment epithelium with age and pathology // Anal. Bioanal. Chem. – 2015. – Vol. 407. – P. 1075–1088. doi: 10.1007/s00216-014-8366-9.
13. Feldman T.B., Yakovleva M.A., Larichev A.V., Arbukhanova P.M., Radchenko A.Sh., Borzenok S.A., Kuzmin V.A., Ostrovsky M.A. Spectral analysis of fundus autofluorescence pattern as a tool to detect early stages of degeneration in the retina and retinal pigment epithelium // Eye. – 2018. – Vol. 32, No. 9. – P. 1440–1448. doi: 10.1038/s41433-018-0090-7.
14. Bourauel L., Vaisband M., Von der Emde L. et al. Spectral analysis of human retinal pigment epithelium cells in healthy and AMD eyes // Invest. Ophthalmol. Vis. Sci. – 2024. – Vol. 65. – P. 10. doi: 10.1167/iovs.65.1.10.
15. Yakovleva M.A., Radchenko A.Sh., Feldman T.B., Kostyukov A.A., Arbukhanova P.M., Borzenok S.A., Kuzmin V.A., Ostrovsky M.A. Fluorescence characteristics of lipofuscin fluorophores from human retinal pigment epithelium // Photochem. Photobiol. Sci. – 2020. – Vol. 19, No. 7. – P. 920–930. doi: 10.1039/C9PP00406H.
16. Schweitzer D., Quick S., Schenke S., Klemm M., Gehlert S., Hammer M., Jentsch S., Fischer J. Comparison of parameters of time-resolved autofluorescence between healthy subjects and patients suffering from early AMD // Ophthalmologe. – 2009. – Vol. 106. – P. 714–722. doi: 10.1007/s00347-009-1975-4.
17. Sauer L., Gensure R.H., Andersen K.M., Kreilkamp K.M., Hageman G.S., Hammer M., Bernstein P.S. Patterns of fundus autofluorescence lifetimes in eyes of individuals with non-exudative age-related macular degeneration // Invest. Ophthalmol. Vis. Sci. – 2018. – Vol. 59. – P. AMD65. doi: 10.1167/iovs.17-23764.
18. Pawley J. (ed.). Handbook of biological confocal microscopy. 3rd. ed. – Springer, 2006. doi: 10.1007/978-0-387-45524-2.
19. Philip J.P., Carlsson K. Theoretical investigation of the signal-to-noise ratio in fluorescence lifetime imaging // J. Opt. Soc. Am. A. – 2003. – Vol. 20. – P. 368–379. doi: 10.1364/JOSAA.20.000368.
20. Becker W. Fluorescence lifetime imaging — techniques and applications // Vol. 247, Is. 2. – 2012. – P. 119–136. doi: 10.1111/j.1365-2818.2012.03618.x.
21. Smirnov K., Divochiy A., Vakhtomin Y., Morozov P., Zolotov P., Antipov A., Seleznev V. NbN single-photon detectors with saturated dependence of quantum efficiency // Superconductor Science and Technology. – 2018. – Vol. 31, No. 3. – P. 035011. doi: 10.1088/1361-6668/aaa56a.
22. Shcheslavskiy V., Morozov P., Divochiy A., Vakhtomin Yu., Smirnov K., Becker W. Ultrafast time measurements by time-correlated single photon counting coupled with superconducting single photon detector // Rev. Sci. Instrum. – 2016. – Vol. 87.– P. 053117. doi: 10.1063/1.4952963.
23. Wang S., Yin Z.-Q., He D.-Y., Chen W., Wang R.-Q., Ye P., Zhou Y., Fan-Yuan G.-J., Wang F.-X.. Zhu Y.-G., Morozov P.V., Divochiy A.V., Zhou Z., Guo G.-C., Han Z.-F. Twin-field quantum key distribution over 830-km fibre // Nature Photonics. – 2022. – Vol. 16. – P. 154–161. doi: 10.1038/s41566-021-00928-2.
24. Dontsov A., Yakovleva M., Trofimova N., Sakina N., Gulin A., Aybush A., Gostev F., Vasin A., Feldman T., Ostrovsky M. Water-soluble products of photooxidative destruction of the bisretinoid A2E cause proteins modification in the dark // Int. J. Mol. Sci. – 2022. – Vol. 23, No. 3. – P. 1534. doi: 10.3390/ijms23031534.
25. Docchio F., Boulton M., Cubeddu R., Ramponi R., Dayhaw-Barker P. Age-related changes in the fluorescence of melanin and lipofuscin granules of the retinal pigment epithelium: a time-resolved fluorescence spectroscopy study // Photochemistry and Photobiology. – 1991. – Vol. 54. – P. 247–253. doi: 10.1111/j.1751-1097.1991.tb02013.x.
26. Semenov A.N., Maksimov E.G., Moysenovich A.M., Yakovleva M.A., Tsoraev G.V., Ramonova A.A., Shirshin E.A., Sluchanko N.N., Feldman T.B., Rubin A.B., Kirpichnikov M.P., Ostrovsky M.A. Protein-mediated carotenoid delivery suppresses the photoinducible oxidation of lipofuscin in retinal pigment epithelial cells // Antioxidants. – 2023. – Vol. 12, No. 2. – P. 413. doi: 10.3390/antiox12020413.
27. Dysli C., Wolf S., Berezin M.Y., Sauer L., Hammer M., Zinkernagel M.S. Fluorescence lifetime imaging ophthalmoscopy // Prog. Retin. Eye Res. – 2017. – Vol. 60. – P. 120–143. doi: 10.1016/j.preteyeres.2017.06.005.
28. Eldred G.E., Katz M.L. Fluorophores of the human retinal pigment epithelium: separation and spectral characterization // Exp. Eye Res. – 1988. – Vol. 47. – P. 71–86. doi: 10.1016/0014-4835(88)90055-2.
29. Sparrow J.R., Wu Y., Kim C.Y., Zhou J. Phospholipid meets all-trans retinal: the making of RPE bisretinoids // J. Lipid Res. – 2009. – Vol. 51. – P. 247–261. doi: 10.1194/jlr.R000687.
30. Miura Y., Bernstein P., Dysli C., Sauer L., Zinkernagel M. Fluorophores in the eye // In: Zinkernagel M., Dysli C. (eds). Fluorescence Lifetime Imaging Ophthalmoscopy. – Cham: Springer International Publishing, 2019. – P. 35–48. doi: 10.1007/978-3-030-22878-1_7.
31. Sonntag S., Klein B., Brinkmann R., Grisanti S., Miura Y. Fluorescence lifetime imaging ophthalmoscopy of mouse models of age-related macular degeneration // Transl. Vis. Sci. Technol. – 2024. – Vol. 13. – P. 24. doi: 10.1167/tvst.13.1.24.

TARGETED DELIVERY OF ANTI-TUBERCULOSIS AND PHOTOSENSITIZING AGENTS TO TUMOR-ASSOCIATED AND *M. TUBERCULOSIS*-INFECTED MACROPHAGES USING NANOCARRIERS

Kochetova A.V., Schwartz Y.S.
Federal state budgetary institution "Novosibirsk tuberculosis research institute" of the Ministry of Health of the Russian Federation, Novosibirsk, Russia

Abstract

Tuberculosis remains a leading cause of mortality among infectious diseases, with drug resistance posing a major challenge to effective treatment. Macrophages serve as the primary cellular reservoir for *M. tuberculosis* (MTB), which upon interaction with this pathogen may acquire a complex phenotype with predominantly anti-inflammatory, immunosuppressive properties and establish a metabolically privileged niche that supports intracellular persistence and survival of MTB. In this review, the phenotype of such macrophages is referred to as M2 (alternatively activated macrophages). This review systematizes current strategies for targeted delivery of anti-tuberculosis agents to MTB-infected macrophages using macromolecular and nanoscale carriers. Passive and active targeting approaches are examined, including the engineering of vector properties through ligand conjugation to M2 macrophage receptors. Strategies for reprogramming macrophage functional phenotype and the development of nanoscale biomimetics are discussed. Special emphasis is placed on targeted delivery of photosensitizers to infected cells for antimicrobial photodynamic therapy. The summarized evidence indicates that combined nanotherapeutic approaches, integrating direct antimicrobial activity with modulation of local immune responses, offer promising strategies for overcoming drug resistance and achieving eradication of MTB.

Key words: Mycobacterium tuberculosis, macrophage, drug resistance, nanoparticle, targeted delivery, antimicrobial photodynamic therapy.

Contacts: Kochetova A.V., e-mail: Ksiomara47@gmail.com

For citations: Kochetova A.V., Schwartz Y.S. Targeted delivery of anti-tuberculosis and photosensitizing agents to tumor-associated and *M. tuberculosis*-infected macrophages using nanocarriers, *Biomedical Photonics*, 2026, vol. 15, no. 2, pp. 27–36. doi: 10.24931/2413–9432–2026–15-2-27-36

НАПРАВЛЕННАЯ ДОСТАВКА ПРОТИВОТУБЕРКУЛЕЗНЫХ И ФОТОСЕНСИБИЛИЗИРУЮЩИХ ПРЕПАРАТОВ В ОПУХОЛЬ-АССОЦИИРОВАННЫЕ И *M. TUBERCULOSIS*-ИНФИЦИРОВАННЫЕ МАКРОФАГИ С ИСПОЛЬЗОВАНИЕМ НАНОНОСИТЕЛЕЙ

А.В. Кочетова, Я.Ш. Шварц
Федеральное государственное бюджетное учреждение «Новосибирский научно-исследовательский институт туберкулеза» Минздрава России, Новосибирск, Россия

Резюме

Туберкулёз остаётся одной из важнейших глобальных проблем общественного здравоохранения, входя в первую десятку основных причин, уносящих человеческие жизни и занимая первое место по смертности среди всех инфекционных заболеваний. При этом наиболее сложной проблемой туберкулеза, как и множества других инфекционных заболеваний, является лекарственная устойчивость возбудителя**.** Основным клеточным резервуаром *M. tuberculosis* (МБТ) являются макрофаги – клетки врожденной иммунной системы, которые во взаимодействии с данным патогеном могут приобретать сложный фенотип с преимущественно антивоспалительными, иммуносупрессивными свойствами и формируют метаболически привилегированную среду, способствующую выживанию и внутриклеточной персистенции МБТ. В настоящем обзоре фенотип таких макрофагов обозначен как М2 (альтернативно активированные макрофаги). В обзоре систематизированы современные подходы к таргетной доставке противотуберкулезных препаратов в МБТ-инфицированные макрофаги с использованием высокомолекулярных и наноразмерных носителей. Рассмотрены

стратегии пассивного и активного таргетирования, включая придание частицам векторных свойств лигандами к рецепторам М2-макрофагов, обсуждаются методы перепрограммирования функционального фенотипа макрофагов и использования наноразмерных биомиметиков; особое внимание уделяется направленной доставке в инфицированные клетки фотосенсибилизаторов для антимикробной фотодинамической терапии. Обобщенные данные свидетельствуют, что комбинированные нанотерапевтические подходы, сочетающие прямой антимикробный эффект с модуляцией локального иммунного ответа, открывают новые возможности для преодоления лекарственной устойчивости и эрадикации МБТ.

Ключевые слова: *Mycobacterium tuberculosis*, макрофаг, М2-поляризация, лекарственная устойчивость, наночастица, таргетная доставка, антимикробная фотодинамическая терапия.

Контакты: Кочетова А.В., e-mail: Ksiomara47@gmail.com

Для цитирования: Кочетова А.В., Шварц Я.Ш. Направленная доставка противотуберкулезных и фотосенсибилизирующих препаратов в опухоль-ассоциированные и *M. tuberculosis*-инфицированные макрофаги с использованием наноносителей // Biomedical Photonics. – 2026. – Т. 15, № 2. – С. 27–36. doi: 10.24931/2413–9432–2026–15-2-27-36

Introduction

Tuberculosis (TB) is an infection caused by *Mycobacterium tuberculosis* (MTB) and remains one of the most serious global public health problems. According to the World Health Organization, in 2023, the incidence of TB was approximately 10.8 million people, with mortality at 1.25 million. The problem is compounded by the increasing spread of multidrug resistance (MDR) of the pathogen: in 2023, approximately 400,000 cases of the disease were caused by MDR strains [1]. The problem of drug resistance is driven by the rate of mutations/acquisition of chemoresistance by MTB, which significantly exceeds the rate of generation of new effective anti-tuberculosis drugs. This fact demonstrates the extreme limitation of the therapeutic potential of traditional approaches to the treatment of MDR-TB and necessitates the development of fundamentally new therapeutic methods.

Macrophages (Mφ) play a central role in the pathogenesis of TB, serving as the first line of defense against the pathogen, but also as the primary host cell within which MTB can persist and proliferate. The interaction between MTB and Mφ determines the outcome of the infection: effective activation of Mφ along the classical pro-inflammatory phenotype leads to the destruction of the bacteria, while activation along the anti-inflammatory M2 (alternatively activated macrophages) phenotype creates conditions for pathogen survival [2]. It is evident that the development of interventions targeting Mφ with persistent MTB could become an effective strategy for overcoming drug resistance of the TB pathogen.

Functional phenotype of macrophages in tuberculosis infection

The nature of the macrophage response to MTB is determined by the influence of the microenvironment and mycobacteria on the functional polarization/formation of the functional phenotype of these cells. Despite the plasticity of the functional phenotype of Mφ, the literature generally uses a binary division into predominantly pro- or anti-inflammatory – M1 (classically activated macrophages) or M2 phenotype – depending on the effector molecules produced by these cells, with corresponding differences in transcriptomic signatures [3, 4]. MTB-induced M1 activation of Mφ is necessary for infection control [5]. Markers of M1-type activation include increased expression of iNOS, STAT-4, CCR7 and high levels of production of pro-inflammatory mediators and cytokines, such as TNF-α, IL-6, IL-12, IL-1β, IL-15, IL-23, CXCL-10, COX-2, reactive oxygen and nitrogen metabolites. Furthermore, in M1-Mφ, the autophagy process is activated, effectively destroying MTB [4, 6]. If MTB are not destroyed by anti-infective factors and survive, they induce a shift in the functional phenotype of Mφ towards M2, which are characterized by the production and expression of large amounts of IL-10, TGF-β, IL-1Ra, CCL17, CCL18, CCL22, Arg-1, fizz-1, Ym-1, COX-1, ALOX, etc. [3]. The functional phenotype of M2-Mφ is oriented towards reducing the biocidal-destructive pro-inflammatory response, tissue regeneration, and fibrogenesis. This phenotype is unable to inhibit the growth and spread of intracellular infections, including MTB [2].

MTB during co-evolution with *Homo sapiens* has developed numerous mechanisms for evading the immune response and manipulating the immune response of Mφ to its advantage [7]. MTB-induced M2 polarization creates a tolerant, privileged intracellular environment for MTB persistence and growth, due to low production of pro-inflammatory and high production of anti-inflammatory mediators and cytokines [3, 6, 8, 9, 10]. Furthermore, the M2 phenotype is associated with fibrosis processes that help maintain the structure of MTB-induced granulomas – the primary tissue niche for MTB persistence in infected Mφ [11, 12].

Targeting MTB-infected Mφ in TB therapy can pursue several goals simultaneously: 1) increasing the effectiveness of therapy through direct killing of MTB in their primary intracellular niche due to increased concentration of anti-tuberculosis chemotherapeutic agents [7, 13]; 2) reducing the side effects of anti-tuberculosis chemotherapeutic agents by lowering their concentration outside the targeting zone; 3) the possibility of overcoming drug resistance through the delivery of anti-tuberculosis agents to Mφ with mechanisms of action alternative to

chemotherapeutic agents [14, 15, 16]; 4) increasing the effectiveness of anti-tuberculosis therapy through the repolarization of Mφ from the M2 to the bactericidal M1 phenotype, induction of autophagy in them, and reprogramming of the immune microenvironment towards pathogen destruction [17].

Targeted delivery of nanoparticles to macrophages: influence of size and charge

Nanoscale carriers are most often used for the effective delivery of therapeutic agents to Mφ. Passive targeting is determined by the ability of Mφ to phagocytose particles of a certain size, surface charge, shape, and hydrophilicity, which affects the dispersion and aggregation of particles, as well as their binding to specific receptors [18, 19]. The surface charge of particles significantly influences cellular uptake and biodistribution of polymeric nanoparticles (NPs). It has been shown that with increasing surface charge (positive or negative), NP uptake by Mφ increased [18, 20]. A high NP charge enhances their phagocytosis by Mφ through opsonization, i.e., adsorption of immunoglobulins A/G/M, C3/C4/C5, complement activation products C3b/C4b/iC3b, laminin, fibronectin, C-reactive protein, etc. [21, 22]. When a negatively charged component such as phosphatidylserine is incorporated into NPs with a photosensitizer (PS), the "eat me" signal is significantly enhanced, providing increased recognition and uptake of NPs by Mφ [23]. Conversely, PEG modification of NPs reduces their charge and uptake by Mφ compared to NPs with highly charged coatings [24, 25].

Regarding the size of NPs, C. He *et al.* showed that increasing NP size from 150 to 300 and 500 nm led to an increase in uptake by 1.1 and 1.3 times, respectively, indicating that phagocytes with greater avidity capture larger NPs [18]. This same relationship was confirmed in a study by B. Prietl *et al*., which showed that carboxylpolystyrene particles sized 500-1000 nm induced phagocytosis and respiratory burst significantly more effectively than particles sized 20-200 nm [25]. The literature also mentions NPs with a diameter of about 500 nm, which are well-suited for passive targeting of alveolar Mφ [26].

Receptor-mediated targeting of anti-tuberculosis drugs and biomolecules to MTB-infected macrophages

Active targeting aimed at target cells assumes that the drug carrier has affinity for receptors expressed on these cells or is modified with a specific ligand recognized by corresponding receptors. The literature describes receptor-dependent phagocytosis involving different types of macrophage receptors, such as the mannose receptor, mannose-fucose (CD206) and fucose receptors, scavenger receptors (SR), Fc receptors, folate receptor alpha, hyaluronic acid receptor (CD44), tuftsin receptor, formyl peptide receptor, and others [26].

In TB infection, Mφ acquire an M2-like phenotype and express a number of specific receptors and signaling pathway molecules that promote MTB survival within cells but can also be used as targets for delivering NPs with active agents. These include, in particular, the mannose and mannose-fucose receptors (CD206), which belong to the large family of C-type lectin receptors (CLR) [27, 28].

Mannosylation is the most common strategy for delivering NPs to Mφ via CD206. Examples of mannosylated NPs are given in Table 1.

Although the literature primarily focuses on the CD206 receptor, targeting of Mφ is also achieved through other receptors. For instance, S.S. Soni *et al*. identified the role of SR-A1 in the uptake of cyclodextrin NPs by Mφ [42]. An example of targeted delivery of anti-tuberculosis drugs to Mφ in tuberculosis infection is the conjugate of moxifloxacin with carboxymethylglucan (M-DCMG), where carboxymethylglucan served as a ligand for Mφ SR [43]. Peptide ligands, such as tuftsin, encapsulated in PLGA (poly(D,L-lactide-co-glycolide)) NPs, increase uptake by monocytes/Mφ and suppression of intracellular MTB growth [44]. Another promising approach is based on the use of β-glucans and other carbohydrates as ligand carriers. For example, E. Jaecklein *et al*. presented a strategy for encapsulating anti-tuberculosis drugs or prodrugs in the hydrophobic core of glucan-lipid NPs derived from baker's yeast *Saccharomyces cerevisiae*. Glucan-lipid NPs can be

Таблица 1
Применение стратегии маннозилирования для таргетинга НЧ
Table 1
Application of the mannosylation strategy for targeting NPs

Тип НЧ Type of NPs	Активное вещество Active substance	Основные эффекты Outcomes	Авторы, год Authors, year
PLGA-PEG-Маннозамин PLGA-PEG-Mannosamine	Рифапентин + Изониазид Rifapentine + Isoniazid	↑ фагоцитоз, медленное высвобождение, ↑антибактериальная активность ↑ phagocytosis, sustained release, ↑ antibacterial activity	Peng C. с соавт., (2025) [29] Peng C. et al., (2025) [29]
PLGA-PEG-Маннозамин PLGA-PEG-Mannosamine	Рифапентин Rifapentine	↑ поглощение макрофагами ↑ macrophage uptake	Luan H. с соавт., (2025) [30] Luan H. et al., (2025) [30]

Липидные НЧ-Манноза Lipid NPs-Mannose	Рифампицин Rifampicin	↑ антибактериальное действие (*M. Intracellulare*), подавление биопленок ↑ antibacterial activity (*M. Intracellulare*), biofilm suppression	Chae J. с соавт., (2023) [31] Chae J. et al., (2023) [31]
Гиалуроновая кислота-Манноза/Хитозан Hyaluronic acid- Mannose/ Chitosan	Изониазид Isoniazid	Сродство к CD206/CD44, стимуляция Т-клеточного ответа Affinity for CD206/CD44, stimulation of T-cell response	Mukhtar M. с соавт., (2022) [32] Mukhtar M. et al., (2022) [32]
GO-PEG-Манноза GO-PEG-Mannose	Рифампицин Rifampicin	↑ захват/накопление в макрофагах, pH-зависимое лизосомальное высвобождение, ↑ бактерицидность (БЦЖ/МБТ) ↑ macrophage uptake/accumulation, pH-dependent lysosomal release, ↑ bactericidal activity (BCG/MTB)	Pi J. с соавт., (2019) [33] Pi J. et al., (2019) [33]
Липидные НЧ-Манноза Lipid NPs-Mannose	Изониазид Isoniazid	↑ поглощение альвеолярными макрофагами, рецептор-зависимое (ингибируется маннозой) ↑ alveolar macrophage uptake, receptor-dependent (inhibited by mannose)	Costa A. с соавт., (2018) [34] Costa A. et al., (2018) [34]
Желатиновые НЧ Gelatin NPs	Глицирризин Glycyrrhizin	↑ захват *in vitro*, ↓ бактериальная нагрузка в легких/селезенке у мышей ↑ *in vitro* uptake, ↓ bacterial burden in lungs/spleen of mice	Viswanathan V. с соавт., (2018) [35] Viswanathan V. et al., (2018) [35]
Дендримерные НЧ-Манноза Dendrimer NPs-Mannose	LXR-L LXR-L	↑ накопление в макрофагах бляшек, активация LXR-ABCA1/ABCG1, замедление атеросклероза, ↓ MMP9/NF-κB и некроза без выраженной липогенности в печени ↑ accumulation in plaque macrophages, activation of LXR-ABCA1/ABCG1, atherosclerosis retardation, ↓ MMP9/NF-κB and necrosis without marked hepatolipotoxicity	He H. с соавт., (2018) [36] He H. et al., (2018) [36]
НЧ на основе бычьего сывороточного альбумина-Манноза Bovine serum albumin NPs-Mannose	miRNA KLK12 miRNA KLK12	pH-чувствительное высвобождение, ↓ бактериальная нагрузка/воспаление *in vivo* pH-sensitive release, ↓ bacterial burden/inflammation *in vivo*	Wang Y. с соавт., 2024 [37] Wang Y. et al., 2024 [37]
Внеклеточные везикулы-VSV-G-α-CD206 Extracellular vesicles-VSV-G-α-CD206	Рекомбинантная люцифераза Recombinant luciferase	↑ поглощение CD206+ клетками ↑ uptake by CD206+ cells	Ovchinnikova LA. с соавт., (2024) [38] Ovchinnikova LA. et al., (2024) [38]
Фукоидан/Хитозан-Манноза/Маннан Fucoidan/Chitosan -Mannose/Mannan		Активация THP-1, ↑ IL-1β, IL-6, TNF-α, поляризация в М1-макрофаги THP-1 activation, ↑ IL-1β, IL-6, TNF-α, polarization towards M1 macrophages	Serrasqueiro F. с соавт., (2023) [39] Serrasqueiro F. et al., (2023) [39]
Полимерные НЧ-двухвалентный маннозный PEG-лиганд Polymer NPs-bivalent mannose PEG ligand		Селективное поглощение М2-макрофагами (в 2.4-11.8 раз), рецептор-зависимое (ингибируется маннаном), плотность маннозного лиганда 1% Selective uptake by M2 macrophages (2.4- to 11.8-fold), receptor-dependent (inhibited by mannan), mannose ligand density 1%	Chen P. с соавт., (2020) [40] Chen P. et al., (2020) [40]
Pluronic F127 -Дубильная кислота-Манноза Pluronic F127-Tannic acid-Mannose		Селективное поглощение М2-макрофагами, рецептор-зависимое (ингибируется маннаном) Selective uptake by M2 macrophages, receptor-dependent (inhibited by mannan)	Hatami E. с соавт., (2019) [41] Hatami E. et al., (2019) [41]

PLGA – поли(D,L-лактид-ко-гликолид); PEG – полиэтиленгликоль; LXR-L – агонист рецептора LXR (Liver X Receptor); KLK12 – калликреин-связанная пептидаза 12.
PLGA – poly(D,L-lactide-co-glycolide); PEG – polyethylene glycol; LXR-L – LXR agonist (Liver X Receptor); KLK12 – kallikrein-related peptidase 12.

modified for controlled release of cargo at low pH and intra-macrophagally after recognition of β-1,3-glucans by dectin-1 and CR3 receptors [25, 45].

Receptor-mediated targeting of photosensitizers to macrophages for photodynamic therapy in oncological and other diseases

Photodynamic therapy (PDT) with receptor-mediated targeting of Mφ is a promising approach for treating tumors, atherosclerosis, and infectious diseases, based on the selective delivery of PS to target cells. This approach is particularly often used for the elimination or reprogramming of tumor-associated macrophages (TAMs), as they have an M2-like phenotype and serve as the main source of immunosuppression in tumor tissue, promoting tumor cell growth and metastasis [17, 46, 47]. Studies show that conjugates of PS with proteins (albumin, transferrin, lipoproteins), polysaccharides (dextran, mannan, beta-glucans), as well as nanoparticles binding to specific receptors, ensure high selectivity of PS accumulation in Mφ. It has been shown that conjugates of hematoporphyrin with lipoproteins [48], albumin, or transferrin [49] are actively taken up by Mφ due to high SR expression on them. Modification of PS-binding proteins with maleic acid enhances the selectivity of PS uptake by Mφ via SR-A1 [50, 51]. Since SR-A1 recognizes and binds negatively charged molecules, F. Tang *et al*. conjugated sodium alginate (polyanion) with the PS 1-[4-(2-aminoethyl)phenoxy] zinc(II) phthalocyanine. *In vivo* biodistribution analysis revealed selective accumulation of conjugates in the tumor, with 87% tumor growth inhibition without systemic toxicity [52]. Conjugates of PS with polysaccharides, such as dextran sulfate, also provide targeted delivery to TAMs. Dextran sulfate conjugated with chlorin e6 was predominantly taken up by TAMs with the M2 phenotype expressing SR-A1 receptors and effectively induced tumor cell apoptosis upon laser irradiation [47]. Similarly, mannose-modified compounds provide targeted delivery to TAMs with an M2-like phenotype via CD206. T. Soyama *et al*. synthesized a conjugate of chlorin e6 with mannose, which selectively targeted CD206 highly expressed on M2-TAMs and led to damage and death of tumor cells [53].

By directly eliminating M2-TAMs, PDT increases the proportion of anti-tumor Mφ with an M1-like phenotype and induces immunogenic cell death [54]. Along with the elimination of some cells, DAMP molecules (e.g., calreticulin) are released, and the antigen-presenting function of Mφ is activated [53, 55, 56]. This leads to a reduction in immunosuppression and enhancement of local anti-tumor immunity [53]. Y. Kimura *et al*. showed that PDT using a mannose-chlorin e6 conjugate increased the amount of calreticulin on the surface of cancer cells, enhancing their phagocytosis by Mφ [55]. In the work of X. Chi *et al*., a nanocomposite was synthesized consisting of chlorin e6 and the α2-adrenergic receptor (α2-AR) agonist guanfacine, which, by activating these receptors, can enhance the effectiveness of photoimmunotherapy. It was shown that α2-AR agonists promoted the repolarization of M2-TAMs towards the M1 phenotype through α2-AR-mediated inhibition of adenylate cyclase [56].

Clinical perspectives of PDT are associated not only with oncology but also with the treatment of pathologies such as atherosclerosis [57, 58], infectious diseases [23, 60, 61, 62, 63, 64, 65, 66, 67], and autoimmune processes [59]. In atherosclerotic lesions, Mφ constitute the most numerous cell population, determining all stages of its development [57]. Furthermore, Mφ play a key role in the initiation and progression of rheumatoid arthritis [59]. S.Y. Lee *et al*. synthesized D-mannosamine-PEG-chlorin e6 for PDT of atherosclerosis, which specifically bound to CD206 and penetrated foam cells derived from Mφ, significantly increasing reactive oxygen species generation after irradiation [58]. J. Huang *et al*. developed a dextran-bovine serum albumin conjugate to create a nanoemulsion with chlorin e6 and dexamethasone for SR-A-mediated delivery to Mφ. PDT using this nanoemulsion enhanced reactive oxygen species production, stimulated autophagy in foam cells, increased expression of the cholesterol efflux-associated protein ABCA1, and reduced secretion of pro-inflammatory cytokines [57]. A new PDT method for treating rheumatoid arthritis was proposed by D.N. Dorst *et al*., in which liposomes containing the PS IRDye700DX were delivered to Mφ in inflamed joints. It was shown that PDT using liposomes containing IRDye700DX caused Mφ death *in vitro* and significantly slowed arthritis development in mice with collagen-induced arthritis, providing local elimination of pro-inflammatory Mφ [59].

Receptor-mediated targeting of photosensitizers to MTB-infected macrophages for antibacterial photodynamic and photothermal therapy

Traditional TB chemotherapy faces problems of long treatment duration, toxicity, and the development of MDR strains. The use of TB treatment strategies alternative to chemotherapy, such as PDT, can overcome MDR-MTB through non-specific action on multiple cellular proteins, lipids, and nucleic acids [14, 15, 16]. Anti-tuberculosis therapy targeted at Mφ can be conducted using nanomaterials, which allows increasing the local concentration of drugs in infection foci, reducing systemic toxicity, and providing a synergistic effect through the combination of direct PDT action and PDT-induced immune response [23].

As noted above, Mφ play an important role in the pathogenesis of TB, being the primary cellular reservoir of MTB. To enhance therapeutic efficacy, NPs modified with ligands or membranes capable of selectively binding to macrophage receptors are used. Within the framework of antibacterial PDT and combined approaches, strategies

for targeting PS to MTB-infected Mφ are being particularly actively developed. An example is the work of N. Tian *et al*., who developed nanocomposites with a core made of a metal-organic framework based on zirconium ions and porphyrin ligands, with internal content of synthetic unmethylated CpG oligonucleotides. Phosphatidylserine was used as a surface coating. By stimulating TLR in immune cells, oligonucleotides can induce an anti-mycobacterial Th1- and M1-type immune response. The obtained NPs combined properties necessary simultaneously for PDT and targeted immunotherapy; as a result, the created NPs showed high bactericidal activity against MTB and immunostimulatory properties [23].

In addition to classical PDT, combined approaches combining photodynamic and photothermal effects have been actively developed in recent years. Mannosylated NPs provide highly effective delivery of anti-tuberculosis drugs through interaction with CD206. S. Fan *et al*. developed mannose-modified polydopamine-based mesoporous NPs loaded with rifampicin. These NPs provided selective drug delivery and photothermal bacterial killing in MTB-infected Mφ. At the same time, these NPs induced an immune response and prevented MTB evasion from immune cells, stimulated autophagy, suppressed lipid peroxidation and ferroptosis of MTB-infected Mφ. In a mouse model of cutaneous TB, such combined therapy significantly reduced bacterial load and decreased pathological changes without systemic side effects [60].

One approach to TB therapy uses NPs coated with the membrane of activated Mφ or erythrocytes. This design ensures precise targeting of granulomas and infected tissues, high biocompatibility, and prolonged circulation in the bloodstream. H. Wang *et al*. created biomimetic NPs coated with erythrocyte membranes to increase blood circulation time and selective accumulation in tuberculous granulomas. Inside these NPs contained a PS excited in the near-infrared range, as well as a photothermal agent – Prussian blue. This construct, upon laser irradiation, destroys bacteria, providing simultaneously PS-mediated reactive oxygen species generation and local thermal effects. As a result, in a mouse model of TB infection, a synergistic effect was observed, leading to suppression of bacterial growth and reduction of granulomatous infiltration [61]. The same group of researchers developed NPs containing macrophage membrane-derived microvesicles with chlorin e6. These NPs circulated in the blood for a long time and accumulated in tuberculous granulomas due to the tropism of microvesicles for infection foci. In a mouse model of tuberculous granulomatosis, microvesicles effectively inhibited pathogen growth and spread, demonstrating good biocompatibility and potential for TB treatment with a low risk of drug resistance development [62]. B. Li *et al*. developed PLGA-based NPs encapsulating a photothermal agent with aggregation-induced emission (AIE), coated with membranes from *M. marinum*-activated RAW 264.7 Mφ. The *M. marinum*-induced increased expression of TLR2/4/6 on the membranes of such Mφ provides targeted transport of NPs to tuberculous granulomas. AIE allows fluorescent visualization of tissues in the near-infrared range (1500-1700 nm). In a mouse model of TB infection, intravenous administration of these NPs provided high-contrast visualization of granulomas in the lungs with resolution surpassing CT, and transcutaneous laser irradiation induced a local photothermal effect eliminating the pathogen [63]. Biomimetic AIE NPs allow not only combined photodynamic/photothermal therapy but also high-contrast visualization of granulomas *in vivo*. In a recent study, Yan D *et al*. synthesized AIE NPs coated with membranes of pre-activated Mφ. Using AIE visualization allowed precise detection of small granulomas about 0.2 mm in diameter in the lungs of infected mice. Upon irradiation with a 1064 nm laser, NPs provided photothermal bacterial killing more effectively than chemotherapy [64].

It should be noted that targeted PDT aimed at destroying intracellularly localized pathogens is effective not only against *M. tuberculosis* but also against other pathogens, including *Staphylococcus aureus* [65], including methicillin-resistant strains [66], *Acinetobacter baumannii* [66], *Salmonella enterica* [67], and others.

Conclusion

The increasing prevalence of MDR-TB and the limited effectiveness of chemotherapeutic agents dictate the need to revise treatment strategies towards alternative highly specific pathogen-oriented and immunomodulatory approaches. The data presented in this review show that Mφ with M2-like polarization are not only a central link in MTB persistence but also a promising therapeutic target. The use of nanoscale carriers with passive and active targeting allows not only to ensure a high intracellular concentration of antibacterial drugs but also to implement fundamentally different mechanisms of action. Of particular interest in this context is the targeted delivery of PS, which underlies antimicrobial PDT. Combined approaches integrating PDT with photothermal effects and immunomodulation demonstrate high efficacy in preclinical models, providing synergistic killing of intracellular pathogens and stimulation of anti-infective immunity. It is important to emphasize that the efficacy of many of the platforms considered has already been confirmed *in vivo* in models of TB infection with MDR pathogen.

Nevertheless, the translation of the obtained results into clinical practice requires solving a number of tasks: optimization of the biodistribution and biocompatibility profile of NPs, standardization of targeted delivery protocols for different routes of administration (inhalation, intravenous), as well as studying the long-term effects of modulating the Mφ phenotype on anti-tuberculosis immunity as a whole.

REFERENCES

1. World Health Organization. Global tuberculosis report 2023. Geneva: World Health Organization, 2023, 75 p. ISBN 978-92-4-008385-1. Available at: https://iris.who.int/handle/10665/373853 (accessed: 21.06.2026).
2. Strizova Z., Benesova I., Bartolini R., Novysedlak R., Cecrdlova E., Foley L.K., Striz I. M1/M2 macrophages and their overlaps–myth or reality? *Clinical Science.* 2023, vol. 137 (15), pp. 1067-1093. doi: 10.1042/CS20220531.
3. Ahmad F., Rani A., Alam A., Zarin S., Pandey S., Singh H., Hasnain S.E., Ehtesham N.Z. Macrophage: a cell with many faces and functions in tuberculosis. *Frontiers in immunology.* 2022, vol. 13, pp. 747799. doi: 10.3389/fimmu.2022.747799.
4. Zhang K., Mishra A., Jagannath C. New insight into arginine and tryptophan metabolism in macrophage activation during tuberculosis. *Frontiers in immunology.* 2024, vol. 15, pp. 1363938. doi: 10.3389/fimmu.2024.1363938.
5. Arrigoni R., Ballini A., Topi S., Bottalico L., Jirillo E., Santacroce L. Antibiotic resistance to Mycobacterium tuberculosis and potential use of natural and biological products as alternative anti-mycobacterial agents. *Antibiotics.* 2022, vol. 11 (10), pp. 1431. doi: 10.3390/antibiotics11101431.
6. Le Y., Cao W., Zhou L., Fan X., Liu Q., Liu F., Gai X., Chang C., Xiong J., Rao Y., Li A., Xu W., Liu B., Wang T., Wang B., Sun Y. Infection of Mycobacterium tuberculosis promotes both M1/M2 polarization and MMP production in cigarette smoke-exposed macrophages. *Frontiers in immunology.* 2020, vol. 11, pp. 1902. doi: 10.3389/fimmu.2020.01902.
7. Shi L., Jiang Q., Bushkin Y., Subbian S., Tyagi S. Biphasic dynamics of macrophage immunometabolism during Mycobacterium tuberculosis infection. *MBio.* 2019, vol. 10 (2), pp. e02550-18. doi: 10.1128/mBio.02550-18.
8. Zhang Y., Li S., Liu Q., Long R., Feng J., Qin H., Li M., Liu L., Luo J. Mycobacterium tuberculosis heat-shock protein 16.3 induces macrophage M2 polarization through CCRL2/CX3CR1. *Inflammation.* 2020, vol. 43 (2), pp. 487-506. doi: 10.1007/s10753-019-01132-9.
9. Refai A., Gritli S., Barbouche M.R., Essafi M. Mycobacterium tuberculosis virulent factor ESAT-6 drives macrophage differentiation toward the pro-inflammatory M1 phenotype and subsequently switches it to the anti-inflammatory M2 phenotype. *Frontiers in cellular and infection microbiology.* 2018, vol. 8, pp. 327. doi: 10.3389/fcimb.2018.00327.
10. Huang L., Nazarova E.V., Tan S., Liu Y., Russell D.G. Growth of Mycobacterium tuberculosis in vivo segregates with host macrophage metabolism and ontogeny. *Journal of Experimental Medicine.* 2018, vol. 215 (4), pp. 1135-1152. doi: 10.1084/jem.20172020.
11. Huang Z., Luo Q., Guo Y., Chen J., Xiong G., Peng Y., Ye J., Li J. Mycobacterium tuberculosis-induced polarization of human macrophage orchestrates the formation and development of tuberculous granulomas in vitro. *PloS one.* 2015, vol. 10 (6), pp. e0129744. doi: 10.1371/journal.pone.0129744.
12. Shang X., Maimaiti N., Fan J., Wang L., Wang Y., Sun H., Lv J., Zhang X., Wang J., Ma X. Triggering receptor expressed on myeloid cells 2 mediates the involvement of M2-type macrophages in pulmonary tuberculosis infection. *Journal of Inflammation Research.* 2024, pp. 1919-1928. doi: 10.2147/JIR.S435216.
13. Fang H., Xiong Y., Fu B., Wu H. Targeting alveolar macrophages in tuberculosis: Exploiting trained immunity for novel therapeutic approaches. *International Immunopharmacology.* 2025, vol. 163, pp. 115211. doi: 10.1016/j.intimp.2025.115211.
14. Gourlot C., Gosset A., Glattard E., Aisenbrey C., Rangasamy S., Rabineau M., Ouk T.S., Sol V., Lavalle P., Gourlaouen C., Ventura B., Bechinger B., Heitz V. Antibacterial photodynamic therapy in the near-infrared region with a targeting antimicrobial peptide connected to a π-extended porphyrin. *ACS Infectious Diseases.* 2022, vol. 8 (8), pp. 1509-1520. doi: 10.1021/acsinfecdis.2c00131.
15. Sabino C.P., Wainwright M., Ribeiro M.S., Sellera F.P., Dos Anjos C., Baptista M.D.S., Lincopan N. Global priority multidrug-resistant pathogens do not resist photodynamic therapy. *Journal of Photochemistry and Photobiology B: Biology.* 2020, vol. 208, pp. 111893. doi: 10.1016/j.jphotobiol.2020.111893.
16. Bekmukhametova A., Ruprai H., Hook J.M., Mawad D., Houang J., Lauto A. Photodynamic therapy with nanoparticles to combat microbial infection and resistance. *Nanoscale.* 2020, vol. 12 (41), pp. 21034-21059. doi: 10.1039/d0nr04540c.
17. Chen X., Zheng R., Zhao L., Kong R., Yang N., Liu Y., Chen A., Wang C., Cheng H., Li S. Photodynamic therapy initiated immunotherapy of self-delivery re-educator by inducing immunogenic cell death and macrophage polarization. *Chemical Engineering Journal.* 2022, vol. 435, pp. 134783. doi: 10.1016/j.cej.2022.134783.
18. He C., Hu Y., Yin L., Tang C., Yin C. Effects of particle size and surface charge on cellular uptake and biodistribution of polymeric

ЛИТЕРАТУРА

1. World Health Organization. Global tuberculosis report 2023 // Geneva: World Health Organization. – 2023. – 75 p. – ISBN 978-92-4-008385-1. – URL: https://iris.who.int/handle/10665/373853 (дата обращения: 21.06.2026).
2. Strizova Z., Benesova I., Bartolini R., Novysedlak R., Cecrdlova E., Foley L.K., Striz I. M1/M2 macrophages and their overlaps–myth or reality? // Clinical Science. – 2023. – Vol. 137 (15). – P. 1067-1093. doi: 10.1042/CS20220531.
3. Ahmad F., Rani A., Alam A., Zarin S., Pandey S., Singh H., Hasnain S.E., Ehtesham N.Z. Macrophage: a cell with many faces and functions in tuberculosis // Frontiers in immunology. – 2022. – Vol. 13. – P. 747799. doi: 10.3389/fimmu.2022.747799.
4. Zhang K., Mishra A., Jagannath C. New insight into arginine and tryptophan metabolism in macrophage activation during tuberculosis // Frontiers in immunology. – 2024. – Vol. 15. – P. 1363938. doi: 10.3389/fimmu.2024.1363938.
5. Arrigoni R., Ballini A., Topi S., Bottalico L., Jirillo E., Santacroce L. Antibiotic resistance to Mycobacterium tuberculosis and potential use of natural and biological products as alternative anti-mycobacterial agents // Antibiotics. – 2022. – Vol. 11 (10). – P. 1431. doi: 10.3390/antibiotics11101431.
6. Le Y., Cao W., Zhou L., Fan X., Liu Q., Liu F., Gai X., Chang C., Xiong J., Rao Y., Li A., Xu W., Liu B., Wang T., Wang B., Sun Y. Infection of Mycobacterium tuberculosis promotes both M1/M2 polarization and MMP production in cigarette smoke-exposed macrophages // Frontiers in immunology. – 2020. – Vol. 11. – P. 1902. doi: 10.3389/fimmu.2020.01902.
7. Shi L., Jiang Q., Bushkin Y., Subbian S., Tyagi S. Biphasic dynamics of macrophage immunometabolism during Mycobacterium tuberculosis infection // MBio. – 2019. – Vol. 10 (2). – P. e02550-18. doi: 10.1128/mBio.02550-18.
8. Zhang Y., Li S., Liu Q., Long R., Feng J., Qin H., Li M., Liu L., Luo J. Mycobacterium tuberculosis heat-shock protein 16.3 induces macrophage M2 polarization through CCRL2/CX3CR1 // Inflammation. – 2020. – Vol. 43 (2). – P. 487-506. doi: 10.1007/s10753-019-01132-9.
9. Refai A., Gritli S., Barbouche M.R., Essafi M. Mycobacterium tuberculosis virulent factor ESAT-6 drives macrophage differentiation toward the pro-inflammatory M1 phenotype and subsequently switches it to the anti-inflammatory M2 phenotype // Frontiers in cellular and infection microbiology. – 2018. – Vol. 8. – P. 327. doi: 10.3389/fcimb.2018.00327.
10. Huang L., Nazarova E.V., Tan S., Liu Y., Russell D.G. Growth of Mycobacterium tuberculosis in vivo segregates with host macrophage metabolism and ontogeny // Journal of Experimental Medicine. – 2018. – Vol. 215 (4). – P. 1135-1152. doi: 10.1084/jem.20172020.
11. Huang Z., Luo Q., Guo Y., Chen J., Xiong G., Peng Y., Ye J., Li J. Mycobacterium tuberculosis-induced polarization of human macrophage orchestrates the formation and development of tuberculous granulomas in vitro // PloS one. – 2015. – Vol. 10 (6). – P. e0129744. doi: 10.1371/journal.pone.0129744.
12. Shang X., Maimaiti N., Fan J., Wang L., Wang Y., Sun H., Lv J., Zhang X., Wang J., Ma X. Triggering receptor expressed on myeloid cells 2 mediates the involvement of M2-type macrophages in pulmonary tuberculosis infection // Journal of Inflammation Research. – 2024. – P. 1919-1928. doi: 10.2147/JIR.S435216.
13. Fang H., Xiong Y., Fu B., Wu H. Targeting alveolar macrophages in tuberculosis: Exploiting trained immunity for novel therapeutic approaches // International Immunopharmacology. – 2025. – Vol. 163. – P. 115211. doi: 10.1016/j.intimp.2025.115211.
14. Gourlot C., Gosset A., Glattard E., Aisenbrey C., Rangasamy S., Rabineau M., Ouk T.S., Sol V., Lavalle P., Gourlaouen C., Ventura B., Bechinger B., Heitz V. Antibacterial photodynamic therapy in the near-infrared region with a targeting antimicrobial peptide connected to a π-extended porphyrin // ACS Infectious Diseases. – 2022. – Vol. 8 (8). – P. 1509-1520. doi: 10.1021/acsinfecdis.2c00131.
15. Sabino C.P., Wainwright M., Ribeiro M.S., Sellera F.P., Dos Anjos C., Baptista M.D.S., Lincopan N. Global priority multidrug-resistant pathogens do not resist photodynamic therapy // Journal of Photochemistry and Photobiology B: Biology. – 2020. – Vol. 208. – P. 111893. doi: 10.1016/j.jphotobiol.2020.111893.
16. Bekmukhametova A., Ruprai H., Hook J.M., Mawad D., Houang J., Lauto A. Photodynamic therapy with nanoparticles to combat microbial infection and resistance // Nanoscale. – 2020. – Vol. 12 (41). – P. 21034-21059. doi: 10.1039/d0nr04540c.
17. Chen X., Zheng R., Zhao L., Kong R., Yang N., Liu Y., Chen A., Wang C., Cheng H., Li S. Photodynamic therapy initiated immunotherapy of self-delivery re-educator by inducing immunogenic cell death and macrophage polarization // Chemical Engineering Journal. – 2022. – Vol. 435. – P. 134783. doi: 10.1016/j.cej.2022.134783.
18. He C., Hu Y., Yin L., Tang C., Yin C. Effects of particle size and surface charge on cellular uptake and biodistribution of polymeric

nanoparticles. *Biomaterials.* 2010, vol. 31 (13), pp. 3657-3666. doi: 10.1016/j.biomaterials.2010.01.065.
19. Fröhlich E. The role of surface charge in cellular uptake and cytotoxicity of medical nanoparticles. *International journal of nanomedicine.* 2012, pp. 5577-5591. doi: 10.2147/IJN.S36111.
20. Xiao K., Li Y., Luo J., Lee J.S., Xiao W., Gonik A.M., Agarwal R.G., Lam K.S. The effect of surface charge on in vivo biodistribution of PEG-oligocholic acid based micellar nanoparticles. *Biomaterials.* 2011, vol. 32 (13), pp. 3435-3446. doi: 10.1016/j.biomaterials.2011.01.021.
21. Sahay G., Alakhova D.Y., Kabanov A.V. Endocytosis of nanomedicines. *Journal of controlled release.* 2010, vol. 145 (3), pp. 182-195. doi: 10.1016/j.jconrel.2010.01.036.
22. Zhou J., Xiang H., Huang J., Zhong Y., Zhu X., Xu J., Lu Q., Gao B., Zhang H., Yang R., Luo Y., Yan F. Role of surface charge of nanoscale ultrasound contrast agents in complement activation and phagocytosis. *International Journal of Nanomedicine.* 2022, vol. 17, pp. 5933. doi: 10.2147/IJN.S364381.
23. Tian N., Duan H., Cao T., Dai G., Sheng G., Chu H., Sun Z. Macrophage-targeted nanoparticles mediate synergistic photodynamic therapy and immunotherapy of tuberculosis. *RSC advances.* 2023, vol. 13 (3), pp. 1727-1737. doi: 10.1039/d2ra06334d.
24. Zahr A.S., Davis C.A., Pishko M.V. Macrophage uptake of core–shell nanoparticles surface modified with poly (ethylene glycol). *Langmuir.* 2006, vol. 22 (19), pp. 8178-8185. doi: 10.1021/la060951b.
25. Prietl B., Meindl C., Roblegg E., Pieber T.R., Lanzer G., Fröhlich E. Nano-sized and micro-sized polystyrene particles affect phagocyte function. *Cell biology and toxicology.* 2014, vol. 30 (1), pp. 1-16. doi: 10.1007/s10565-013-9265-y.
26. Gairola A., Benjamin A., Weatherston J.D., Cirillo J.D., Wu H.J. Recent developments in drug delivery for treatment of tuberculosis by targeting macrophages. *Advanced therapeutics.* 2022, vol. 5 (6), pp. 2100193. doi: 10.1002/adtp.202100193.
27. Rajaram M.V.S., Arnett E., Azad A.K., Guirado E., Ni B., Gerberick A.D., He L.Z., Keler T., Thomas L.J., Lafuse W.P., Schlesinger L.S. M. tuberculosis-initiated human mannose receptor signaling regulates macrophage recognition and vesicle trafficking by FcRγ-chain, Grb2, and SHP-1. *Cell reports.* 2017, vol. 21 (1), pp. 126-140. doi: 10.1016/j.celrep.2017.09.034.
28. Rajaram M., Ni B., Arnett E., Abul A., Schlesinger L. FcRγ-chain, Grb2 and SHP-1 are invovled in mannose receptor (CD206)-mediated signaling in relation to tuberculosis (INC4P. 329). *The Journal of Immunology.* 2015, vol. 194 (1_Supplement), pp. 125.8-125.8. doi: 10.4049/jimmunol.194.Supp.125.8.
29. Peng C., Luan H., Shang Q., Xiang W., Yasin P., Song X. Mannosamine-Modified Poly (lactic-co-glycolic acid)-Polyethylene Glycol Nanoparticles for the Targeted Delivery of Rifapentine and Isoniazid in Tuberculosis Therapy. *Bioconjugate Chemistry.* 2025, vol. 36 (5), pp. 1021-1033. doi: 10.1021/acs.bioconjchem.5c00062.
30. Luan H., Peng C., Yasin P., Shang Q., Xiang W., Song X. Mannosamine-Engineered Nanoparticles for Precision Rifapentine Delivery to Macrophages: Advancing Targeted Therapy Against Mycobacterium Tuberculosis. *Drug Design, Development and Therapy.* 2025, pp. 2081-2102. doi: 10.2147/DDDT.S505682.
31. Chae J., Kang S.H., Kim J., Choi Y., Kang S.H., Choi J. Targeted and efficient delivery of rifampicin to macrophages involved in non-tuberculous mycobacterial infection via mannosylated solid lipid nanoparticles. *Nanoscale advances.* 2023, vol. 5 (17), pp. 4536-4545. doi: 10.1039/d3na00320e.
32. Mukhtar M., Csaba N., Robla S., Varela-Calviño R., Nagy A., Burian K., Kókai D., Ambrus R. Dry powder comprised of isoniazid-loaded nanoparticles of hyaluronic acid in conjugation with mannose-anchored chitosan for macrophage-targeted pulmonary administration in tuberculosis. *Pharmaceutics.* 2022, vol. 14 (8), pp. 1543. doi: 10.3390/pharmaceutics14081543.
33. Pi J., Shen L., Shen H., Yang E., Wang W., Wang R., Huang D., Lee B.S., Hu C., Chen C., Jin H., Cai J., Zeng G., Chen Z.W. Mannosylated graphene oxide as macrophage-targeted delivery system for enhanced intracellular M. tuberculosis killing efficiency. *Materials Science and Engineering: C.* 2019, vol. 103, pp. 109777. doi: 10.1016/j.msec.2019.109777.
34. Costa A., Sarmento B., Seabra V. Mannose-functionalized solid lipid nanoparticles are effective in targeting alveolar macrophages. *European Journal of Pharmaceutical Sciences.* 2018, vol. 114, pp. 103-113. doi: 10.1016/j.ejps.2017.12.006.
35. Viswanathan V., Mehta H., Pharande R., Bannalikar A., Gupta U., Mukne A. Mannosylated gelatin nanoparticles of licorice for use in tuberculosis: formulation, in vitro evaluation, in vitro cell uptake, in vivo pharmacokinetics and in vivo anti-tubercular efficacy. *Journal of Drug Delivery Science and Technology.* 2018, vol. 45, pp. 255-263. doi: 10.1016/j.jddst.2018.01.017.
36. He H., Yuan Q., Bie J., Wallace R.L., Yannie P.J., Wang J., Lancina M.G. 3rd, Zolotarskaya O.Y., Korzun W., Yang H., Ghosh S. Development

nanoparticles // Biomaterials. – 2010. – Vol. 31 (13). – P. 3657-3666. doi: 10.1016/j.biomaterials.2010.01.065.
19. Fröhlich E. The role of surface charge in cellular uptake and cytotoxicity of medical nanoparticles // International journal of nanomedicine. – 2012. – P. 5577-5591. doi: 10.2147/IJN.S36111.
20. Xiao K., Li Y., Luo J., Lee J.S., Xiao W., Gonik A.M., Agarwal R.G., Lam K.S. The effect of surface charge on in vivo biodistribution of PEG-oligocholic acid based micellar nanoparticles // Biomaterials. – 2011. – Vol. 32 (13). – P. 3435-3446. doi: 10.1016/j.biomaterials.2011.01.021.
21. Sahay G., Alakhova D.Y., Kabanov A.V. Endocytosis of nanomedicines // Journal of controlled release. – 2010. – Vol. 145 (3). – P. 182-195. doi: 10.1016/j.jconrel.2010.01.036.
22. Zhou J., Xiang H., Huang J., Zhong Y., Zhu X., Xu J., Lu Q., Gao B., Zhang H., Yang R., Luo Y., Yan F. Role of surface charge of nanoscale ultrasound contrast agents in complement activation and phagocytosis // International Journal of Nanomedicine. – 2022. – Vol. 17. – P. 5933. doi: 10.2147/IJN.S364381.
23. Tian N., Duan H., Cao T., Dai G., Sheng G., Chu H., Sun Z. Macrophage-targeted nanoparticles mediate synergistic photodynamic therapy and immunotherapy of tuberculosis // RSC advances. – 2023. – Vol. 13 (3). – P. 1727-1737. doi: 10.1039/d2ra06334d.
24. Zahr A.S., Davis C.A., Pishko M.V. Macrophage uptake of core–shell nanoparticles surface modified with poly (ethylene glycol) // Langmuir. – 2006. – Vol. 22 (19). – P. 8178-8185. doi: 10.1021/la060951b.
25. Prietl B., Meindl C., Roblegg E., Pieber T.R., Lanzer G., Fröhlich E. Nano-sized and micro-sized polystyrene particles affect phagocyte function // Cell biology and toxicology. – 2014. – Vol. 30 (1). – P. 1-16. doi: 10.1007/s10565-013-9265-y.
26. Gairola A., Benjamin A., Weatherston J.D., Cirillo J.D., Wu H.J. Recent developments in drug delivery for treatment of tuberculosis by targeting macrophages // Advanced therapeutics. – 2022. – Vol. 5 (6). – P. 2100193. doi: 10.1002/adtp.202100193.
27. Rajaram M.V.S., Arnett E., Azad A.K., Guirado E., Ni B., Gerberick A.D., He L.Z., Keler T., Thomas L.J., Lafuse W.P., Schlesinger L.S. M. tuberculosis-initiated human mannose receptor signaling regulates macrophage recognition and vesicle trafficking by FcRγ-chain, Grb2, and SHP-1 // Cell reports. – 2017. – Vol. 21 (1). – P. 126-140. doi: 10.1016/j.celrep.2017.09.034.
28. Rajaram M., Ni B., Arnett E., Abul A., Schlesinger L. FcRγ-chain, Grb2 and SHP-1 are invovled in mannose receptor (CD206)-mediated signaling in relation to tuberculosis (INC4P. 329) // The Journal of Immunology. – 2015. – Vol. 194 (1_Supplement). – P. 125.8-125.8. doi: 10.4049/jimmunol.194.Supp.125.8.
29. Peng C., Luan H., Shang Q., Xiang W., Yasin P., Song X. Mannosamine-Modified Poly (lactic-co-glycolic acid)-Polyethylene Glycol Nanoparticles for the Targeted Delivery of Rifapentine and Isoniazid in Tuberculosis Therapy // Bioconjugate Chemistry. – 2025. – Vol. 36 (5). – P. 1021-1033. doi: 10.1021/acs.bioconjchem.5c00062.
30. Luan H., Peng C., Yasin P., Shang Q., Xiang W., Song X. Mannosamine-Engineered Nanoparticles for Precision Rifapentine Delivery to Macrophages: Advancing Targeted Therapy Against Mycobacterium Tuberculosis // Drug Design, Development and Therapy. – 2025. – P. 2081-2102. doi: 10.2147/DDDT.S505682.
31. Chae J., Kang S.H., Kim J., Choi Y., Kang S.H., Choi J. Targeted and efficient delivery of rifampicin to macrophages involved in non-tuberculous mycobacterial infection via mannosylated solid lipid nanoparticles // Nanoscale advances. – 2023. – Vol. 5 (17). – P. 4536-4545. doi: 10.1039/d3na00320e.
32. Mukhtar M., Csaba N., Robla S., Varela-Calviño R., Nagy A., Burian K., Kókai D., Ambrus R. Dry powder comprised of isoniazid-loaded nanoparticles of hyaluronic acid in conjugation with mannose-anchored chitosan for macrophage-targeted pulmonary administration in tuberculosis // Pharmaceutics. – 2022. – Vol. 14 (8). – P. 1543. doi: 10.3390/pharmaceutics14081543.
33. Pi J., Shen L., Shen H., Yang E., Wang W., Wang R., Huang D., Lee B.S., Hu C., Chen C., Jin H., Cai J., Zeng G., Chen Z.W. Mannosylated graphene oxide as macrophage-targeted delivery system for enhanced intracellular M. tuberculosis killing efficiency // Materials Science and Engineering: C. – 2019. – Vol. 103. – P. 109777. doi: 10.1016/j.msec.2019.109777.
34. Costa A., Sarmento B., Seabra V. Mannose-functionalized solid lipid nanoparticles are effective in targeting alveolar macrophages // European Journal of Pharmaceutical Sciences. – 2018. – Vol. 114. – P. 103-113. doi: 10.1016/j.ejps.2017.12.006.
35. Viswanathan V., Mehta H., Pharande R., Bannalikar A., Gupta U., Mukne A. Mannosylated gelatin nanoparticles of licorice for use in tuberculosis: formulation, in vitro evaluation, in vitro cell uptake, in vivo pharmacokinetics and in vivo anti-tubercular efficacy // Journal of Drug Delivery Science and Technology. – 2018. – Vol. 45. – P. 255-263. doi: 10.1016/j.jddst.2018.01.017.
36. He H., Yuan Q., Bie J., Wallace R.L., Yannie P.J., Wang J., Lancina M.G. 3rd, Zolotarskaya O.Y., Korzun W., Yang H., Ghosh S. Development

of mannose functionalized dendrimeric nanoparticles for targeted delivery to macrophages: use of this platform to modulate atherosclerosis. *Translational Research.* 2018, vol. 193, pp. 13-30. doi: 10.1016/j.trsl.2017.10.008.

37. Wang Y., Liu Y., Long M., Dong Y., Li L., Zhou X. Nanoparticles target M2 macrophages to silence kallikrein-related peptidase 12 for the treatment of tuberculosis and drug-resistant tuberculosis. *Acta Biomaterialia.* 2024, vol. 188, pp. 358-373. doi: 10.1016/j.actbio.2024.09.026.
38. Ovchinnikova L.A., Tanygina D.Y., Dzhelad S.S., Evtushenko E.G., Bagrov D.V., Gabibov A.G., Lomakin Y.A. Targeted macrophage mannose receptor (CD206)-specific protein delivery via engineered extracellular vesicles. *Heliyon.* 2024, vol. 10 (24), pp. e40940. doi: 10.1016/j.heliyon.2024.e40940.
39. Serrasqueiro F., Barbosa A.I., Lima S.A.C., Reis S. Targeting the mannose receptor with functionalized fucoidan/chitosan nanoparticles triggers the classical activation of macrophages. *International Journal of Molecular Sciences.* 2023, vol. 24 (12), pp. 9908. doi: 10.3390/ijms24129908.
40. Chen P., Zhang X., Venosa A., Lee I.H., Myers D., Holloway J.A., Prud'homme R.K., Gao D., Szekely Z., Laskin J.D., Laskin D.L., Sinko P.J. A novel bivalent mannosylated targeting ligand displayed on nanoparticles selectively targets anti-inflammatory M2 macrophages. *Pharmaceutics.* 2020, vol. 12 (3), pp. 243. doi: 10.3390/pharmaceutics12030243.
41. Hatami E., Mu Y., Shields D.N., Chauhan S.C., Kumar S., Cory T.J., Yallapu M.M. Mannose-decorated hybrid nanoparticles for enhanced macrophage targeting. *Biochemistry and biophysics reports.* 2019, vol. 17, pp. 197-207. doi: 10.1016/j.bbrep.2019.01.007.
42. Soni S.S., Kim K.M., Sarkar B., Rodell C.B. Uptake of cyclodextrin nanoparticles by macrophages is dependent on particle size and receptor-mediated interactions. *ACS applied bio materials.* 2024, vol. 7 (8), pp. 4856-4866. doi: 10.1021/acsabm.3c00985.
43. Schwartz Y.S., Dushkin M.I., Vavilin V.A., Melnikova E.V., Khoschenko O.M., Kozlov V.A., Agafonov A.P., Alekseev A.Y., Rassadkin Y., Shestapalov A.M., Azaev M.S., Saraev D.V., Filimonov P.N., Kurunov Y., Svistelnik A.V., Krasnov V.A., Pathak A., Derrick S.C., Reynolds R.C., Morris S., Blinov V.M. Novel conjugate of moxifloxacin and carboxymethylated glucan with enhanced activity against Mycobacterium tuberculosis. *Antimicrobial agents and chemotherapy.* 2006, vol. 50 (6), pp. 1982-1988. doi: 10.1128/AAC.00362-05.
44. Horváti K., Gyulai G., Csámpai A., Rohonczy J., Kiss É., Bősze S. Surface Layer modification of poly (d, l-lactic-co-glycolic acid) nanoparticles with targeting peptide: a convenient synthetic route for Pluronic F127–Tuftsin conjugate. *Bioconjugate chemistry.* 2018, vol. 29 (5), pp. 1495-1499. doi: 10.1021/acs.bioconjchem.8b00156.
45. Jaecklein E., Papavinasasundaram K., Ostroff G.R., Sassetti C., Soto E.R. Targeted delivery of antitubercular drugs using glucan lipid particles. *Microbiology Spectrum.* 2025, vol. 13 (3), pp. e02744-24. doi: 10.1128/spectrum.02744-24.
46. Yu T.T., Sang X.Y., Han N., Peng X.C., Li Q.R., Xu X., Xiao R.C., Xu H.Z., Chen X., Wang M.F., Li T.F. Macrophages mediated delivery of chlorin e6 and treatment of lung cancer by photodynamic reprogramming. *International Immunopharmacology.* 2021, vol. 100, pp. 108164. doi: 10.1016/j.intimp.2021.108164.
47. Deng H., Wang H., Zhang Y., Liu R., Hou W., Wang L., Xu H., Zhang W. Tumor-associated macrophage-mediated delivery of nano-photosensitizer enables light-induced metabolic programming for immuno-photodynamic therapy. *Protein & Cell.* 2025, vol. 16 (12), pp. 1060-1065. doi: 10.1093/procel/pwaf064.
48. Park K., Ahn J.W., Kim J.H., Kim J.W. Tumor-associated macrophage-targeted photodynamic cancer therapy using a dextran sulfate-based nano-photosensitizer. *International journal of biological macromolecules.* 2022, vol. 218, pp. 384-393. doi: 10.1016/j.ijbiomac.2022.07.159.
49. Hamblin M.R., Newman E.L. Photosensitizer targeting in photodynamic therapy II. Conjugates of haematoporphyrin with serum lipoproteins. *Journal of Photochemistry and Photobiology B: Biology.* 1994, vol. 26 (2), pp. 147-157. doi: 10.1016/1011-1344(94)07036-9.
50. Hamblin M.R., Newman E.L. Photosensitizer targeting in photodynamic therapy I. Conjugates of haematoporphyrin with albumin and transferrin. *Journal of Photochemistry and Photobiology B: Biology.* 1994, vol. 26 (1), pp. 45-56. doi: 10.1016/1011-1344(94)85035-6.
51. Hamblin M.R., Miller J.L., Ortel B. Scavenger-Receptor Targeted Photodynamic Therapy. *Photochemistry and Photobiology.* 2000, vol. 72 (4), pp. 533-540. doi: 10.1562/0031-8655(2000)072<0533:srtpt>2.0.co;2.
52. Liu Q., Hamblin M.R. Macrophage-targeted photodynamic therapy: scavenger receptor expression and activation state. *International journal of immunopathology and pharmacology.* 2005, vol. 18 (3), pp. 391-402. doi: 10.1177/039463200501800301.

of mannose functionalized dendrimeric nanoparticles for targeted delivery to macrophages: use of this platform to modulate atherosclerosis // Translational Research. – 2018. – Vol. 193. – P. 13-30. doi: 10.1016/j.trsl.2017.10.008.

37. Wang Y., Liu Y., Long M., Dong Y., Li L., Zhou X. Nanoparticles target M2 macrophages to silence kallikrein-related peptidase 12 for the treatment of tuberculosis and drug-resistant tuberculosis // Acta Biomaterialia. – 2024. – Vol. 188. – P. 358-373. doi: 10.1016/j.actbio.2024.09.026.
38. Ovchinnikova L.A., Tanygina D.Y., Dzhelad S.S., Evtushenko E.G., Bagrov D.V., Gabibov A.G., Lomakin Y.A. Targeted macrophage mannose receptor (CD206)-specific protein delivery via engineered extracellular vesicles // Heliyon. – 2024. – Vol. 10 (24). – P. e40940. doi: 10.1016/j.heliyon.2024.e40940.
39. Serrasqueiro F., Barbosa A.I., Lima S.A.C., Reis S. Targeting the mannose receptor with functionalized fucoidan/chitosan nanoparticles triggers the classical activation of macrophages // International Journal of Molecular Sciences. – 2023. – Vol. 24 (12). – P. 9908. doi: 10.3390/ijms24129908.
40. Chen P., Zhang X., Venosa A., Lee I.H., Myers D., Holloway J.A., Prud'homme R.K., Gao D., Szekely Z., Laskin J.D., Laskin D.L., Sinko P.J. A novel bivalent mannosylated targeting ligand displayed on nanoparticles selectively targets anti-inflammatory M2 macrophages // Pharmaceutics. – 2020. – Vol. 12 (3). – P. 243. doi: 10.3390/pharmaceutics12030243.
41. Hatami E., Mu Y., Shields D.N., Chauhan S.C., Kumar S., Cory T.J., Yallapu M.M. Mannose-decorated hybrid nanoparticles for enhanced macrophage targeting // Biochemistry and biophysics reports. – 2019. – Vol. 17. – P. 197-207. doi: 10.1016/j.bbrep.2019.01.007.
42. Soni S.S., Kim K.M., Sarkar B., Rodell C.B. Uptake of cyclodextrin nanoparticles by macrophages is dependent on particle size and receptor-mediated interactions // ACS applied bio materials. – 2024. – Vol. 7 (8). – P. 4856-4866. doi: 10.1021/acsabm.3c00985.
43. Schwartz Y.S., Dushkin M.I., Vavilin V.A., Melnikova E.V., Khoschenko O.M., Kozlov V.A., Agafonov A.P., Alekseev A.Y., Rassadkin Y., Shestapalov A.M., Azaev M.S., Saraev D.V., Filimonov P.N., Kurunov Y., Svistelnik A.V., Krasnov V.A., Pathak A., Derrick S.C., Reynolds R.C., Morris S., Blinov V.M. Novel conjugate of moxifloxacin and carboxymethylated glucan with enhanced activity against Mycobacterium tuberculosis // Antimicrobial agents and chemotherapy. – 2006. – Vol. 50 (6). – P. 1982-1988. doi: 10.1128/AAC.00362-05.
44. Horváti K., Gyulai G., Csámpai A., Rohonczy J., Kiss É., Bősze S. Surface Layer modification of poly (d, l-lactic-co-glycolic acid) nanoparticles with targeting peptide: a convenient synthetic route for Pluronic F127–Tuftsin conjugate // Bioconjugate chemistry. – 2018. – Vol. 29 (5). – P. 1495-1499. doi: 10.1021/acs.bioconjchem.8b00156.
45. Jaecklein E., Papavinasasundaram K., Ostroff G.R., Sassetti C., Soto E.R. Targeted delivery of antitubercular drugs using glucan lipid particles // Microbiology Spectrum. – 2025. – Vol. 13 (3). – P. e02744-24. doi: 10.1128/spectrum.02744-24.
46. Yu T.T., Sang X.Y., Han N., Peng X.C., Li Q.R., Xu X., Xiao R.C., Xu H.Z., Chen X., Wang M.F., Li T.F. Macrophages mediated delivery of chlorin e6 and treatment of lung cancer by photodynamic reprogramming // International Immunopharmacology. – 2021. – Vol. 100. – P. 108164. doi: 10.1016/j.intimp.2021.108164.
47. Deng H., Wang H., Zhang Y., Liu R., Hou W., Wang L., Xu H., Zhang W. Tumor-associated macrophage-mediated delivery of nano-photosensitizer enables light-induced metabolic programming for immuno-photodynamic therapy // Protein & Cell. – 2025. – Vol. 16 (12). – P. 1060-1065. doi: 10.1093/procel/pwaf064.
48. Park K., Ahn J.W., Kim J.H., Kim J.W. Tumor-associated macrophage-targeted photodynamic cancer therapy using a dextran sulfate-based nano-photosensitizer // International journal of biological macromolecules. – 2022. – Vol. 218. – P. 384-393. doi: 10.1016/j.ijbiomac.2022.07.159.
49. Hamblin M.R., Newman E.L. Photosensitizer targeting in photodynamic therapy II. Conjugates of haematoporphyrin with serum lipoproteins // Journal of Photochemistry and Photobiology B: Biology. – 1994. – Vol. 26 (2). – P. 147-157. doi: 10.1016/1011-1344(94)07036-9.
50. Hamblin M.R., Newman E.L. Photosensitizer targeting in photodynamic therapy I. Conjugates of haematoporphyrin with albumin and transferrin // Journal of Photochemistry and Photobiology B: Biology. – 1994. – Vol. 26 (1). – P. 45-56. doi: 10.1016/1011-1344(94)85035-6.
51. Hamblin M.R., Miller J.L., Ortel B. Scavenger-Receptor Targeted Photodynamic Therapy // Photochemistry and Photobiology. – 2000. – Vol. 72 (4). – P. 533-540. doi: 10.1562/0031-8655(2000)072<0533:srtpt>2.0.co;2.
52. Liu Q., Hamblin M.R. Macrophage-targeted photodynamic therapy: scavenger receptor expression and activation state // International journal of immunopathology and pharmacology. – 2005. – Vol. 18 (3). – P. 391-402. doi: 10.1177/039463200501800301.

53. Tang F., Xie W., Li S., Hu Q., Zheng B., Ke M., Huang J. Alginate-zinc (II) phthalocyanine conjugates: Synthesis, characterization and tumor-associated macrophages-targeted photodynamic therapy. *Carbohydrate polymers.* 2020, vol. 240, pp. 116239. doi: 10.1016/j.carbpol.2020.116239.
54. Soyama T., Sakuragi A., Oishi D., Kimura Y., Aoki H., Nomoto A., Yano S., Nishie H., Kataoka H., Aoyama M. Photodynamic therapy exploiting the anti-tumor activity of mannose-conjugated chlorin e6 reduced M2-like tumor-associated macrophages. *Translational oncology.* 2021, vol. 14 (2), pp. 101005. doi: 10.1016/j.tranon.2020.101005.
55. Kimura Y., Aoki H., Soyama T., Sakuragi A., Otsuka Y., Nomoto A., Yano S., Nishie H., Kataoka H., Aoyama M. Photodynamic therapy using mannose-conjugated chlorin e6 increases cell surface calreticulin in cancer cells and promotes macrophage phagocytosis. *Medical Oncology.* 2022, vol. 39 (6), pp. 82. doi: 10.1007/s12032-022-01674-3.
56. Chi X., Wang S.H., Gao J., Su J., Du Y.Z., Xu X.L. Carrier-Free Nanocombo-Sensitized Photoimmunotherapy via Activation of α2-Adrenergic Receptors. *ACS Applied Materials & Interfaces.* 2025, vol. 17 (11), pp. 16437-16452. doi: 10.1021/acsami.4c18052.
57. Huang J., Xu S., Liu L., Zhang J., Xu J., Zhang L., Zhou X., Huang L., Peng J., Wang J., Gong Z., Chen Y. Targeted treatment of atherosclerosis with protein–polysaccharide nanoemulsion co-loaded with photosensitiser and upconversion nanoparticles. *Journal of Drug Targeting.* 2023, vol. 31 (10), pp. 1111-1127. doi: 10.1080/1061186X.2023.2284093.
58. Lee S.Y., Kim J.H., Song J.W., Min J.S., Kim H.J., Kim R.H., Ahn J.W., Yoo H., Park K., Kim J.W. Macrophage-mannose-receptor-targeted photoactivatable agent for in vivo imaging and treatment of atherosclerosis. *International journal of pharmaceutics.* 2024, vol. 654, pp. 123951. doi: 10.1016/j.ijpharm.2024.123951.
59. Dorst D.N., Boss M., Rijpkema M., Walgreen B., Helsen M.M.A., Bos D.L., van Bloois L., Storm G., Brom M., Laverman P., van der Kraan P.M., Buitinga M., Koenders M.I., Gotthardt M. Photodynamic therapy targeting macrophages using irdye700dx-liposomes decreases experimental arthritis development. *Pharmaceutics.* 2021, vol. 13 (11), pp. 1868. doi: 10.3390/pharmaceutics13111868.
60. Fan S., Zhao D., Wang J., Ma Y., Chen D., Huang Y., Zhang T., Liu Y., Xia J., Huang X., Lu Y., Ruan Y., Xu J.F., Shen L., Yang F., Pi J. Photothermal and host immune activated therapy of cutaneous tuberculosis using macrophage targeted mesoporous polydopamine nanoparticles. *Materials Today Bio.* 2024, vol. 28, pp. 101232. doi: 10.1016/j.mtbio.2024.101232.
61. Wang H., Li B., Sun Y., Ma Q., Feng Y., Jia Y., Wang W., Su M., Liu X., Shu B., Zheng J., Sang S., Yan Y., Wu Y., Zhang Y., Gao Q., Li P., Wang J., Ma F., Li X., Yan D., Wang D., Zou X., Liao Y. NIR-II AIE luminogen-based erythrocyte-like nanoparticles with granuloma-targeting and self-oxygenation characteristics for combined phototherapy of tuberculosis. *Advanced Materials.* 2024, vol. 36 (38), pp. 2406143. doi: 10.1002/adma.202406143.
62. Wang H., Li X., Li P., Feng Y., Wang J., Gao Q., Men B., Wang W., Yan Y., Zhang Y., Shi H., Wu Y., Ma F., Jia Y., Sang S., Fu X., Duan H., Zeng Q., Li X., Ma W., Li B., Liao Y. Uptake of Biomimetic Nanovesicles by Granuloma for Photodynamic Therapy of Tuberculosis. *ACS omega.* 2025, vol. 10 (7), pp. 6679-6688. doi: 10.1021/acsomega.4c08127.
63. Li B., Wang W., Zhao L., Wu Y., Li X., Yan D., Gao Q., Yan Y., Zhang J., Feng Y., Zheng J., Shu B., Wang J., Wang H., He L., Zhang Y., Pan M., Wang D., Tang B.Z., Liao Y. Photothermal therapy of tuberculosis using targeting pre-activated macrophage membrane-coated nanoparticles. *Nature Nanotechnology.* 2024, vol. 19, pp. 834-845. doi: 10.1038/s41565-024-01618-0.
64. Yan D., Li X., Wang H., Li B., Wang W., Liao Y., Tang B.Z., Wang D. NIR-II aggregation-induced emission nanoparticles camouflaged with preactivated macrophage membranes for phototheranostics of pulmonary tuberculosis. *Nature Protocols.* 2025, vol. 20 (9), pp. 2560-2585. doi: 10.1038/s41596-025-01146-8.
65. Cai Q., Fei Y., An H.W., Zhao X.X., Ma Y., Cong Y., Hu L., Li L.L., Wang H. Macrophage-instructed intracellular Staphylococcus aureus killing by targeting photodynamic dimers. *ACS applied materials & interfaces.* 2018, vol. 10 (11), pp. 9197-9202. doi: 10.1021/acsami.7b19056.
66. Wang Z., Wu A., Cheng W., Li Y., Li D., Wang L., Zhang X., Xiao Y. Adoptive macrophage directed photodynamic therapy of multidrug-resistant bacterial infection. *Nature Communications.* 2023, vol. 14 (1), pp. 7251. doi: 10.1038/s41467-023-43074-9.
67. Kim H.J., Jeong E.K., Lee H.J., Jung Y.J. The photosensitizer DH-I-180-3 regulates intracellular bacterial growth by increasing the secretion of proinflammatory cytokines via the NF-κB-and MAPK-mediated signaling pathways and promoting phagosome maturation in Salmonella-infected mouse macrophages. *Journal of Microbiology (Seoul, Korea).* 2025, vol. 63 (6), pp. e2502003-e2502003. doi: 10.71150/jm.2502003.

53. Tang F., Xie W., Li S., Hu Q., Zheng B., Ke M., Huang J. Alginate-zinc (II) phthalocyanine conjugates: Synthesis, characterization and tumor-associated macrophages-targeted photodynamic therapy // Carbohydrate polymers. – 2020. – Vol. 240. – P. 116239. doi: 10.1016/j.carbpol.2020.116239.
54. Soyama T., Sakuragi A., Oishi D., Kimura Y., Aoki H., Nomoto A., Yano S., Nishie H., Kataoka H., Aoyama M. Photodynamic therapy exploiting the anti-tumor activity of mannose-conjugated chlorin e6 reduced M2-like tumor-associated macrophages // Translational oncology. – 2021. – Vol. 14 (2). – P. 101005. doi: 10.1016/j.tranon.2020.101005.
55. Kimura Y., Aoki H., Soyama T., Sakuragi A., Otsuka Y., Nomoto A., Yano S., Nishie H., Kataoka H., Aoyama M. Photodynamic therapy using mannose-conjugated chlorin e6 increases cell surface calreticulin in cancer cells and promotes macrophage phagocytosis // Medical Oncology. – 2022. – Vol. 39 (6). – P. 82. doi: 10.1007/s12032-022-01674-3.
56. Chi X., Wang S.H., Gao J., Su J., Du Y.Z., Xu X.L. Carrier-Free Nanocombo-Sensitized Photoimmunotherapy via Activation of α2-Adrenergic Receptors // ACS Applied Materials & Interfaces. – 2025. – Vol. 17 (11). – P. 16437-16452. doi: 10.1021/acsami.4c18052.
57. Huang J., Xu S., Liu L., Zhang J., Xu J., Zhang L., Zhou X., Huang L., Peng J., Wang J., Gong Z., Chen Y. Targeted treatment of atherosclerosis with protein–polysaccharide nanoemulsion co-loaded with photosensitiser and upconversion nanoparticles // Journal of Drug Targeting. – 2023. – Vol. 31 (10). – P. 1111-1127. doi: 10.1080/1061186X.2023.2284093.
58. Lee S.Y., Kim J.H., Song J.W., Min J.S., Kim H.J., Kim R.H., Ahn J.W., Yoo H., Park K., Kim J.W. Macrophage-mannose-receptor-targeted photoactivatable agent for in vivo imaging and treatment of atherosclerosis // International journal of pharmaceutics. – 2024. – Vol. 654. – P. 123951. doi: 10.1016/j.ijpharm.2024.123951.
59. Dorst D.N., Boss M., Rijpkema M., Walgreen B., Helsen M.M.A., Bos D.L., van Bloois L., Storm G., Brom M., Laverman P., van der Kraan P.M., Buitinga M., Koenders M.I., Gotthardt M. Photodynamic therapy targeting macrophages using irdye700dx-liposomes decreases experimental arthritis development // Pharmaceutics. – 2021. – Vol. 13 (11). – P. 1868. doi: 10.3390/pharmaceutics13111868.
60. Fan S., Zhao D., Wang J., Ma Y., Chen D., Huang Y., Zhang T., Liu Y., Xia J., Huang X., Lu Y., Ruan Y., Xu J.F., Shen L., Yang F., Pi J. Photothermal and host immune activated therapy of cutaneous tuberculosis using macrophage targeted mesoporous polydopamine nanoparticles // Materials Today Bio. – 2024. – Vol. 28. – P. 101232. doi: 10.1016/j.mtbio.2024.101232.
61. Wang H., Li B., Sun Y., Ma Q., Feng Y., Jia Y., Wang W., Su M., Liu X., Shu B., Zheng J., Sang S., Yan Y., Wu Y., Zhang Y., Gao Q., Li P., Wang J., Ma F., Li X., Yan D., Wang D., Zou X., Liao Y. NIR-II AIE luminogen-based erythrocyte-like nanoparticles with granuloma-targeting and self-oxygenation characteristics for combined phototherapy of tuberculosis // Advanced Materials. – 2024. – Vol. 36 (38). – P. 2406143. doi: 10.1002/adma.202406143.
62. Wang H., Li X., Li P., Feng Y., Wang J., Gao Q., Men B., Wang W., Yan Y., Zhang Y., Shi H., Wu Y., Ma F., Jia Y., Sang S., Fu X., Duan H., Zeng Q., Li X., Ma W., Li B., Liao Y. Uptake of Biomimetic Nanovesicles by Granuloma for Photodynamic Therapy of Tuberculosis // ACS omega. – 2025. – Vol. 10 (7). – P. 6679-6688. doi: 10.1021/acsomega.4c08127.
63. Li B., Wang W., Zhao L., Wu Y., Li X., Yan D., Gao Q., Yan Y., Zhang J., Feng Y., Zheng J., Shu B., Wang J., Wang H., He L., Zhang Y., Pan M., Wang D., Tang B.Z., Liao Y. Photothermal therapy of tuberculosis using targeting pre-activated macrophage membrane-coated nanoparticles // Nature Nanotechnology. – 2024. – Vol. 19. – P. 834-845. doi: 10.1038/s41565-024-01618-0.
64. Yan D., Li X., Wang H., Li B., Wang W., Liao Y., Tang B.Z., Wang D. NIR-II aggregation-induced emission nanoparticles camouflaged with preactivated macrophage membranes for phototheranostics of pulmonary tuberculosis // Nature Protocols. – 2025. – Vol. 20 (9). – P. 2560-2585. doi: 10.1038/s41596-025-01146-8.
65. Cai Q., Fei Y., An H.W., Zhao X.X., Ma Y., Cong Y., Hu L., Li L.L., Wang H. Macrophage-instructed intracellular Staphylococcus aureus killing by targeting photodynamic dimers // ACS applied materials & interfaces. – 2018. – Vol. 10 (11). – P. 9197-9202. doi: 10.1021/acsami.7b19056.
66. Wang Z., Wu A., Cheng W., Li Y., Li D., Wang L., Zhang X., Xiao Y. Adoptive macrophage directed photodynamic therapy of multidrug-resistant bacterial infection // Nature Communications. – 2023. – Vol. 14 (1). – P. 7251. doi: 10.1038/s41467-023-43074-9.
67. Kim H.J., Jeong E.K., Lee H.J., Jung Y.J. The photosensitizer DH-I-180-3 regulates intracellular bacterial growth by increasing the secretion of proinflammatory cytokines via the NF-κB-and MAPK-mediated signaling pathways and promoting phagosome maturation in Salmonella-infected mouse macrophages // Journal of Microbiology (Seoul, Korea). – 2025. – Vol. 63 (6). – P. e2502003-e2502003. doi: 10.71150/jm.2502003.

ФОТОСЕНСИБИЛИЗАТОР хлоринового ряда для фотодинамической терапии

«ФОТОДИТАЗИН®» концентрат для приготовления раствора для инфузий — лекарственное средство РУ ЛП-№(007290)-(РГ-RU) от 17.10.2024 г.

«ФОТОДИТАЗИН®» применяется для флюоресцентной диагностики и фотодинамической терапии онкологических заболеваний различных нозологических форм, а также патологий неонкологического характера в следующих областях медицины:

- нейрохирургия
- гинекология
- торакальная хирургия
- урология
- стоматология
- гнойная хирургия
- дерматология
- комбустиология
- травматология и ортопедия

Фотодинамическая терапия внесена в клинические рекомендации МЗ РФ.

Фотодинамическая терапия включена в перечень видов высокотехнологичной медицинской помощи Программы государственных гарантий бесплатного оказания гражданам медицинской помощи, утверждаемой Правительством РФ.

ООО «ВЕТА-ГРАНД»
123056, г. Москва, ул. Красина, д. 27, стр. 2
Тел.: +7 (929) 971-44-46, +7 (499) 250-40-00
E-mail: veta-grand@mail.ru

fotoditazin.com
фотодитазин.рф